ผลของการห่อหุ้มตัวเร่งปฏิกิริยาโครเมียม-ซิงก์ออกไซด์และคอปเปอร์-ซิงก์ออกไซด์-อะลูมินาด้วยซิลิโกอะลูมิโนฟอสเฟตต่อการสังเคราะห์ไดเมทิลอีเทอร์จากแก๊สสังเคราะห์

นางสาวกิติมา ปิ่นแก้ว

วิทยานิพนธ์นี้เป็นส่วนหนึ่งของการศึกษาตามหลักสูตรปริญญาวิทยาศาสตรดุษฎีบัณฑิต
สาขาวิชาเคมีเทคนิค ภาควิชาเคมีเทคนิค
คณะวิทยาศาสตร์ จุฬาลงกรณ์มหาวิทยาลัย
ปีการศึกษา 2555

EFFECTS OF ENCAPSULATION OF Cr-ZnO AND Cu-ZnO-Al_2O_3 CATALYSTS WITH SILICOALUMINOPHOSPHATES ON DIMETHYL ETHER SYNTHESIS FROM SYNGAS

Miss Kitima Pinkaew

A Dissertation Submitted in Partial Fulfillment of the Requirements
for the Degree of Doctor of Philosophy Program in Chemical Technology
Department of Chemical Technology
Faculty of Science
Chulalongkorn University
Academic Year 2012

Thesis Title	EFFECTS OF ENCAPSULATION OF Cr-ZnO AND Cu-ZnO-Al_2O_3 CATALYSTS WITH SILICOALUMINOPHOSPHATES ON DIMETHYL ETHER SYNTHESIS FROM SYNGAS
By	Miss Kitima Pinkaew
Field of Study	Chemical Technology
Thesis Advisor	Associate Professor Tharapong Vitidsant, Ph.D.
Thesis Co-advisor	Professor Noritatsu Tsubaki, Ph.D.

Accepted by the Faculty of Science, Chulalongkorn University in Partial Fulfillment of the Requirements for the Doctoral Degree

.....Dean of the Faculty of Science

(Professor Supot Hannongbua, Dr. rer. nat.)

THESIS COMMITTEE

.....Chairman

(Associate Professor Kejvalee Pruksathorn, Dr.de l'INPT.)

.....Thesis Advisor

(Associate Professor Tharapong Vitidsant, Ph.D.)

.....Thesis Co-advisor

(Professor Noritatsu Tsubaki, Ph.D.)

.....Examiner

(Assistant Professor Prasert Reubroycharoen, Ph.D.)

.....Examiner

(Assistant Professor Chawalit Ngamcharussrivichai, Ph.D.)

.....External Examiner

(Associate Professor Apinya Duangchan, Ph.D.)

กิติมา ปิ่นแก้ว : ผลของการห่อหุ้มตัวเร่งปฏิกิริยาโครเมียม-ซิงก์ออกไซด์และคอปเปอร์-ซิงก์ออกไซด์-อะลูมินาด้วยซิลิโกอะลูมิโนฟอสเฟตต่อการสังเคราะห์ไดเมทิลอีเทอร์จากแก๊สสังเคราะห์, (EFFECTS OF ENCAPSULATION OF Cr-ZnO AND Cu-ZnO-Al_2O_3 CATALYSTS WITH SILICOALUMINOPHOSPHATES ON DIMETHYL ETHER SYNTHESIS FROM SYNGAS) อ.ที่ปรึกษาวิทยานิพนธ์หลัก : รศ.ดร.ธราพงษ์ วิทิตศานต์, อ.ที่ปรึกษาวิทยานิพนธ์ร่วม : Prof. Noritatsu Tsubaki, Ph.D., 137 หน้า

ในผลศึกษานี้ได้แบ่งการทดลองออกเป็นสามส่วนหลักๆ ได้แก่ ส่วนแรกเกี่ยวกับการศึกษาชนิดของซีโอไลท์ในตัวเร่งปฏิกิริยาแบบผสม ส่วนที่สองเป็นการศึกษาเกี่ยวกับตัวเร่งปฏิกิริยาชนิดแคปซูล และส่วนสุดท้ายเป็นการศึกษาการออกแบบการทดลองแบบแฟกทอเรียล ตัวเร่งปฏิกิริยาชนิดแคปซูลถูกเตรียมโดยวิธีการแบบใหม่ทางกายภาพ ตัวเร่งปฏิกิริยาที่ถูกเคลือบได้แก่ โครเมียม-ซิงก์ออกไซด์เคลือบทับโดยซิลิโกอะลูมิโนฟอสเฟตชนิด 46 และคอปเปอร์-ซิงก์ออกไซด์-อะลูมินาเคลือบทับด้วยซิลิโกอะลูมิโนฟอสเฟตชนิด 11 ตัวเร่งปฏิกิริยาชนิดแคปซูลที่เตรียมโดยวิธีทางกายภาพนี้สามารถเตรียมได้ในภาวะบรรยากาศปกติโดยที่ไม่ต้องใช้เครื่องมือพิเศษชนิดอื่นๆ เพิ่มเติม และจากผลการวิเคราะห์สมบัติของตัวเร่งปฏิกิริยา เช่น SEM EDSและ XRD ต่างยืนยันว่า ตัวเร่งปฏิกิริยาชนิดแคปซูลแบบใหม่มีพื้นผิวที่แน่นและเคลือบติดบนตัวเร่งปฏิกิริยาแกนที่อยู่ด้านใน ในส่วนผลการทดสอบปฏิกิริยาแสดงให้เห็นว่า ตัวเร่งปฏิกิริยาชนิดแคปซูลทั้งสองชนิดช่วยเร่งทำให้ค่าการเลือกเกิดของไดเมทิลอีเทอร์สูงกว่าตัวเร่งปฏิกิริยาแบบผสมปกติ ผลของการทดสอบปฏิกิริยายังแสดงให้เห็นว่า มีค่าร้อยละการเลือกเกิดไดเมทิลอีเทอร์และค่าร้อยละการเกิดไดเมทิลอีเทอร์สูงมากอยู่ที่ 90 และ 83 ตามลำดับบนตัวเร่งปฏิกิริยาคอปเปอร์-ซิงก์ออกไซด์-อะลูมินาที่เคลือบทับด้วยซิลิโกอะลูมิโนฟอสเฟตชนิด 11 นอกจากนี้ในส่วนของการศึกษาชนิดของซีโอไลท์ในตัวเร่งปฏิกิริยาแบบผสมโครเมียม-ซิงก์ออกไซด์และซีโอไลท์ชนิดต่างๆ ได้แก่ อะลูมิโนฟอสเฟสชนิด 5 และ 11 และซิลิโกอะลูมิโนฟอสเฟสชนิด 11 และ 46 พบว่าซิลิโกอะลูมิโนฟอสเฟตชนิด 11 เป็นตัวที่ความเหมาะสมสำหรับปฏิกิริยาการสังเคราะห์ไดเมทิลอีเทอร์จากแก๊สสังเคราะห์ จากการทดลองแบบแฟกทอเรียลสามารถทำนายสมการสำหรับค่าการเปลี่ยนของแก๊สสังเคราะห์และค่าการเลือกเกิดไดเมทิลอีเทอร์ได้

ภาควิชา เคมีเทคนิค ลายมือชื่อนิสิต .....

สาขาวิชา เคมีเทคนิค ลายมือชื่อ อ.ที่ปรึกษาวิทยานิพนธ์หลัก .....

ปีการศึกษา 2555 ลายมือชื่อ อ.ที่ปรึกษาวิทยานิพนธ์ร่วม .....

5273894323 : MAJOR CHEMICAL TECHNOLOGY

KEYWORDS : DIMETHYL ETHER SYNTHESIS / CAPSULE CATALYST / SAPOs / FACTORIAL DESIGN

KITIMA PINKAEW : EFFECTS OF ENCAPSULATION OF Cr-ZnO AND Cu-ZnO-Al_2O_3 CATALYSTS WITH SILICOALUMINOPHOSPHATES ON DIMETHYL ETHER SYNTHESIS FROM SYNGAS. ADVISOR : ASSOC. PROF. THARAPONG VITIDSANT, Ph.D., CO-ADVISOR : PROF. NORITATSU TSUBAKI, Ph.D., 137 pp.

In this thesis, the experimental is divided into three parts, the catalyst mixture of Cr-ZnO catalyst and various types of zeolite, the main study of capsule catalyst, and the experimental design. The capsule catalyst was prepared by the new method named physical coating. The new coating catalysts are Cr-ZnO encapsulated by SAPO-46, and Cu-ZnO-Al_2O_3 encapsulated by SAPO-11. The capsule catalyst is simple and can be prepared without using any extra equipment. All catalysts have been characterized by SEM, EDS and XRD. All characterization techniques confirm the new capsule catalyst is compact. The total catalytic activities of capsule catalyst are higher than the conventional mixed catalyst. The reaction results show remarkably higher DME selectivity due to the spatial core-shell-like structure of capsule catalyst. The physical CuZnAl/SAPO11-PhyC catalyst showed extremely high DME selectivity at 90% and DME yield at 83%. Moreover, the study on the mixture catalyst of Cr-ZnO and SAPO-11 presented the best catalytic performance among those four types of molecular sieve ($AlPO_4$-5, $AlPO_4$-11, SAPO-11 and SAPO-46). The acidity properties and framework structure of zeolites were considered as the important factors. The optimum mathematical model was obtained from 2^k factorial design among three variables, W/F ratio, reaction temperature and weight ratio of SAPO11: Cr-ZnO.

Department : Chemical Technology Student's Signature .....

Field of Study : Chemical Technology Advisor's Signature .....

Academic Year : 2012 Co-advisor's Signature .....

ACKNOWLEDGEMENTS

This work would not be accomplished without the considerable assistance of the following persons and organizations:

I would like to thank my advisor Assoc. Prof. Dr Tharapong Vitidsant for giving me a great opportunity for this scholarship and my co-advisor Prof. Dr. Noritatsu Tsubaki who really supported me for this work, provided me so many suggestions and contributed help for the work and my living when I was in Japan. I would like to give Guohui Yang very great thanks for being my mentor I would say this because without him I would not be able to learn many things I have been through all year in Prof. Tsubaki's laboratory and still after I come back to Thailand, his help had been sending to me for suggesting and correcting my publication. There were also so many people supported me for the work, many friends in the laboratory all senior and junior friends I have to thank to for helping me, Itou san who is the secretary of Prof. Tsubaki she helped me everything about the living when I was there. I'm very grateful to what she did for me.

I would like to thank all the thesis committee Assoc. Prof. Kejvalee Pruksathorn for serving as the chairman, Asst. Professor Prasert Reubroycharoen, Asst. Prof. Chawalit Ngamcharussrivichai, and Assoc. Prof. Apinya Duangchan for serving as the committee.

I would like to acknowledge Chulalongkorn University for providing financial support to me by Dutsadi Phiphat Scholarship all the time I have been studied in Doctoral degree.

And the last one, I would like to thank my parents, families and all friends both in Thailand and in Japan and also junior and senior friends at Chemical Technology who really supported me when I have problems.

CONTENTS

Page

Page

Page

List of Tables

Page

Page

List of Figures

Page

Page

Page

CHAPTER I

INTRODUCTION

The role of synthetic fuels has gained more important nowadays in many processes including petrochemical, industrial or commercial use. Due to the large increase of the population in the world, the petroleum fuel has been brought to serve the increasing necessities of the world's demands. Petroleum and natural gas resources are accounted for 60% of the overall world's energy consumption. The other resources such as coal, nuclear, hydroelectric and other sources are accounted for 27, 6, 6 and 1%, respectively. The world energy consumption in 2012 has been increased from the last century (based on year 2000) for around 35% of world energy use and is forecasted to reach 65% by 2025. The more energy use has been gradually increased and can be roughly divided into 4 major sectors; industrial, transportation, commercial and residential. Among these four types, the industrial use has gained the large amount of increment due to the growth of world economic nowadays. The industrial section has reached the highest proportion of the world energy use. The petroleum-based fuels are mostly the fuels used in many industrial. And the long-term energy demand in the world is forecasted to be increased; for this reason, the new alternative choice such as synthetic fuel has been researched in a number of studies nowadays. The other alternative fuel candidates are methane, hydrogen, methanol, ethanol, biofuels, Fisher-Tropsch fuels, and dimethyl ether (DME). The alternative fuels like DME has been gained much more attention in researches due to the ability to replace the petroleum-based fuels.

The process of synthetic fuels from natural gas such as the formation of CH_4 to syngas is the very first processes of the indirect way of conversion of methane to higher hydrocarbons. Methane will be transformed to syngas (CO, CO_2 and hydrogen) by steam reforming and then the syngas can be transformed to olefins or gasoline by Fischer-Tropsch synthesis, or firstly by methanol synthesis. And then the methanol

can be transformed to higher hydrocarbons by methanol-to olefin (MTO) or methanol-to-gasoline (MTG). The methanol synthesis process has mostly been derived from syngas production step. The overall process of producing downstream products from natural gas is shown in the Figure 1.1 below.

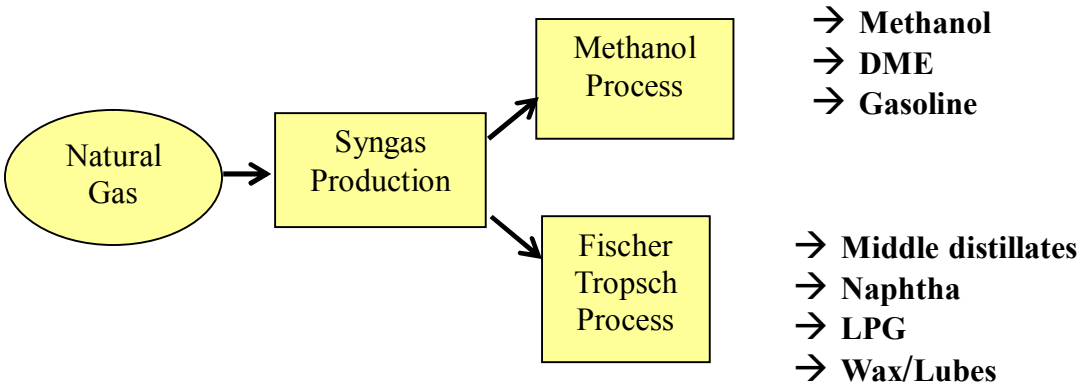

Figure 1.1 The process of downstream products from natural gas

Up to date, many types of substitute fuels have been more researched including DME. DME is generally synthesized via the STD reaction and the filed that has gained more interesting nowadays is developing on catalyst system. The STD catalyst has been studied widely to find out the optimum point for both of catalyst properties and operating conditions. For methanol synthesis catalyst, it has been known that Cu-Zn-Al catalyst is typical for low temperature process and also practical in industrial use. The high methanol synthesis process usually uses Cr_2O_3-ZnO as a catalyst. For methanol dehydration catalyst, solid acid catalysts for instance, γ- Al_2O_3 or zeolite have been selected for DME synthesis. In methanol dehydration, the acid properties and pore structure were believed to be an important key to determine the catalytic performance. Besides the aluminosilicate zeolite, there are also the other classes of zeolite that present mild acidic properties compare with aluminosilicate zeolite [1, 2]. Usually, the SAPO zeolites are employed as acidic catalysts for many reactions, such as hydrocarbon isomerization, conversion of methanol to light olefins (MTO), as well as the process of DME synthesis by methanol dehydration [1, 3-6]. Therefore in this study, the various aluminophosphate (AlPOs) and silicoaluminophosphate (SAPOs) were prepared to perform the DME synthesis from

synthesis gas. The mixed catalysts of Cr/ZnO and AlPOs or SAPOs were used for STD synthesis. Moreover, the main part of this study is about the capsule catalysts which were performed for STD synthesis as well. The outstanding catalytic performance is shown in Chapter 5.

In this research work, the Cr/ZnO and other kinds of molecular sieve (these are AlPOs, and SAPOs) have been introduced in the direct DME synthesis. The new capsule catalyst was prepared by the physical coating method. Silicoaluminophosphate membrane was coated on the methanol synthesis catalyst pellet, Cr/ZnO or CuZnAl, and which was called "capsule catalyst". In the reaction, the reactant gas ($CO+H_2$) passed through the silicoaluminophosphate membrane and reached the core catalyst. Then the methanol occurred there at the center part and diffused out. And when the methanol diffused out through the SAPO membrane, most of them had high probability to reach the acidic sites inside the SAPO and dehydrated to DME or isomerized into higher hydrocarbons. For higher hydrocarbons or long-chain hydrocarbons, their low diffusion rate will keep themselves stay in the SAPO channel longer which tend to increase the chance to have isomerization or cracking inside its channel. The benefit of the restricted structure is the key to success which lead to the higher total activity of the reaction. This capsule catalyst has an advantage over conventional mixed catalyst. This is the main rationale of this research work.

The experimental design study has also gained more attention nowadays. The 2^k factorial design is also one of the designs which can evaluate the optimum mathematical model to determine the set of experiment in order to minimize the number of resources, time, and obtain the reliable archetype of that experiment. In general, factorial designs are most efficient for study the effects of two or more factors; the effect of a factor is defined to be the result in response produced by a change in a level of the factor. In this study, the factorial designs are done to evaluate the mathematical model of CO conversion and DME selectivity.

In brief, this study can be divided into three parts. The first part is about the studying of mixed catalyst of Cr/ZnO and various types of aluminophosphate ($AlPO_4$-5 and $AlPO_4$-11) and silicoaluminophosphate (SAPO-11 and SAPO-46) in STD reaction. The catalytic performance of these catalysts is shown in Chapter 4. The

second part is the study of capsule catalysts; the new coating catalyst is Cr/ZnO encapsulated by SAPO-46 and CuZnAl encapsulated by SAPO-11. The capsule catalyst was approached by new method named physical coating which is simple and can be prepared without using any extra equipment. The results show remarkably higher DME selectivity due to the suitable catalyst structure of capsule catalyst. The details were discussed more in Chapter 5. And the third part is the study of 2^k factorial design on three parameters; W/F ratio, reaction temperature and weight ratio of SAPO-11: Cr/ZnO to obtain the optimum conditions among the range of maximum and minimum condition. The results have been presented in Chapter 6.

CHAPTER II

THEORY AND LITERATURE REVIEWS

2.1 Dimethyl ether

Dimethyl ether (DME) is gaining worldwide recognition as a multisource, multipurpose clean fuel and chemical feedstock for the 21st century. It is a technically mature, environmentally friendly, and market acceptable alternative fuel. As shown in **Figure 2.1**, DME can be produced from a variety of sources, and its end use includes a number of important applications. Dimethyl ether can be manufactured in large quantities from coal, natural gas, biomass and municipal solid waste.

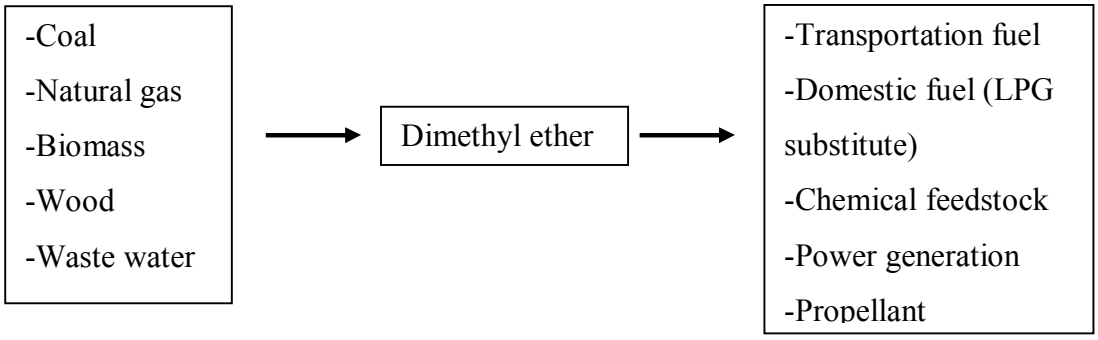

Figure 2.1 DME as a multisource and multipurpose chemical [7]

The simplest ether compound, DME has been shown to be both nontoxic and environmentally benign. Dimethyl ether has a variety of uses in the fuel and the chemical industries. Currently, the major use of DME is a propellant in the aerosols industry, Its cetane number (a quantitative indicator of the ignition quality of diesel engines) is high, ranging from 55 to 60, so that it can be used in diesel engines. Its flame is visible blue flame similar to that of natural gas, and it can be used just as it is

in an LPG cooking stove, and it does not produce any aldehydes. The toxicity of DME is low, about the same as that of LPG and even lower than that of methanol. Because of DME‘s restrictive use, current world capacity is only 150,000 metrictons/yr. Future megaplant technology providers include NKK, Haldor Topsoe, Lurgi, Toyo Engineering, Mitsubishi Gas Chemical, Kvaerner, Synetix, etc.

The technology of DME production is various nowadays. Many countries have developed the applications of DME as a diesel fuel for example China and Australia. The societal interest would be seen more in Europe and Japan. The initial pilot plant scale of DME production nowadays has been developed for produce five ton per day which was already established in Japan. Later this plant has developed the capability of DME production into one-hundred ton per day (year 2006). And in some Europe countries, in Sweden, the demonstration plant was put into operation in 2010. Nowadays the total amount of DME production is beyond in the past.

2.1.1 Properties of dimethyl ether

DME is the simplest ether with the formula CH_3OCH_3. DME is a colorless gas at ambient temperature, chemically stable, with a boiling point of -24.9 °C and as its vapor pressure is about 0.6 MPa at 25 °C, DME is easily liquefied. The properties of DME are similar to those of liquefied petroleum gas (LPG). DME burns with a visible blue flame. Unlike methane, DME does not require addition of odor because it has sweet ether-like odor. The physical properties of DME compared to other fuels are detailed in **Table 2.1.** Those values of conventional gasoline and diesel are shown in the table.

Table 2.1 Physical and thermo-physical properties of fuels [8]

Formula	Methane CH_4	Methanol CH_3OH	DME CH_3OCH_3	Ethanol CH_3CH_2OH	Gasoline C_7H_{16}	Diesel $C_{14}H_{30}$
Molecular weight (g mol^{-1})	16.04	32.04	46.07	46.07	100.2	198.4
Density (g cm^{-3})	0.00072[a]	0.792	0.661[b]	0.785	0.737	0.856
NBP[c] (°C)	-162	64	-24.9	78	38-204	125-400
LHV (kJ cm^{-3})	0.0346	15.82	18.92	21.09	32.05	35.66
LHV (kJg^{-1})	47.79	19.99	28.62	26.87	43.47	41.66
Exergy (MJL^{-1})	0.037	17.8	20.63	23.1	32.84	33.32
Exergy ($MJkg^{-1}$)	51.76	22.36	30.75	29.4	47.46	46.94
Carbon content (wt.%)	74	37.5	52.2	52.2	85.5	87
Sulfur content (ppm)	~7-25	0	0	0	~200	~250

[a] Values per cm^3 of vapor at standard temperature and pressure.

[b] Density at P = 1 atm and T =−25 ◦C.

[c] Normal boiling point

From the properties shown in **Table 2.1**, we can see the better properties of DME compared with other commonly used fuels e.g. the zero sulfur content, higher calorific value compared with methanol.

2.1.2 DME production nowadays and its applications

DME is the very useful clean energy source, the nonpetroleum-based fuels. The main application of DME is using as a spray propellant or other interesting one is using instead of diesel fuels which do not producing soot during combustion and its cetane number properties are relative close to those of diesel fuels. The burning of DME in diesel engines results in a lower NOx and SOx. The pollutions came from

diesel oil and liquefied petroleum gas such as soot, particular matter, and NOx or SOx could be replaced by using a substitute DME to avoid more serious problems. The advantages of using DME in the diesel engine are very low NOx emission, reduced engine noise, and soot-free combustion. Moreover, DME is a useful intermediate for the preparation of many important chemicals including methyl acetate, acetic acid, DMET (for further convert into ethylene glycol), aromatics and premium gasoline. Besides substitution for diesel fuel, DME can also substitute for transportation fuel, power generation fuel and domestic fuel. Use of DME, a clean burning oxygenates, has a very positive impact on these problems. Properties of DME are compared with those of diesel in **Table 2.2**.

Table 2.2 Comparison between DME and Diesel [9]

Property	DME	Diesel
Normal boiling point (°C)	-25.1	180-370
Liquid density (g/cm^3)	0.67	0.84
Igition temperature (°C)	235	250
Explosion limit (%)	3.4-17	0.60-0.65
Cetane number	55-60	40-55
Net heating value (kJ/kg)	28,882	42,612

DME can be synthesized by methanol dehydration over acid catalyst (Eq. (2)) and the other is direct methanol synthesis from syngas over hybrid catalyst (Eq. (1), (2)). This one-step controlled synthesis from syngas will occur sequentially; the first reaction is methanol synthesis from syngas (Eq. (1)) and followed by the methanol dehydration (Eq. (2)). The water gas shift reaction (WGS) usually occurs with the one-step controlled synthesis from syngas. The hybrid catalyst is generally combined of metal oxide and acid catalyst. Each reaction step of DME synthesis is shown as below.

Methanol synthesis:

$CO + 2H_2 \rightarrow CH_3OH$, $\Delta H°_{rxn} = -90.3\ kJmol^{-1}$ (1)

Methanol dehydration:

$2CH_3OH \rightarrow CH_3OCH_3 + H_2O$, $\Delta H°_{rxn} = 23.4\ kJ\ mol^{-1}$ (2)

Water–gas shift:

$H_2O + CO \rightarrow H_2 + CO_2$, $\Delta H°_{rxn} = 40.9\ kJmol^{-1}$ (3)

Net reaction:

$3H_2 + 3CO \rightarrow CH_3OCH_3 + CO_2$, $\Delta H°_{rxn} = 258.6\ kJmol^{-1}$ (4)

Generally, dimethyl ether (DME) can be produced via two processes, one-step syngas to dimethyl ether synthesis or individually occurred. For one-step process it composes of three reactions that is methanol synthesis from syngas, and then methanol dehydration to DME. And water-gas shift reaction (WGS) incorporated occurs accelerating the methanol synthesis reaction shift into the right hand side and also favoring the methanol dehydration rate. Both of one step process and two steps process are now commercially available. And DME can also convert itself into olefins or higher hydrocarbons.

The catalyst that has been widely known as a catalyst for methanol synthesis is Cu-based one. This catalyst shows good activity for hydrogenation reaction and also has been used as the conventional catalyst for methanol synthesis [10]. Cu-based catalyst was normally been used in low temperature synthesis, whereas the Cr-based catalyst can be used for higher temperature and pressure synthesis. Generally, methanol synthesis can be classified in to two groups: low pressure and high pressure synthesis. In low pressure process, the typical catalysts is $Cu/ZnO/Al_2O_3$ operates within the pressure and temperature range from 5-10 MPa and 240-270 °C, respectively. Whereas, the high pressure process could be operated within the condition of 24-30 MPa and 350-400 °C. The typical catalyst for high pressure process is Cr_2O_3-ZnO.

2.2 Using of aluminophosphate and silicoaluminophosphate molecular sieve in a role of acid catalyst

The new class molecular sieve aluminophosphate ($AlPO_4$) has been found in this recent 30 years. Nowadays, many applications have been applied with many kinds of molecular sieve have been used for many applications nowadays. The acidity properties can be one referred by Si/Al ratio; the ratio could be varied from 1 to ∞. The Al and P atom incorporates forming the crystalline framework structure. Other element, such as B, Ge, Zn, P, and transition elements, can also be incorporated into the framework and are also referred to as crystalline molecular sieves. Aluminophosphates (AlPOs) have strictly alternating AlO_2^- and PO_2^+ units, and the framework is neutral, organophillic, and nonacidic. The alternation of Al or P leads to structures lacking in odd-numbered rings. Substitution of P by Si leads to silicoaluminophosphates (SAPOs), with cation exchange abilities. Metal cations can also be introduced into the framework, including transition metal ions such as Co, Fe, Mn, Zn or Ti producing varied Bronsted acidity [11, 12]. Many types of substituted metal aluminophosphate have been discovered nowadays. Moreover, the other acidity properties could be referred by the amount of acid site; it has been known that the amount of acid site and its framework structure of each kind of silicoaluminophosphates and aluminophosphate affect the catalytic properties and selectivity of the final products. For methanol to olefin (MTO) process, many researches have been studied about the amount of acidic properties, both of acid amount and strength, and also the framework structure that were the main reason affected the designed products (light olefin ethane and/or propene). In those process DME or methanol is fed repeatedly to the mechanism and then formed longer hydrocarbons via alkylation or hydrogen transfer or poly condensation. But in this study, the DME in the designed product will be obtained from the one-step syngas to dimethyl ether synthesis. The overall reaction steps were occurred by first methanol synthesis reaction from syngas and then methanol dehydration to obtained DME and byproducts water. Moreover, water is the reactant in the water-gas shift reaction will drive overall process to occur more CO_2. There have many studies about the helpful

of using CO_2 in syngas for DME synthesis and it helps accelerating the overall reaction more favorable than without it.

2.3 Mixed catalyst and capsule catalyst

The mixed catalysts have been used for catalysis of reactions composed of two or more elementary reactions occurring via different pathways; for example, WO_3/SiO_2 for the cross-metathesis and self-metathesis of butenes, Cu/ZnO/ZSM-5 for direct DME synthesis or other reactions, etc. The acid catalyst has been applied in many applications nowadays. Mostly, the physical blending catalyst is the most common used nowadays due to the easy preparation method by mixing between the first and the second active catalysts for two different reactions. The conventional mixed catalysts that have been used for DME synthesis in most commonly used are Cu-based catalyst and acid catalyst zeolite. The most popular zeolite used for this reaction in the past are H-ZSM-5 or γ-Al_2O_3 due to the acidic properties itself. Besides those aluminosilicate zeolite, the other class of zeolite named aluminophosphated-based is becoming a talent acid catalyst as well. SAPO-34 and SAPO-18 were some examples of them that have been used in MTO process nowadays. There are so many types of zeolite acid catalyst, each type provides different framework structures and also leads to different catalytic behaviors. More study about the role of structure of zeolite and acidic properties should be more researched in the future. It has been known that the mild to moderate acid catalyst is more suitable for DME synthesis than the stronger acid catalyst due to the unnecessary further dehydration ability into higher hydrocarbons. Therefore in order to synthesize DME products, selecting the mild to moderate acid catalyst should be considered as the first variable. The less acidic zeolite such as aluminosilicate-base or silicoalumino- phosphate zeolite is one class of zeolite that has mild to moderate acid properties. As a result, they were brought into this study for more understanding on this STD synthesis. The mixed catalyst of Cr/ZnO and various zeolites such as $AlPO_4$-5, $AlPO_4$-11, SAPO-11, and SAPO-46 has been prepared. Altogether with the capsule catalyst of Cr/ZnO with SAPO-46 and SAPO-11 and CuZnAl with SAPO-46 were prepared. The role of core-shell-like structure has been proved that is better than the

unorganized structure of mixed catalyst. This core-shell-like structure provides that a sequential order of methanol synthesis occur at the core catalyst and methanol dehydration occur at the shell membrane of the whole catalyst. And also the shell membrane is working as a protecting layer and keeps the longer hydrocarbon stay inside the pore of zeolite. This will help increasing contact time and the chance of cracking higher hydrocarbon. The cross sectional view of capsule catalyst is demonstrated in **Figure 2.2.**

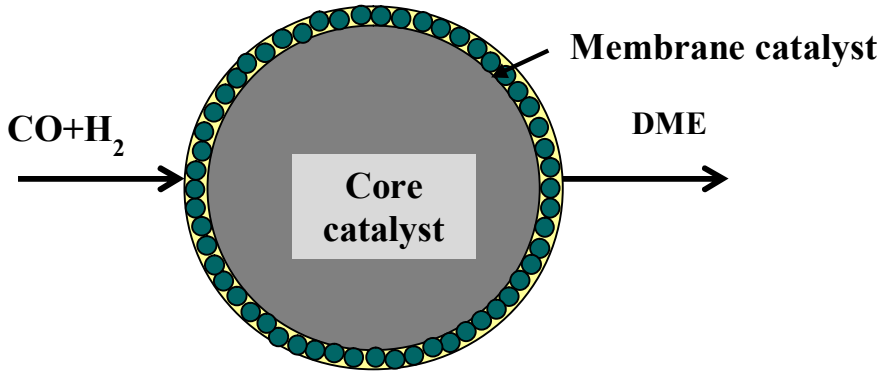

Figure 2.2 The cross sectional view of capsule catalyst

2.4 Aluminophosphate

The amount of Al can be varied with many Si/Al ratios which can represent acidity; the ratio could be varied from 1 to ∞. Aluminophosphate is one of the classifications of molecular sieve substance. The Al and P atom incorporates forming the crystalline framework structure. Other element, such as B, Ge, Zn, P, and transition elements, can also be incorporated into the framework and are referred to as crystalline molecular sieves. Aluminophosphates (AlPOs) have strictly alternating AlO_2^- and PO_2^+ units, and the framework is neutral, organophillic, and nonacidic. The alternation of Al or P leads to structures lacking in odd-numbered rings. Substitution of P by Si leads to silicoaluminophosphates (SAPOs), with cation exchange abilities. Metal cations can also be introduced into the framework, including transition metal

ions such as Co, Fe, Mn, and Zn. Discovery of these solids has led to development of several new structures.

Table 2.3 Framework structures and pore channel of $AlPO_4$s and SAPOs [13]

Sample	Framework	Channels
$AlPO_4$-5	AFI	[001] **12** 7.3x7.3* (1-D)
$AlPO_4$-11	AEL	[001] **10** 4.0x6.5* (1-D)
SAPO-11	AEL	[001] **10** 4.0x6.5* (1-D)
SAPO-46	AFS	[001] **12** 7.0x7.0* $\leftrightarrow \perp$ [001] **8** 4.0x4.0 (3-D)

Phosphate –based zeolites and molecular sieves [14]

The family of crystalline, microporous three-dimensional oxide structures can be divided into silicate-based and phosphate-based types. This new class of molecular sieve has been discovered in the last 30 years. Currently, the number of phosphate-based zeolites and molecular sieves has been substantial researched more generally compare with silicate-based zeolites. A large number of poro-tecto-aluminophosphate structures are denoted with the acronym '$AlPO_4$-n' referring to three dimensional oxide framework with P/Al ratios equal to 1 : 1. The number 'n' refers to the specific crystallographic structure. The numbering is arbitrary. analogous materials containing other elements besides Al and P are conveniently thought of as being derived from an imaginary, isostructure $AlPO_4$, in which Al, or P, or both, have undergone partial or even complete isomorphic substitution. The nature of the isomorphic substitution is currently indicated in the acronym, e.g., SAPO-5 is a silicoaluminophosphate with structure type No.5, CoAPO-11 is a coboalt-aluminophosphate with structure type No.11, etc. For the naming of materials, several researchers have used codes derived from the name of their institute or company. For

instance, the code name ‘TAMU’ stands for ‘Texas A & M University’, ‘VPI’ for ‘Virginia Polytechnic Institute’ and ‘JDF’ for ‘Jilin David Faraday’.

2.4.1 Structural, synthetic and physicochemical concepts relevant to poro-tecto- phosphates

2.4.1.1 $AlPO_4$ ($GaPO_4$)

The well-known phosphate-based molecular sieve nowadays is microporous materials with three dimensional, phosphorus has four-coordinated with five electron valency , aluminum is three-coordinated and its valency can be IV, V, or VI. Usually, the aluminum with four ligands are oxogen bridges with framework phosphorus atoms, but sometime the guest molecule such as hydroxyl, fluoro, phosphate, aquo or other species will occupy with the fifth and sixth ligand positions. The ‘$AlPO_4$’ structural concept occurs from the remark that, when ignoring the secondary coordinations of aluminum, $AlPO_4$ structure can be represented by an idealized framework composed of strictly sharing, alternating AlO_4 and PO_4 tetrahedral.

Due to each oxygen of the framework is two-connected, the three-dimentional network of linked AlPl and PO_4 tetrahedral can be symbolized by a short straight line showing the branches between adjacent Al and P atoms. In the short straight line, the centers of the oxygen tetrahedral tie at the nodes, each node stand for an Al or P atom.

The corner of Al and P in the tetrahedral nodes of the idealized framework prevents the existence of odd-membered ring of tetrahedral in poro-tecto-phosphate. In poro-tecto-silicates, the odded five membered-rings are very common.

Zeolites and molecular sieves are often classified according to their pore size. The pore size is measured as the number of nodes in the structure. The framework element at the specific crystallographic locations have only three instead of four oxogen bridges to neighboring framework elements, increasing a systematic interruption of the three-dimensional network. At the framework interruptions at P, Al and Ga elements, the coordination is surrounded with a hydroxyl ligand; the

coordination of lower valent elements such as Zn is surrounded typically with an aquo ligand.

2.4.1.2 Al (Ga) coordination concept

The Aluminium shows lots of coordination in $AlPO_{4S}$. The water molecules or fluoride, hydroxide, or phosphate anion was adsorbed in the pore will be interact with aluminium atoms and form Al^{V} and Al^{VI} matching. In most cases, only some Al atoms located at specific crystallographic locations exhibit this interaction with guest molecules. It will be shown that the physicochemical properties of an $AlPO_4$ material are determined by the coordination chemistry of aluminum and, therefore, it is useful to classify the materials according to the coordinations embraced by the framework aluminum atoms.

The as-synthesized form of Al coordination in $AlPO_4$ phase is easy to use as reference. After the crystallization of hydrothermal required conditions, the microporous crystals are filled with organic structurizing agents (templates), water and other cationic or anionic molecular species. Negative electronic charges of the framework anions are balanced by the positive charges of organic and/or inorganic cations that are encapsulated in the micropores. For mostly of $AlPO_4$ phases, the Al coordination has been indicated either by structure alteration based on XRD diffraction data or high resolution ^{27}Al solid state NMR. The as-synthesized $AlPO_4$ materials can be subdivided according to the Al coordination into (i) four-coordination $AlPO_4$s, (ii) $AlPO_4$-hydrates, (iii) $AlPO_4$-hydroxides, (iv) $AlPO_4$-fluorides, and (v) $AlPO_4$-phosphate. It has to be highlighted that the Al coordination does not depend only on the nature of the organic structurizing agent that is encapsulated during the crystallization, but also an instrinsic property. The different Al coordinations are illustrated in **Figure 2.3**. In four coordinated $AlPO_4$s, all frameworks Al atoms are four-coordinated (Al^{IV}). In $AlPO_4$ hydrates, Al atoms at specific crystallographic framework positions are six-coordinated (Al^{VI}) and have two aqua ligands excluding the four oxogen bridges to framework P atoms. This type of aluminum is denoted as ‘aluminum dihydrate’. In $AlPO_4$-hydroxides, a number of specific Al atoms are five- or six-coordinated depending on whether these atoms are

linked either to one hydroxo ligand (Al^{VI}). Fluorine shows a similar chemistry in the coordination sphere of Al atoms of $AlPO_4$-fluorides. In $AlPO_4$-phosphates a phosphate anion not belonging to the framework is trapped in a systematic way in specific cages. The oxygens of these phosphate anions occupy a fifth coordination site of framework Al^V atoms. Whereas aqua ligands connect to one Al atom, hydroxo, fluoro and phosphate ligands are always connect to two Al atoms at least (**Figure 2.3**)

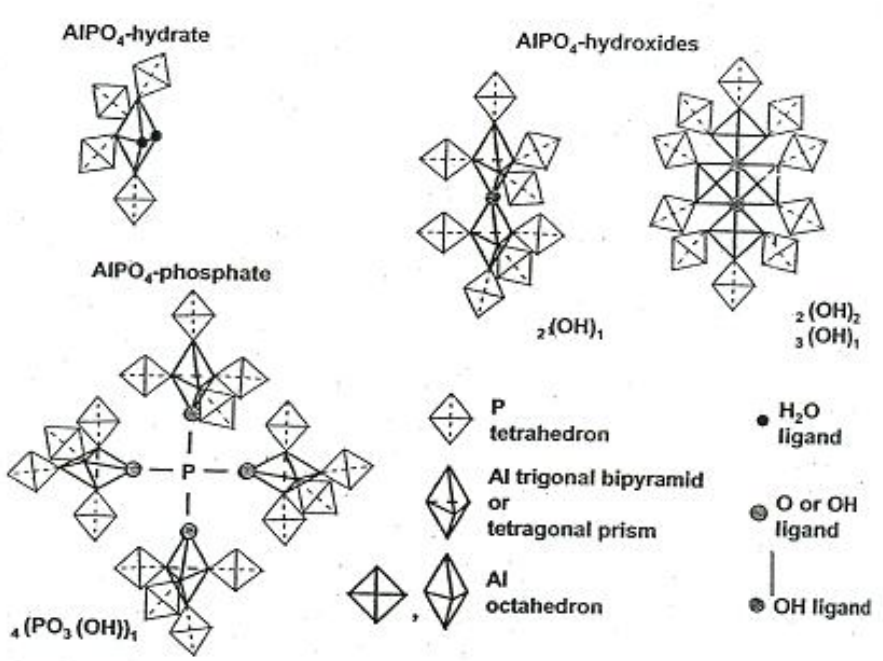

Figure 2.3 Al coordinations occurring in as-synthesized $AlPO_4$-hydrated, $AlPO_4$-hydroxides and $AlPO_4$-phosphates.

2.4.2 Rationalizaion of properties of poro-tecto-phosphates with structural, synthetic and physicochemical concepts

2.4.2.1 Isomorphic substitution

By definition, isomorphic substitution is similar to an additional element in a crystalline lattice by another element analogous cation radius and coordination requirements. Isomorphic substitution in $AlPO_4$s is currently achieved during crystallization by adding the element to be incorporated into the synthesis mixture. In poro-tecto-phosphates, many types of isomorphic substitution are possible. The complexity arises from the existence of two types of atoms, Al and P, which are both capable to substitute, and form the variety of coordinations of the framework Al atoms (IV, V, and VI).

The first $AlPO_4$-based materials reported in 1982 contained Al and P only. The additional of Si to the Al and P framework elements had been done in 1984 in the synthesis of silicoaluminophosphate (SAPO) molecular sieves. Later, in 1985 and 1986, microporous metal aluminophosphate with framework containing Mg, Mn, Fe, Co or Zn were successfully prepared, and the other element including Li, B, Be, Ti, Mn, Ga, and As was achieved to incorporate in the framework. Many possible framework elements in AlPO-based materials are still extending include, e.g. Cr, Ni, V and Sn. Moreover, there seems to be no upper limit to the number of elements that can be incorporated instantaneously. The synthesis of six different framework elements had been claimed.

For phosphates following the $AlPO_4$ idea or having alteration frameworks element with Al, or P , three mechanisms of isomorphic substitution have been claimed: substitutions of Al atoms (SM I), substitution of P atoms (SM II), and substitution of pairs of adjacent Al and P atoms (SM III) (**Figure 2.4**).

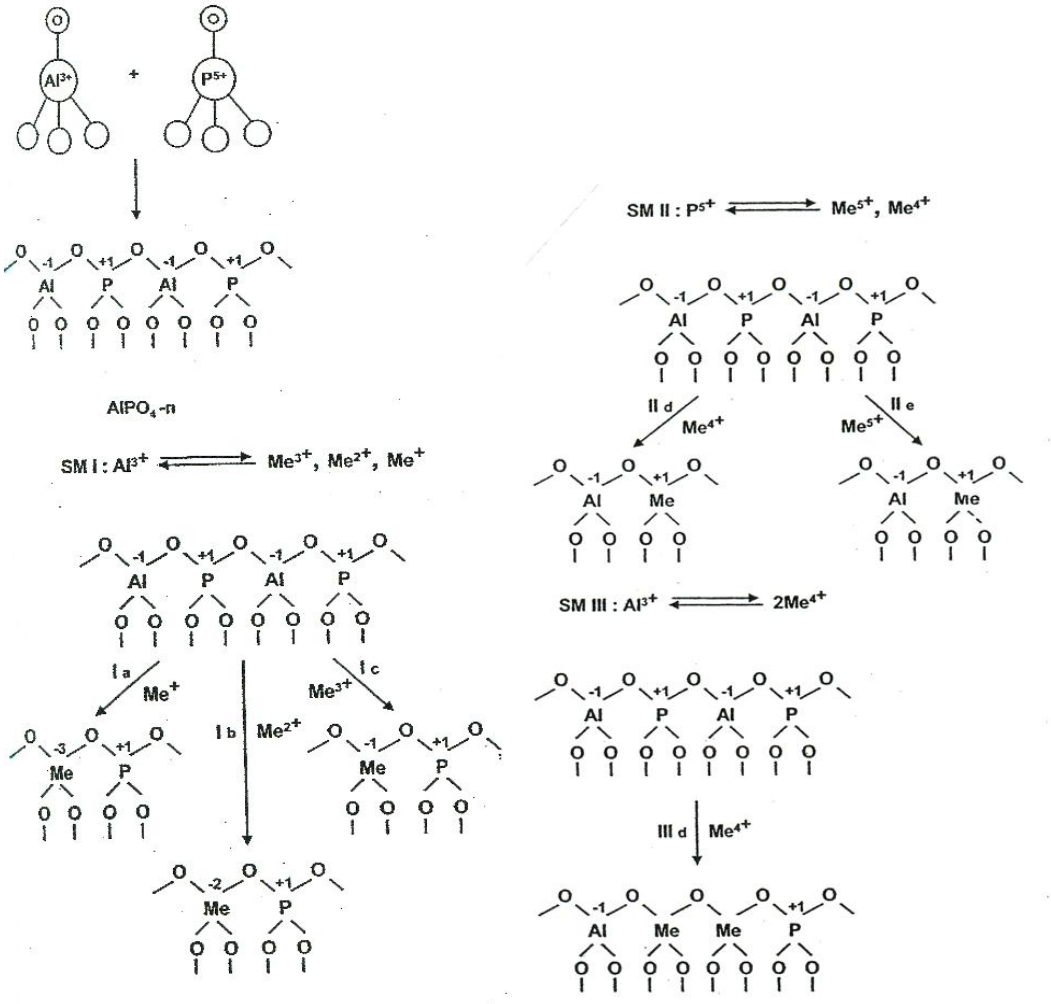

Figure 2.4 Isomorphic substitution mechanisms in $AlPO_4$ molecular sieves

Silica was observed in only SM III mechanisms. The SM I and SM II mechanisms can be separated according to the normal charge of the element substituted (**Figure 2.4**). Other types of substituted element not mentioned in **Figure 2.4** are not clear. They would lead either to positively charged frameworks or to a too high negative framework charge density.

2.4.2.2 Si incorporation according to SM III

Generating Si and AlP domains

Silicon is the only element showing SM III. The formation of framework charges could be avoided if we replaced thoroughly Al and P atoms with Si in a

certain segment of the crystal starting from the external surface. A transition form of an aluminophosphate with silicate compositional domain in an AFI type of framework is illustrated in **Figure 2.5**. The neutral of electron in the framework is generated, producing an $AlPO_4$ core (AlP domain) and topotactic SiO_2 overlayer(s) (Si domains). At the boundary of the two crystal domains, Si (3Si, 1Al) environments are present (**Figure 2.5**). It has to be emphasized that the framework charges must not necessarily be related with these Si environments.

SMIII usually occurs in four-coordinated $AlPO_4$s framework structure. In AEL frameworks, the general SM III mechanism has been considered mainly of the crystals with the high amount of Si (reach to 46% of the T atoms). In many SAPO materials, Si atom is incorporated according to a combination if SM IIa and SM III mechanisms.

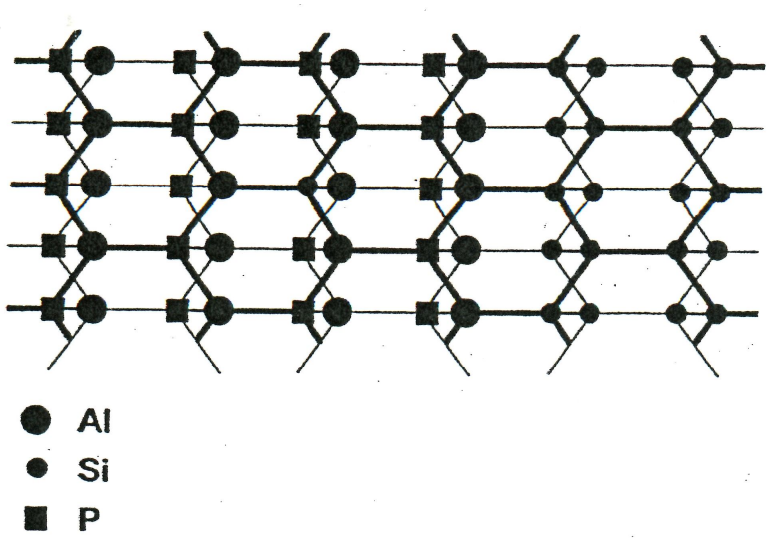

Figure 2.5 Example of heterogeneous framework composition in a silicoalumino-phosphate with AFI topology, generated through SM III substitutions

2.4.2.3 Si incorporation according to combinations of SM IIa and SM III

Generating SiAl and SiAlP domains

Most of SAPO materials have been reported based on a combination of the substitution of SM IIa and SM III mechanism. The combination of two types of

mechanism is possible for mostly Si domain. The silicoaluminophosphate compositions of the Si, Al, P ternary framework composition is presented in **Figure 2.6**. The chemical composition in individual SAPO crystals is varied. Some part of a SAPO crystal corresponds chemically to a silicate with SiO_2 composition (Si domain). This may happen where some Si atoms are replaced by Al atoms, thus generating negative framework charges in an aluminosilicate (SiAl domain). The other parts combining Al, P, and Si elements are generated by the SM IIa mechanisms, and contain isolated Si atoms having four Al neighbors in the framework (SiAlP domain).

The four-coordinated AlPO4s are subject to Si incorporation via a combination of SM IIa and SM III mechanisms. For instance, SAPO-5 crystals containing large layers of SiO_2 composition represents the oxide lattice up to 25%. At the surface of crystal the silicon is always concentrated.

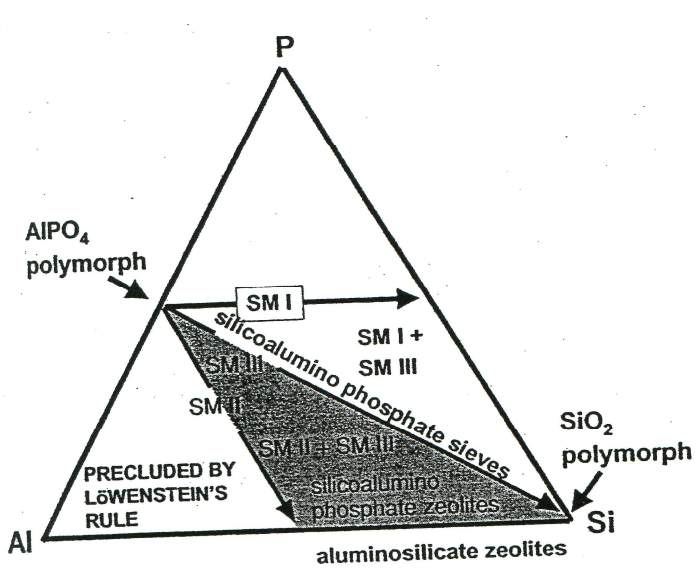

Figure 2.6 Si, Al, P composition diagram for silicoaluminophosphate zeolites and molecular sieves. Actually observed compositions are situated in the shaded area

Silicon incorporation according to SM IIa and SM III combination is also possible in some specific $AlPO_4$; SAPO-31 and SAPO-34, but the amount of silicon incorporated is lower.

From the mechanisms of Si incorporation in SAPOs, (the concept of Si incorporated in lattice is pointless in the catalytic activity performance). In SAPO crystals containing of Si or SiAl and SiAl and SiAlP domains, Bronsted acid sites are located in the SiAlP domains, in the SiAl domains and at the domain interfaces. It can be said that the catalytic performance of the different types of acid sites is strongly dependent on the structure type.

In SAPO-11 incorporated with pure SM III mechanism, the catalytic activity is a result of the location of acid sites at SiAlP-Si interfaces.

2.4.3 Framework type data **[13]**

SAPO-46 could be synthesized via several structure directing reagent, in this study di-propyamine (DPA) was used. SAPO-11 was generally synthesized by using DPA as the template. The material with the similar framework structure but different in the substituted element could have been referred with the similar framework type data as well due to the overall framework unit still present the similar XRD diffraction line. Therefore, in this study MAPSO-46 framework type was used as reference of SAPO-46. The framework type data of MAPSO-46 and SAPO-11 molecular sieves were showed below.

For SAPO-46

Crystal material data: $|(C_6H_{16}N)_8\ (H_2O)_{14}|\ [Mg_6Al_{22}P_{26}Si_2O_{112}]$

$(C_6H_{16}N)_8$ = dipropylammonium

Channels: [001] **12** 7.0×7.0* ↔ [001] **8** 4.0 × 4.0**

Idealized cell data: hexagonal, $P6_3/mcm$, $a = 13.1\,\text{Å}, c = 25.9\,\text{Å}$

Secondary building unit: 6*1

Composite building unit:

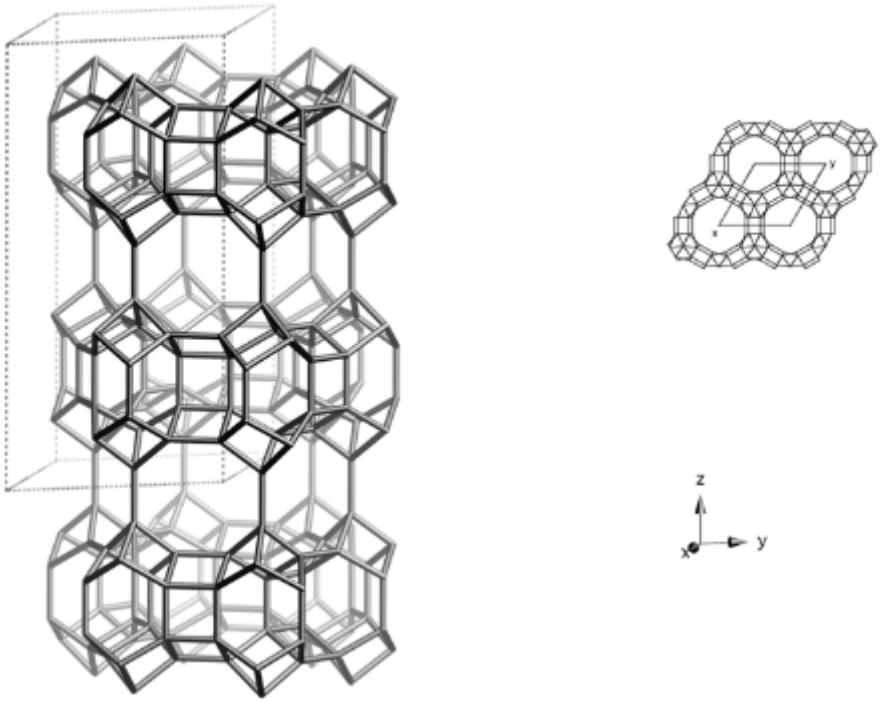

Figure 2.7 Framework viewed along [001] plane (upper right: projection down [001])

For SAPO-11

Crystal chemical data: $[Al_{20}P_{20}O_{80}]$

Orthorhombic, Ibm2, $a = 13.53\,\text{Å}, b = 18.42\,\text{Å}, c = 8.370\,\text{Å}$

(Relationship to unit cell of Framework Type: $a' = c, b' = b, c' = a$

Channels: [001] **10** 4.0 × 6.5*

Idealized cell data: orthorhombic, Imma, $a = 8.3\,\text{Å}, b = 18.7\,\text{Å}, 13.4\,\text{Å}$

Secondary building unit: 4-1

Composite building unit:

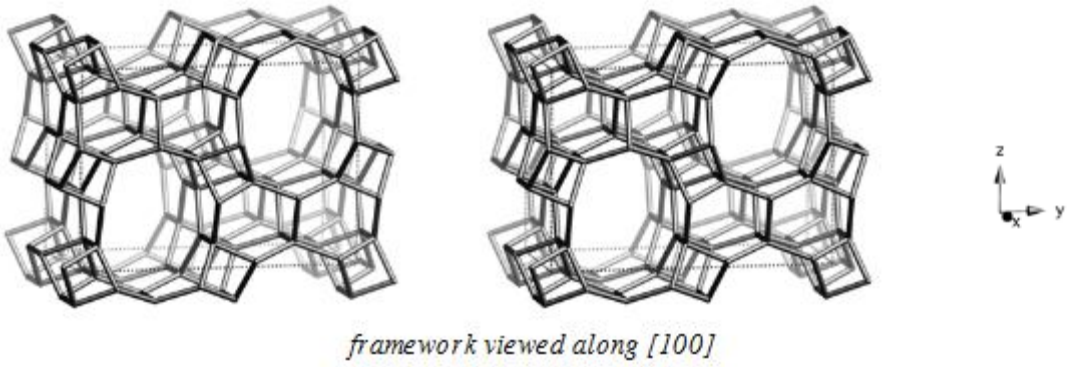

Figure 2.8 Framework viewed along [100] plane

2.5 Experimental design (2^k factorial design) [15]

P-Value in the hypothesis test

One way to report the hypothesis is to show weather the main hypothesis will be rejected or not at the value α which is normally been set at 0.05 or in other word to have 95% interval. The definition of P-value is the statistic test that has at least value as much or equal to the observation value when the main hypothesis is true which has been used as an evidence to reject the main hypothesis H_0. Furthermore, the other definition is the minimum significant value which leads to consider rejecting the main hypothesis H_0.

Generally, we usually consider the statistic test shows significant meaning when the main hypothesis is rejected; therefore, we might consider the P-value as the minimum α that can be acceptable.

Analysis of Variance (ANOVA)

In this section, it is about how to compare equal ability of the many mean values of the data set of the experiment. The ANOVA is one of the appropriate ways to conclude this kind of statistic. The ANOVA is divided into small part, so we get Total Corrected Sum of Square

$$SS_T = \sum_{i=1}^{a}\sum_{j=1}^{n}(y_{ij} - \bar{y}_{..})^2$$

For the overall level of variance of the data set, we should divided with them by the degree of freedom N-1 when N-1 is the amount of total data then we will get the example of variance of sample y

The total variance will collected from the Total Corrected Sum of Square which can be divided into the sum of square of different between mean value of each level and overall mean plus a summation of square of difference between the data and the mean of each set of data. The difference between the mean value of each data and the overall mean value can differentiate the difference between mean value of each set

of data whereas the difference between the data and the mean value of each set of data is the random error. We can write the equation as

$$SS_T = SS_{Treatment} + SS_E$$

When $SS_{Treatment}$ can be calculated from

$$SS_{Treatment} = n\sum_{i=1}^{a}(\bar{y}_{i.} - \bar{y}_{..})^2$$

The degree of freedom is a-1 and SS_E is the sum of square from the error, the degree of freedom is N-a. Mean square can be obtained from the sum of square divided by degree of freedom.

$$MS_{Treatment} = \frac{SS_{Treatment}}{a-1}$$

And

$$MS_E = \frac{SS_E}{a-1}$$

And we can find F_0 for doing the test of hypothesis by

$$F_0 = \frac{MS_{Treatment}}{MS_E}$$

We will rejectH_0 when $F_0 > F_{\alpha, \alpha\text{-}1, N\text{-}1}$ and conclude that it has difference between the mean value and data. In the contrast, when $F_0 < F_{\alpha, \alpha\text{-}1, N\text{-}1}$ means vise versa. That is no difference between the two mean values.

Coding

In order to evaluate the set of data by subtract with the overall mean value to obtain the smaller number which will normally line between 0 to 1 will make the analysis evaluated much more easier.

Factorial design

The factorial design is an effective way to design the set of experiment in case of having factors more than 2 parameters. The design of factorial will consider the sum of level of every parameters in the experiment. The design of factorial has benefited in many cases but has benefited the best point in reducing the number of experiment but still obtain the full significance of data.

2k factorial design

Factorial design has been used with the set of data that has many factors to study in order to study more on response that consequence from each effect. In case, it has k factors, each factor compose of 2 levels, high and low, with only 1 replicate, the overall number of set of experiment will be $2 \times 2 \times 2 \times 2 \times ... \times 2 = 2^k$. We call this design as 2^k factorial.

The general form of evaluating is

$$AB...K = \frac{2}{n2^k}(Contrast_{AB..K})$$

Then we will calculate the overall sum square of each evaluating

$$SS_{AB...K} = \frac{1}{n2^k}(Contrast_{AB...K})^2$$

When n represent the number of replicate. The last thing we have to do is put the all data in the ANOVA table; calculate F_0 or P-value then consider which effect has significant effect to the response. However, in order to obtain the right analysis, this 2^k factorial design still needs to analyze the residual if it has normal curve distribution.

Adding center point for 2^k factorial design

The main hypothesis we need to consider before using 2^k factorial design is about the Linearity of the graph. The 2^k design still work out when it is only the approximate Linearity analysis, but in fact if the term of interaction effect tend to be significant in First order model, there has another model that can responsible for the curvature surface in the response graph. This curvature occurred from the effect of interaction but however, in some case the curvature term does not adequate to determine the First order model. Therefore, the quadratic effect needed to be added in the Second order model.

In the 2^k factorial design, the First order model is more preferred but in some case we might find that the second order term seems more appropriate to fit with the data. In that case, some more replicate of the experiment need to be add in the 2^k factorial design to reassure the curvature term of the model. Moreover, this will help find the estimate error randomly. This method is made from adding center point to the 2k factorial design and we will repeat n_0 replicate at that center point. This adding the center point n_0 replicate to the design does not cause any change to the normal 2^k factorial design but only increase the more calculation. To find the summation of square for curvature term in pure quadratic with the degree of freedom equal 1 is

$$SS_{Pure\ quadratic} = \frac{n_F n_C (\bar{y}_F - \bar{y}_C)^2}{n_F + n_C}$$

When n is the number of experiment in the factorial design. The result from the calculation will be further calculated F_0 or P-value and analyzed. If the calculation from the quadratic term shows significant effect, it would need to add more

experiment to increase the level of parameter into the 2^k factorial design called Face Center Cube adding.

Regression model

Regression model has been used often in the unplanned experiment which might happen from collecting data of the uncontrolled variable or from the data in the past. Moreover, the regression model is still good for the planned experiment in case there has something wrong happen. The example of the regression model is

$$y = \beta_0 + \beta_1 X_1 + \beta_2 X_2 + \varepsilon$$

We will focus on how to create the regression model; let assume we have to create the model obtained from the experiment which will show the relationship between the viscosity of polymer, temperature, and catalyst feed rate. The model that will show this relationship is

$$y = \beta_0 + \beta_1 x_1 + \beta_2 x_2 + \varepsilon$$

When y is viscosity, x_1 is temperature, x_2 is catalyst feed rate

The regression model composes of two dependent factors which will be called Predicted Variable or Regressor. The term of Linearity has been introduced due to the linear function of unknown variable β_0, β_1 and β_2. If the model show more than two plane of x1 and x2, parameter β_0 will controlled intersect point of the planes. Sometime we call β_1 and β_2 as Partial Regression Coefficient due to β_1 will show the change of value y to one unit change of x_1 when x_2 is constant. And β_2 will show the change of value y to one unit change of x_2 when x_1 is constant.

Generally, the response y will contain k Predicted variable, which the model is

$$y = \beta_0 + \beta_1 x_1 + \beta_2 x_2 + \ldots + \beta_k x_k + \varepsilon$$

This equation called Multiple Linear Regression Model with k Regressor Variables and the parameter β_j, when j= 0, 1,…,k are called regression coefficient. This model

will represents hyperplane with k dimension of regression coefficient (x_i) parameter β_j represents change to value y to one unit change of x_1 when all left parameter x_i ($i \neq j$) is constant

For complicated model might be analyzed by the technique of Multiple Linear Regression Model. For example, consider model of case adding interaction term into the First order model that has two parameters

$$y = \beta_0 + \beta_1 x_1 + \beta_2 x_2 + \beta_{12} x_1 x_2 + \varepsilon$$

If we let $x_3 = x_1 x_2$ and $\beta_3 = \beta_{12}$,then the equation can be change to

$$y = \beta_0 + \beta_1 x_1 + \beta_2 x_2 + \beta_3 x_3 + \varepsilon$$

Which it is the Multiple Linear Regression Model with three regressors. Another example is Response surface model with two variables.

$$y = \beta_0 + \beta_1 x_1 + \beta_2 x_2 + \beta_{11} x_1^{\,2} + \beta_{22} x_2^{\,2} + \beta_{12} x_1 x_2 + \varepsilon$$

If we let $x_3 = x^2_1$, $x_4 = x^2_2$, $x_5 = x_1 x_2$, $\beta_3 = \beta_{11}$, $\beta_4 = \beta_{22}$ and $\beta_5 = \beta_{12}$ therefore, the equation will be

$$y = \beta_0 + \beta_1 x_1 + \beta_2 x_2 + \beta_3 x_3 + \beta_4 x_4 + \beta_5 x_5 + \varepsilon$$

Which that is the Linear regression. Normally, any regression model that has linear parameter will mean to the linear regression automatically without considering the shape of response surface.

Estimate parameter in Linear Regression Model

The least square method is normally been used in order to estimate the regression coefficient for Multiple Linear Regression Model. If n > k is the cause of

response variable that is y_1, y_2, …y_n. For any y_i there will have its involved regression variable.

In the least square method, we will select β in the equation in order to make the minimum summation of square of error. The least square function is

$$L = \sum_{i=1}^{n} \varepsilon_i^{\,2}$$

$$= \sum_{i=1}^{n} (y_i - \beta_0 - \sum_{j=1}^{k} \beta_j x_{ij})^2$$

It will be easier if we solve these equations in the form of matrix, therefore we will write these equations in the form of matrix that is

$$y = X\beta + \varepsilon$$

Where

$$y = \begin{bmatrix} y_1 \\ y_2 \\ . \\ . \\ . \\ y_n \end{bmatrix} \qquad X = \begin{bmatrix} 1 & x_{11} & x_{12} & \dots & x_{1k} \\ 1 & x_{21} & x_{22} & \dots & x_{2k} \\ . & . & . & & . \\ . & . & . & & . \\ . & . & . & & . \\ 1 & x_{n1} & x_{n2} & \dots & x_{nk} \end{bmatrix}$$

$$\beta = \begin{bmatrix} \beta_0 \\ \beta_1 \\ . \\ . \\ . \\ \beta_k \end{bmatrix} \quad \text{and} \qquad \varepsilon = \begin{bmatrix} \varepsilon_1 \\ \varepsilon_2 \\ . \\ . \\ . \\ \varepsilon_n \end{bmatrix}$$

Which can be simplify into

In order to solve it we have to multiply both side of the equation with the Inverse of $X'X$ therefore, we get the least square coefficient is

$$\hat{\beta} = (X'X)^{-1} X'y$$

The least square method can be solved to get the predicted value or fitted value, therefore this method is one easy way to analyze and evaluate the model. Moreover the residual of the model will be taken to analyze the precision of the model by many methods as similar to normal analysis of variance. The least square method can be applied to other calculations such as the summation of square term of any variable. Firstly, find the summation of total square term of the model then, test the least square coefficient one by one or can be analyzed in a group (reduce to amount of data to leave only sum square of unwanted variable). Calculate sum of square of the model and compare between the sum of square terms we obtained. Finally we will get the sum of square term we needed.

2.6 Literature review

MTO process and SAPO catalysts [16]

The work studied about silicoaluminoaliminophosphates (SAPO) in the methanol to olefin process. SAPO-34 and SAPO-41 exhibited almost 100% of methanol conversion (MTO process) and showed a good selectivity to light olefin (propene and ethane) at the reaction temperature 723 K (450°C) and maintained it until 10 h. The Bronsted acid site was determined by H MAS NMR spectroscopy technique, this technique was used to determine the type and number of OH group including the studying after loading ammonia to determine the amount of acid sites. The obstruct particles on the catalyst surface after the reaction were characterized by several techniques, UV/vis spectroscopy, thermogravimetry-differential thermal analysis (TG-DTA), and gas chromatography-mass spectrometry (GC-MS). The effects of Bronsted acid sites and framework structures played an important role on the catalytic performance of SAPO in the MTO process. The amount of Bronsted acid sites affected the adsorption of methanol and the formation of hydrocarbon pool compound as well as the catalyst deactivation. Besides, the framework structures of SAPO also affected the influenced diffusion product and consequently affected the product selectivity of MTO process.

In the past, light olefin was produced by thermal cracking or catalytic cracking of crude oil. But the crude oil price is being unpredictable; therefore, the interesting of alternative way to produce oil is gained increasingly. The MTO reaction consist of methanol dehydrated to dimethyl ether (DME), the equilibrium of methanol, DME, and water to convert to light olefin. The light olefins further react to paraffins, aromatic, naphthenes, and higher olefins via hydrogen transfer—alkylation and poly condensation.The accepted mechanism is "hydrocarbon pool" that is a group of large olefin compounds and cyclic organic species in the cages of SAPO—microporous solid acid. The reactants, methanol and DME, were fed to these hydrocarbon pool, whereas the olefins were formed and leaved out the channel. The acidity and framework structure were two key factors controlling the catalytic performance. SAPO-34 has moderate Bronsted acid sites and 8-ring window framework structure which was reported the good catalyst and exhibited the maximum conversion to 80%.

The polyalkylaromatics found inside the cage of SAPO-34 were reported the most active hydrocarbon pool compound (diameter of 9.4Å) causing the formation of light olefin on the Bronsted acid sites. The 8-ring windows (diameter of 3.8 Å) restricted the heavy hydrocarbon and branch hydrocarbon to enter the pore; therefore, bring to the high selectivity of light olefins. Because of its moderate acid sites, SAPO-34 showed the better resistance to coking and resulted in long-lifetime in MTO process. SAPO-11 is the one-dimensional pore system with no cage. And it has been reported not a good catalyst for MTO process. SAPO-34 and SAPD-46 have structure with cages while, SAPO-11 and SAPO-41 have the one-dimensional 10-ring systems.

This study focused on relationship between framework structure and catalytic performance (selectivity and deactivation), type and number of Bronsted acid sites, methanol adsorption capacity and pore structure of zeolite.

Methyl halide to olefins and gasolines over zeolites and SAPO catalysts [4]

As an alternative way for MTO or MTG process with syngas as the intermediate, the process of natural gas-methyl halide-higher hydrocarbons, with methyl halide as the intermediate, gave a new and promising route for the natural gas

utilization. Many MTG catalysts were also employed as the catalyst and promising results have been obtained in the production of hydrocarbons in gasoline range from methyl halides. The application of SAPO molecular sieves made the light olefins production from the conversion of methyl halide a very potential way. Chloromethane could be very selectively transferred to light olefins, especially ethylene and propylene, under a mild condition over SAPO-34 catalyst.

Some mechanisms for methyl halide conversion to higher hydrocarbons were proposed based on different catalysts. Some studies suggested that methyl halide conversion over zeolite catalysts started from framework-bound methoxy species and the key step of C-C bond formation was related with a carbide species, while some study of methyl chloride conversion over SAPO-34 presented that the conversion went through an induction period in which cyclic organic reaction center formed and the C-C bond formation from C_1-reactants follow an indirect reaction route. Hydrocarbon pool mechanism which has been proposed for methanol conversion was employed in the explanation of methyl halide conversion to hydrocarbons.

Influence of solid acid catalyst on DME production [6]

This research studied on the effect of various kinds of SAPOs in methanol dehydration (from methanol) and STD (from syn gas). They studied on various types of SAPOs; SAPO-5, SAPO-11, SAPO-18, and SAPO-34. They concluded that the structure of SAPO-34, and SAPO-18 played an important role on the stability of the catalyst, the strong acidity of SAPO-34 and SAPO-18 is the cause of a lot of blockage coke in the pore of SAPOs. And SAPO-34 and SAPO-18 themselves were known for having strong acid strength (as also seeing from NH_3 TPD results). The XRD of spent catalyst confirms this idea. They also examined these catalysts by TGA analysis and the result was in accordance with those from XRD analysis. SAPO-34 was found the most instability catalyst in this research.

This research studied the effect of solid acid catalyst on the catalytic performance of direct DME synthesis. SAPO-5,-11, 18 and -34 were selected for

methanol dehydration. SAPO-18 and-34 showed rapidly deactivation due to the formation of coke inside the pore. In contrast SAPO-5 and -11 showed lower activity but higher stability. They concluded that this stability contributed to the mild acid sites and desirable pore structure. And they also studied direct DME synthesis from syngas, the admixed catalysts were prepared from $Cu/ZnO/Al_2O_3$ and various SAPO catalysts. Those admixed catalysts showed different catalytic activities in direct DME synthesis when compared with the SAPO catalysts in methanol dehydration. The results showed that the admixed SAPO-5 and -11 had better catalytic stability than the others admixed catalysts. Therefore they suggested that the stability of solid catalyst is an importance factor to determine catalytic performance in the reaction.

Catalytic dehydration of methanol to dimethyl ether over AlPOs and SAPO [17]

A series of aluminophosphate and silico-aluminophosphate AlPO-5, ALPO-11, AlPO-41, SAPO-5, SPAO-11, and SAPO-41 were synthesized and tested for their catalytic performance in methanol dehydration. The SAPO-11 showed the best performance among the others with the DME yield of 84.1% and selectivity of 100% at 250°C. The effects of reaction temperature. From NH_3-TPD, similar desorption peak at around 170°C appeared corresponding to the Lewis acid sites for aluminophosphates. For silico-aluminophosphates, two similar desorption peaks were observed at around 170°C corresponding to mild acid sites and at around 300°C corresponding to moderate acid sites. They suggested that addition of silica atoms into the framework structure not only lead to existence of moderate acid but also increasing the amount of mild acid sites. The amount of moderate acid sites was similar among SAPO-5, SAPO-11, and SAPO-41. For silico-aluminophosphate SAPO-5, SAPO-11, and SAPO-41, the methanol conversion increased while increasing reaction temperature but DME selectivity decreased. Especially, the high DME yield of 84% was achieved at reaction temperature of 250°C. For aluminophosphate AlPO-5, AlPO-11, and AlPO-41, DME was the main product in every reaction temperature and the large amount of DME yield (higher than 80%) was achieved at reaction temperature of 350°C. They suggested that AlPO-5, AlPO-11, AlPO-41, and SAPO-11 were the promising catalyst for methanol dehydration. From

TG-DTA analysis, the main reason of deactivation of catalyst was the formation of coking. The weight lost at lower 200°C corresponding to endothermic peaks in DTA curves and was attributed to desorption of weakly adsorbed water or organic molecule. The weight lost at higher 400°C corresponding to exothermic peaks in DTA curves and was attributed to the combustion of blocked organic materials in molecular sieves. For aluminophosphate series, only weakly adsorbed molecules were detected indicating that coke materials should not be formed during the reaction for AlPO-5, AlPO-11, and AlPO-41 catalysts. Whereas blocked organic materials were detected in silico-aluminophosphate series, SAPO-5, SAPO-11, and SAPO-41 which was resulted from presence of moderate acid sites in acid catalysts. The amount of coke related to the amount of moderate acid site in acid catalysts.

They claimed that the one dimensional pore structure allows small molecules to easily diffuse to acid sites. At high reaction temperature, moderate acid sites in silico-aluminophosphate series boosted up the side reactions leading to lower DME yield.

Study on the thermal stability of Bronsted acid sites in SAPOs [18]

The thermal stability and dehydroxylation of the microporous silicoaluminophosphates SAPO-11, SAPO-18, SAPO-31, and SAPO-34 were investigated after thermal treatment at temperatures of 773–1173 K. There was no change of the crystallinity upon thermal treatment at 1173K found by X-ray diffraction. The ^{27}Al and ^{29}Si MAS NMR spectroscopy showed the dehydroxylation is not accompanied by a dealumination but rather by a removal of silicon (desilication) in the local structures of the former bridging OH groups. The dehydroxylation and desilication of the silicoaluminophosphate framework do not lead to the formation of defectable OH groups as evidenced by ^{1}H MAS NMR spectroscopy.

Kinetic study on methanol synthesis [10, 19]

They studied the kinetic model of methanol synthesis with focusing on the effect of CO_2 fraction as a function of temperature in order to find the optimization of methanol synthesis. A mathematical model of the bench-scale reactor for the synthesis

of methanol over $Cu/ZnO/Al_2O_3/ZrO_2$ catalyst is developed. Several optimizations are suggested to maximize the methanol yield. The trajectory for wall temperature along the reactor axis as well as the optimal CO_2 fraction at the inlet of the reactor is found to be the best strategy in the sense of methanol production per unit amount of feed. The optimization strategy also considers on the variation of reactor in the reactor and synergetic effect on the production rate.

Moreover, kinetic parameters estimation shows that the combination of the surface reaction of a methoxy species, the hydrogenation of a formate intermediate HCO_2, and the formation of a formate intermediate for CO and CO_2 hydrogenations and WGS reaction, respectively, is the best to fit the model.

DME synthesis on CuZnAl catalyst [20]

The results of this study revealed that at the typical syngas-to-DME reaction temperature (260 ◦C) the zeolite dehydration activity (derived from independent methanol dehydration experiments) was mostly determined by the density of strong Brønsted acid sites with a non-negligible contribution of EFAL-related strong Lewis acid sites (if present in the zeolite). The same conclusion hold true for the syngas-to-DME process when the overall reaction becomes controlled by the methanol dehydration step, that is, when using CZA/ZSM-5 hybrid catalysts with a low zeolite concentration.

The effect of zeolite particle size of Mo/HZSM-5 [21]

The effect of the particle size of HZSM-5 on the activity of Mo/HZSM-5 in the non-oxidative CH_4 dehydroaromatization was studied. The crystalline parent HZSM-5 of an average particle size of 4 μm and four ball-milled samples with their average particle sizes being 1.9, 1.0, 0.5 and 0.2μm were prepared and loaded with Mo using conventional impregnation method. The crystallinity and Bronstead acidity of the ball-milled sample became lower and lower as the average particle size of zeolite decreased in the range of <1.9 μm. This reason resulted in undispersed of Mo

particle on the 1.0, 0.5 and 0.2 of the ball-milled zeolite lead to low activities in CH_4 dehydroaromatization.

Using surfactant to control morphology and mesoporosity of SAPOs [22]

This synthesis method used surfactant to control the mesoporosity and morphology of silicoaluminophosphates using designed templates with silicon or phosphorus head groups. The result showed that crystalline silicoaluminophosphates with different structure and morphology could be synthesized by using different surfactants, Cab-osil, $C_{12}H_{25}OPO(OH)_2$ and silylated polymer. All the as-synthesized presented the crystalline structure

Influence of template on Si distribution on SAPO11 [23]

SAPO-11 was synthesized by using several structure directing agents such as diethylamine (DEA), di-iso-propylamine (DIPA) and di-n-propylamine (DPA) or a mixture of DEA and DIPA (named DEPA). The as-synthesized SAPO-11 zeolites showed different physico-chemical properties. SAPO-11 synthesized with DEPA as template showed high crystallinity compared with other samples and was free from phase impurity. The ^{29}Si MAS NMR showed that the SAPO-11 synthesized with the mixed template was better than the single template, leading to a better Si distribution and increased number of acid sites. For the isomerization reaction, the as-synthesized SAPO-11 with DPA showed the best catalytic activity.

The synthesize of micro-mesoporous silicoaluminophosphate (MUS-5) [24]

The MUS-5 had been first synthesized with controlled morphology in a two-step process. They studied the effect of the pH of the solution system varied in the range of 2.0 to 5.0. The different morphologies were obtained i.e. chain-like, flower-like and barrel-like. These novel morphologies have a strong correlation with the pH

value of the solution system. The performance of the cracking 1,3,5-triisopropylbenzene heavy aromatics exhibited a better catalytic activity with using the MUS-5 catalyst rather than the conventional SAPO-5. The author proposed the reaction process of TIPB over SAPO-5 and MUS-5 catalysts.

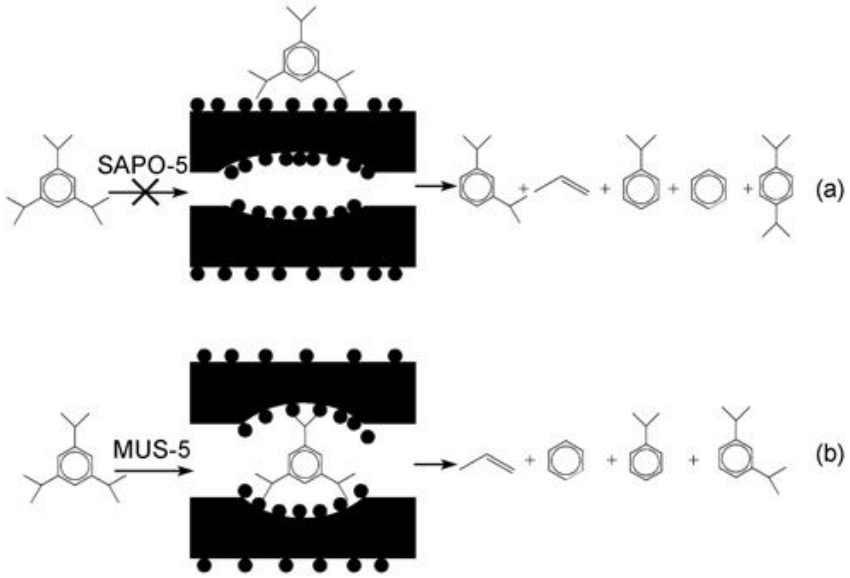

Figure 2.9 Demonstration inside pore channel of SAPO-5 and modified MUS-5

Methanol to olefin conversion catalysts [25]

The methanol to olefin (MTO) process is becoming more popular compared with the other gas utilization processes or naphtha cracking processes. This paper reviewed about the SAPO catalysts used in MTO process for instance; Ni-SAPO-34, MeAPO-5 (Me = Co, Mn, Mg, Zn, Ni, Cr, Zr) catalysts, CoSAPO-34. The experimental results indicated that the Si precursor take part in the crystalline of Si in the first stage (< 2.5 h) with isolated Si(4Al) and obtained great crystallinity. Whereby Si(3Al), Si(2Al), Si(1Al) and Si(0Al) appeared at the later stage. This results implied that the fast crystallization take advantage to SAPO-34 catalyst led to the good catalytic performance. The mechanism involved with methanol to olefin is C-C bonds. Methanol adsorption on the surface of the catalyst should be the first step for reaction. There are two main mechanisms suggested, the first one, consecutive-type

mechanism: ethylene is be first formed in the reaction. The second one, olefin occurs through a carbonaceous species.

Study of the interaction between components in hybrid CuZnAl/HZSM-5 [26]

In this study, the hybrid CuZnAl(CZA)/HZSM-5 catalysts were prepared in order to investigate interactions between components and their impact in the STD process. The three mixing methods were studied; (a) grinding of powders prior to pelletizing (grinding method), (b) slurrying the two solids in water followed by drying and pelletizing (slurry method), and (c) physical mixing of pre-pelletized components. The CZA/HZ hybrids prepared by grinding and slurrying together the respective component powders leading to detrimental interactions between the components that significantly reduced their efficiency for the STD reaction as compared to hybrids obtained by a simple physical mixture of the individual pellets and thus having no chance for interactions.

Surface acidity and the dehydration of methanol to dimethyl ether [27]

The $Ti(SO_4)_2$ has been modified on γ-Al_2O_3 and the result suggested that its presence of sulfur may prevent its use as an acidic catalyst with $Cu/ZnO/Al_2O_3$ for the STD synthesis rather than the use of $Cu/ZnO/Al_2O_3$ with other acidic catalysts which is sensitive to sulfur poison. And this study has been used HZSM-5 and steam de-aluminated H-Y zeolite (SDY) zeolites possess strong Bronsted acidity for methanol dehydration to DME synthesis. However, these catalysts catalyzed high methanol to DME conversion and also coke. In contrast, the γ-Al_2O_3 possessed strong Lewis acidity, showed lower catalytic activity of methanol dehydration. Therefore the modification of Ti $(SO_4)_2$ on γ-Al_2O_3 enhanced the amount of surface Bronsted acidity.

STD synthesis over rare earth modified zeolite-Y [28]

A series of zeolite Y modified with La, Ce, Pr, Nd, Sm and Eu were prepared via ion-exchange method. The reaction were performed in a fixed bed reactor at 245° C, 2.0 MPa, $H_2/CO = 3/2$ and 1500 h^{-1}. They claimed that these rare earth metals were encapsulated in the supercage of zeolite Y and resulted in its enhanced acidity. Among these rare earth, La, Ce, Pr, and Nd were found enhancing the catalytic activity and stability rather than only pure zeolite-Y for the step of methanol dehydration to DME. For the methanol synthesis catalyst, they had modified by adding Mn in Cu/ZnO catalyst and combined with modified zeolite-Y. The results found that the Cu–Mn–Zn/La–Y and Cu–Mn–Zn/Ce–Y catalysts were more active than Cu–Mn–Zn/pure-HY. Moreover, they had written about the moderate acid strength of these dual catalysts had that affected the activity of STD synthesis.

Effect of precursor to AlPOs synthesis on methanol dehydration [29]

The aluminium phosphates (Al/P = 1) were prepared with various types of precursors. Those catalysts were tested in methanol dehydration to DME. They claimed that the crystalline phases (α-crystobalite and berlinite) are inactive for the dehydration reaction and only amorphous $AlPO_4$ seems to be active in catalyzing the dehydration of methanol to DME. Therefore the preparation method is very important to the morphology and properties of aluminium phosphate which led to a difference in catalytic activity. They concluded that the introduction of phosphate ion prior to the hydrolysis of aluminum salt by ammonia is a way to prepare the suitable methanol dehydration catalyst.

Effect of acid properties on STD on Cu-Zn-Ga catalyst [30]

The various acid catalysts were examined on STD synthesis. The activity of Lewis acid sites was depressed by adsorbed water. Therefore, Brønsted acid–Lewis base pair sites became the major active sites for the dehydration of methanol in the

STD process. The silica-rich silica-alumina catalyst was the most favorable STD catalyst with showed high DME yield (55%) along with a good selectivity (93.5%). The water adsorbed on Lewis acid sites suppressed DME formation in the mean while the catalyst with Brønsted acid site with moderate strength was the promising catalyst for STD synthesis. And the modification of methanol synthesis catalyst with Pd enhanced the catalytic activity.

The capsule catalyst study of three-component capsule catalyst [31]

The Pd modified Co/Al_2O_3-H-beta capsule catalyst was prepared by hydrothermal synthesis method and used in isoparaffin direct synthesis via FTS reaction. The results showed that the olefins were mostly converted to isoparaffins by in-situ hydrogenation on the Pd modified Co/Al_2O_3-H-beta capsule catalyst with C_{iso}/C_n 0.96. The Co/Al_2O_3 capsule catalyst and the core Co/Al_2O_3 were prepared as reference as well. The ratio of C_{iso}/C_n of these catalyst were decreased in order Pd-Co/Al_2O_3-H-Beta > Co/Al_2O_3-H-Beta > Co/Al_2O_3.

Kinetic study of methanol dehydration using Clinoptilolite zeolite [32]

The kinetic study of methanol dehydration to dimethyl ether been have studied on the dimethyl ether synthesis for the bubbling fluidized bed reactor. They investigated the effects of operating parameters such as partial pressure of methanol, temperature, superficial gas velocity, and catalyst particle size on the dehydration of methanol reaction. The Langmuir-Hinshelwood mechanism was considered for the reaction. They purposed the reaction mechanism, the relation and the rate expression, including calculated rate constant and methanol equilibrium constant. They designed the optimum operating parameters and studied the response of each on the reaction by using Taguchi experimental design method and composed an L9 ANOVA table in an analysis of 4 factors with 3 levels. They suggested that the particle size and superficial gas velocity have great effects on hydrodynamic behavior of fluidized bed reactor, while the methanol partial pressure and temperature have both effects on

hydrodynamic behavior and reaction kinetics. In brief, the optimum operating temperature was 350°C, the increasing of temperature may promote the side reaction and sintering of the catalyst. The increasing of methanol partial pressure enhanced the rate of DME. The increasing of gas velocity affected the shorter residence time within the reactor, resulting in a bad effect on the reaction.

Design and development of Cu-Zn catalyst using artificial neural network [33]

The design and development of Cu/ZnO in the hybrid catalyst mixed with γ-alumina were studied with an artificial neural network (ANN) in order to find the effective additives for Cu/ZnO in the hybrid for STD synthesis. Eight elements (X) i.e. B, K, Nb, Re, Cd, Ce, Sm, and Tl were selected. These elements were selected in the wide range of physicochemical properties. The activities of Cu/ZnO-X + γ-alumina hybrid catalyst and the physicochemical properties of the eight elements were used as training data for ANN. The trained ANN predicted the promising additives Al, Ti, V, and Nb. They optimized the design by using design of experiment (DOE), ANN, and a grid search, the composition of heptarnary oxide catalyst. The catalyst was confirmed to be an active and stable catalyst with the final long run. The catalyst with the optimized composition showed stable and high activity. And with the assistance of DOE, the number of experiments was reduced.

CHAPTER III

EXPERIMENTAL

This chapter consists of experimental procedures and analytical technique used in this study which is divided to four main parts including the aluminophosphate and silicoaluminophosphate synthesis procedure, the catalyst preparation, the catalytic performance test, and the design experiment of 2^k factorial.

The first part (section 3.1) is described on preparation of molecular sieve such as $AlPO_4$-5, $AlPO_4$-11, SAPO-11, SAPO-46 by hydrothermal synthesis. The preparation of capsule catalyst by new method named physical coating method and also including the mixed catalyst preparation. The second part (section 3.2) explained the catalyst performance test of STD synthesis. The third part (section 3.3) is explained about the catalyst characterization that had been used in this study such as X-ray diffractometer (XRD), energy dispersive X-ray spectroscopy (EDX), scanning electron microscopy and energy dispersive spectroscopy (SEM&EDS), N_2 adsorption-desorption measurement, temperature program desorption of NH_3 (NH_3-TPD)

3.1 Chemical Materials

The details of chemical sources for as-synthesized aluminophosphate ($AlPO_4$) and silicoaluminophisphate (SAPO) molecular sieves are shown in the Table 3.1.

Table 3.1 Chemical sources and reactants used in preparation of catalysts

Source	Chemical
Structure directing agent	Di-n-propylamine (n-DPA, 99% from Sigma-ALDRICH)
	TEA (Triethylamine)

Table 3.1 Chemical sources and reactants used in preparation of catalysts (Cont.)

Source	Chemical
Phosphorous	Phosphoric acid (H_3PO_4, 85% from Chameleon reagent)
Al_2O_3	Aluminium isopropoxide (from ALDRICH)
SiO_2	Silica sol LUDOX 40 wt%.(from ALDRICH)
$Cr(NO_3)_3.9H_2O$	Chromium nitrate (from Kanto Chemical)
$Cu(NO_3)_2.3H_2O$	Cupper nitrate (from Kanto Chemical)
$Zn(NO_3)_2.6H_2O$	Zinc nitrate (from Kanto Chemical)
$Al(NO_3)_3.9H_2O$	Aluminium nitrate (from Kanto Chemical)
$H_2C_2O_4$	Oxalic acid (from Kanto Chemical)
C_2H_5OH	Dehydrated ethanol (99.5%)
NaOH	Sodium hydroxide

3.2 Aluminophosphate and silicoaluminophosphate preparation

Aluminophosphate and silicoaluminophosphate can be synthesized by hydrothermal synthesis method. For SAPO-11, it was prepared in the molar composition of $1.2Al_2O_3$: $3.0H_3PO_4$: $0.6SiO_2$: 2.0 Di-n-propylamine: $100H_2O$. The dilution of solid H_3PO_4 (85%, Chemerion Reagent) was added slowly over the solid aluminium isopropoxide (99%, Sigma-Aldrich) and keep stirring for 2 h until it becomes homogenous white solution. The certain amount of di-n-propylamine (DPA) was added slowly into the mixture under vigorous continuous stirring for 3 h. Finally, the dilute silica sol was added slowly to the mixture under vigorous stirring and continued for 6 h. The obtained mixture was transferred to a Teflon container with a stainless steel autoclave and placed into the hydrothermal unit (DRM-420DA, Hiro Company, Japan) at 453 K for 48 h. After crystallization, the product was separated from the precursor solution by centrifuge, dried at 393 K overnight and treated by

calcination in a muffle oven at the constant heating rate rise (2 K /min) from room temperature to 773 K and hold for 2 h to eliminate the template residual. For SAPO-46, the similar procedure was used, but the gel composition and conditions was prepared in different formula and aging time, and temperature. For $AlPO_4$-5, Triethylamine (TEA) was used as the template. For $AlPO_4$-11, n-DPA was used as the template. The synthesis procedures are as similar as above.

Table3.2 Gel composition and synthesis conditions of AlPOs and SAPOs

Sample	**Gel composition**	**Temperature (°C)**	**Time (h)**
$AlPO_4$-5	$1.2Al_2O_3$: $3H_3PO_4$: 1TEA: $100H_2O$	180	48
$AlPO_4$-11	$1.2Al_2O_3$: $3H_3PO_4$: 1DPA: $100H_2O$	180	48
SAPO-11	$1.2Al_2O_3$: $3H_3PO_4$: $0.6SiO_2$: 2DPA: $100H_2O$	180	48
SAPO-46	$1.2Al_2O_3$: $3H_3PO_4$: $0.6SiO_2$: 4DPA: $100H_2O$	180	144

Figure 3.1 Hydrothermal unit apparatus

3.3 Core catalyst preparation

3.3.1 Cr/ZnO catalyst preparation

The Cr/ZnO catalyst (Cr:Zn = 1:2 in molar) was prepared by the co-precipitation method as in the literature [34]. Aqueous solutions of Cr $(NO_3)_3 \cdot 9H_2O$ 0.01 mol and $Zn(NO_3)_2 \cdot 6H_2O$ 0.02 mol were first mixed in 200 ml distilled water. Aqueous solution 100 mL of NaOH solution 1M was added slowly into the mixed metal nitrate solution under continuous stirring at 273 K for 2 h. The mixture solution was kept aging for 30 minutes under the same condition before moved and sealed in the Teflon lined container and placed in the hydrothermal synthesis unit (DRM-420DA, Hiro Company) at 393 K for10 h. After the hydrothermal treatment, the precipitate was washed with a lot of deionized water to eliminate the Na^+ residuals, dried in the oven at 393 K overnight and treated with calcination at 773 K for 2 h in sequence. The

calcined catalyst was pressurized and crashed into the granule size of 0.85-1.7mm before loading into the reactor. The catalyst was named as Cr/ZnO.

3.3.2 CuZnAl catalyst preparation

The $Cu/ZnO/Al_2O_3$ catalysts, the tricomponent of Cu, Zn, and Al was prepared by the conventional oxalate coprecipitation method [35, 36]. The mixed nitrates of copper, zinc, and aluminum and 20% excess oxalic acid were dissolved with ethanol. Two solutions were mixed rapidly at room temperature under vigorous stirring. The gel-like precipitates were formed and aged at room temperature for 24 h. After aging the precipitated powder was separated by centrifuge, dried at 393 K for 6 h and followed by calcination in muffle oven at 643 K for 1 h. Consequently, the catalyst was pressurized and ground into the pellet size of 0.85 - 1.70 mm. The sample was named as CuZnAl catalyst, was used in methanol synthesis under low temperature synthesis.

3.4 Physical coating catalyst preparation

The granule pellet core catalyst the size range of 0.85- 1.7 mm was used to coat zeolite powder onto it by a simple method. The solution silica sol (Ludox 40wt% suspension, Aldrich) was diluted with deionize water in the weight ratio of 1:1.5. The core catalyst pellet was soaked by using the diluted solution of silica and then put zeolite powder onto it, shake it in the round-bottom flask till it form the uniform layer outside the core. Finally, the whole catalyst was treated by calcination in a muffle furnace at the temperature of 500 °C for 2 h.

Table 3.3 The details of experiment set up for capsule catalyst.

Sample	Weight increment (%)	Core catalyst	Membrane
Cr/ZnO/SAPO46	< 5	Cr/ZnO	SAPO-46
CuZnAl/SAPO11	~ 20	CuZnAl	SAPO-11

3.5 Mixed catalyst preparation

The conventional mixed catalyst of two kinds of catalyst were mixed mechanically by blending together in the calculated weight ratio. Then it will be pressed at 60 MPa, ground into the desired range of size 0.85-1.7 mm.

Table 3.4 Summary of catalyst preparation of mixed catalyst

Sample	Weight ratio	Studying
Cr/ZnO: SAPO-46	10:1	Capsule catalyst
CuZnAl: SAPO-11	10:2	Capsule catalyst
Cr/ZnO: SAPO-11	10:1	2k factorial design
	10:5	2k factorial design
	10:9	2k factorial design
Cr/ZnO: $AlPO_4$-5	10:2	Various zeolite
Cr/ZnO/$AlPO_4$-11	10:2	Various zeolite

3.6 Characterization techniques

3.6.1 X-ray diffraction (XRD)

XRD was performed to determine the bulk crystalline phases of the sample and also used as fingerprint of the substance to identify them. XRD was conducted using a Ringaku RINT 2400 X-ray powder diffractometer equipped with CuK_α radiation (λ = 0.15406 nm) source at 40 KV and 40 mA.

Figure 3.2 XRD diffractometer unit; a Ringaku RINT 2400 X-ray powder diffractometer equipped with CuK_{α} radiation

3.6.2 Energy dispersive X-ray spectroscopy and scanning electron microscopy

An independent energy dispersive X-ray spectroscopy (EDX, SHIMADZU Rayny EDX-700) was employed to determine the elemental composition of the synthesized SAPO-46 molecular seive. Additionally, the morphologies and elemental composition of core catalyst Cr/ZnO and capsule catalyst were analyzed by another scanning electron microscopy (SEM, JEOL JSM-6360LV) equipped with an energy dispersive X-ray spectroscopy analysis (EDS, JED-2300). Before analysis, the samples were firstly coated a platinum layer by using an auto fine coater (JEOL, JFC-1600).

Figure 3.3 Elemental analysis unit; a) an EDX, SHIMADZU Rayny EDX-700, b) an SEM (JEOL JSM-6360LV) equipped with an EDS analysis (EDS, JED-2300)

3.6.3 N_2 physisorption

The surface area, pore volume and pore diameter of catalysts were measured by an Autosorb-1 (Quantachrome, Japan), the automatic gas adsorption system by N_2 adsorption. Before analysis, the samples were degassed at 573 K for 4 h.

Figure 3.4 An Autosorb-1 (Quantachrome) N_2 adsorption unit

3.6.4 TPD-NH_3

The desorption of NH_3 is used to examine the acidity of the catalysts. A flow apparatus on a BELCAT-B-TT (BEL, Japan) Autochem analyzer was used for temperature programmed desorption. In the typical TPD-NH_3, all catalysts were carried out in a quartz-made reactor using 0.03 g dried catalyst in flowing He at 150°C for 1 h, the followed adsorption NH_3 with a speed of 20 ml/min at 80°C for 20

min. The desorption process was first disposed at 80°C for 30 min and gradually increased from 80°C to 600°C at temperature rate 5°C/min in Helium atmosphere.

3.7 Catalyst activity test

The syngas to dimethyl ether synthesis (STD) reaction was carried out in the fixed bed reactor with the reaction temperature of 523 K and 623 K and reaction pressure of 5 MPa and 5.3 MPa, $W_{Cr/ZnO}/F_{syngas}$ = 10 g.h/mol, respectively. At the middle of the reactor, the mixture of quart wool, 4.0 g of glass bead, 0.5 g of Cr/ZnO with 3.0 g of quart sand and quartz wool were packed in sequence. All the catalysts were reduced in situ with pure H_2 flow 50 mL/min from room temperature to 673 K with the temperature ramp rate of 5 K/min and hold at this temperature for 10 h prior to the STD reaction. The syngas composition was 58.10% H_2: 33.80% CO: 5.10% CO_2: 3.09% Ar. In the reaction line apparatus, the effluent products were kept in gaseous state by electronic heater and analyzed online by a gas chromatograph with thermal conductivity detector (TCD, SHIMAZDU GC-8A) equipped with a Porapak N column identifying the concentration of CO and CO_2 in the product stream, by which 3.09% Ar in the feed gas acted as the internal standard. The product gas was further passed through the gas chromatograph with flame ionization detector (FID, SHIMADZU GC-8A) equipped with Gastopack and Porapak Q column to detect the concentration of methanol product. Since the separation and detection of FID GC-8A was not satisfied to determine the other hydrocarbons products; therefore, the product gas stream was further connected to the ice trap to capture some condensed methanol before analyzed online by another gas chromatograph with a hydrogen flame ionization detector (FID, SHIMADZU GC-14B) equipped with Gs-Alumina column. The light hydrocarbons, DME including higher hydrocarbons were determined to calculate the selectivity of hydrocarbons product based on carbon mole.

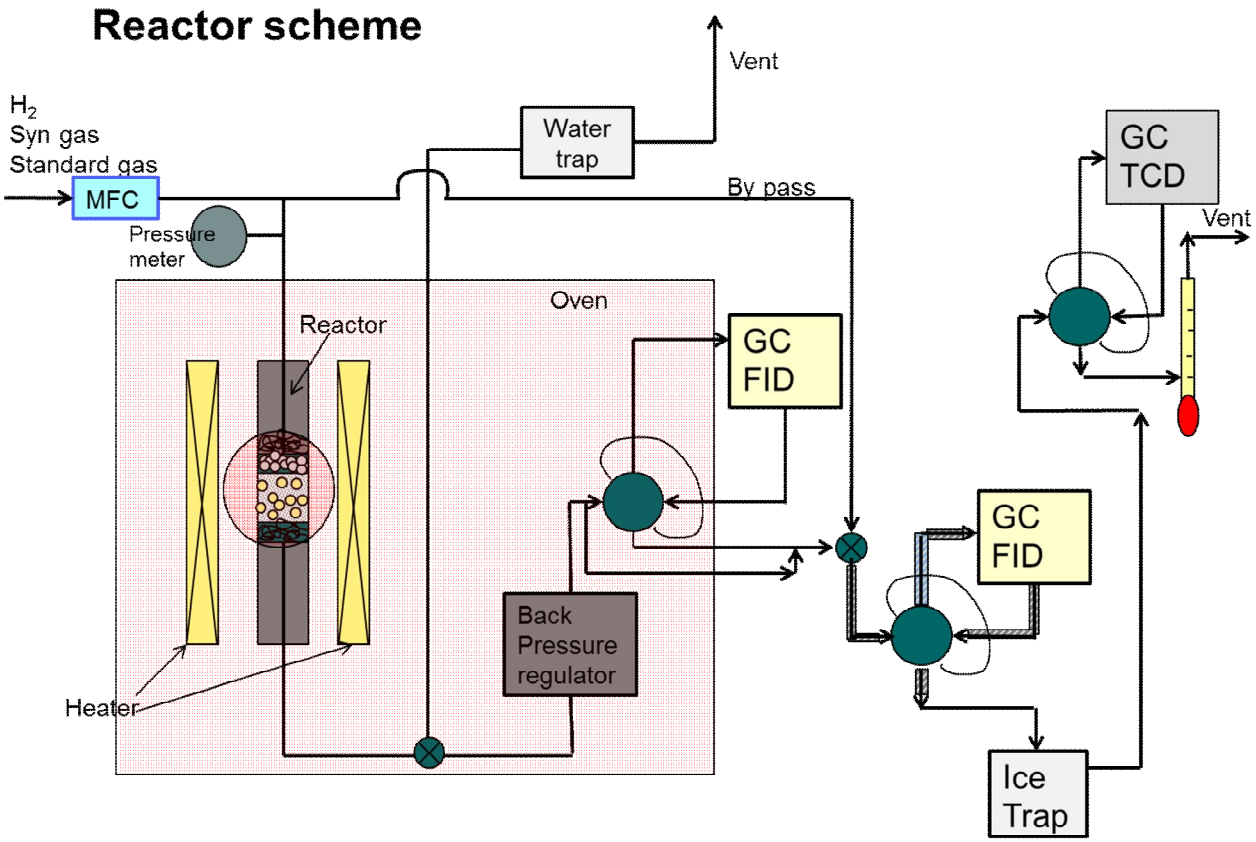

Figure 3.5 Reactor diagram of STD synthesis

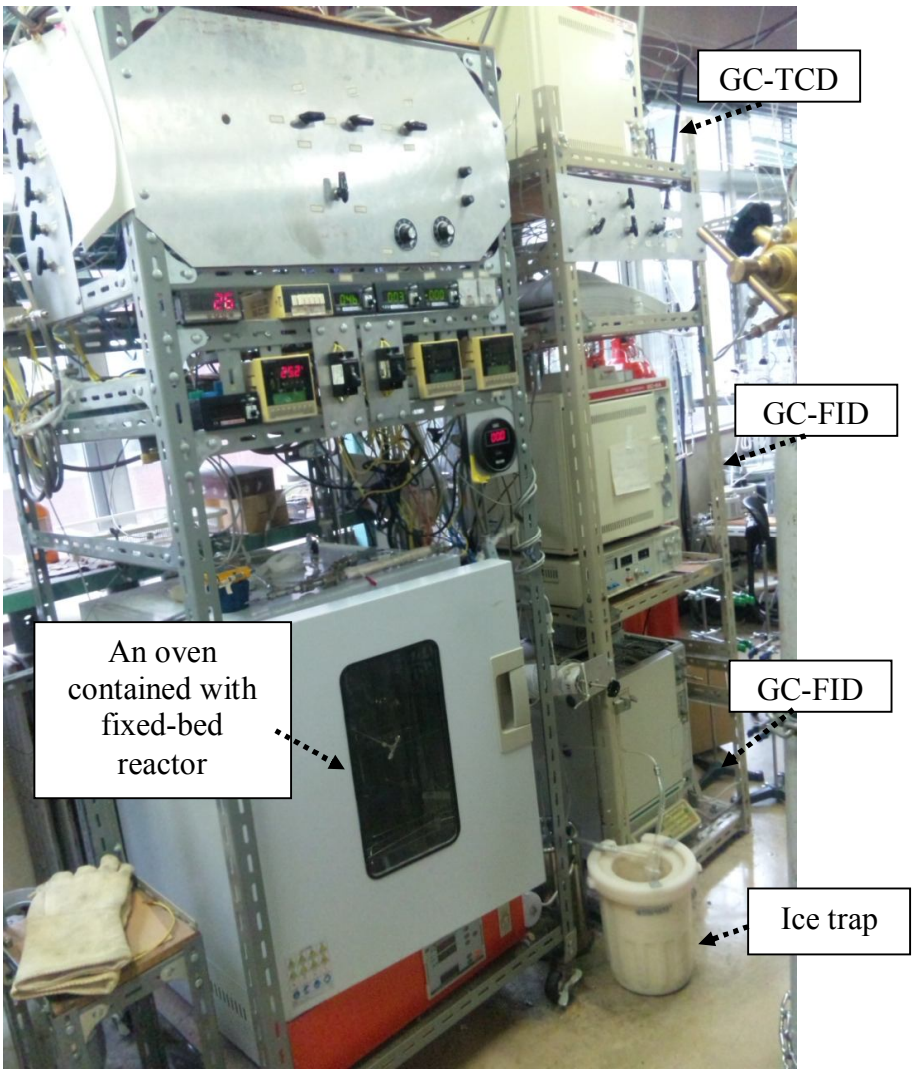

Figure 3.6 Reactor set and the analytical GC

3.8 Factorial design (2^3 experiment)

The 2^k factorial design was conducted in the same procedure as above. The high and low value of parameters in this study is shown in **Table 3.5**. All experiments in this design are labeled and shown in **Table 3.6**.

Table 3.5 The range of maximum and minimum values in the design

Variable	Name	(-1) Low	(0) Center	(+1) High	[unit]
A	$W_{Cr/ZnO}/F_{sysgas}$ ratio	10	15	20	
B	Temperature	300	350	400	°C
C	SAPO11:Cr/ZnO wt ratio	0.1	0.5	0.9	

Table 3.6 The label and condition for calculating effect in 2^3 design

Std	A	B	C	Labels
1	-	-	-	1
2	+	-	-	a
3	-	+	-	b
4	+	+	-	ab
5	-	-	+	c
6	+	-	+	ac
7	-	+	+	bc
8	+	+	+	abc
9	0	0	0	center
10	0	0	0	center
11	0	0	0	center
12	-	0	0	fcc center
13	+	0	0	fcc center
14	0	-	0	fcc center
15	0	+	0	fcc center
16	0	0	-	fcc center
17	0	0	+	fcc center

CHAPTER IV

MIXED CATALYST WITH VARIOUS MOLECULAR SIEVES

The mixed catalyst of Cr/ZnO and various kinds of SAPOs and AlPOs were studied in direct dimethyl ether synthesis from syngas. The preliminary study is about the various types of zeolite framework structure; that is $AlPO_4$-5, $AlPO_4$-11, SAPO-11, and SAPO-46. The mixed catalyst of Cr/ZnO and $AlPO_4$-5, $AlPO_4$-11, SAPO-11, and SAPO-46 were prepared at the weight ratio of 10:2.

Study on various $AlPO_4$s and SAPOs

Aluminophosphate (AlPO) is one of the molecular sieve materials which compose of Al and P atom in the framework structure. The acidity of its own is generally less than aluminosilicate zeolite such as HZSM-5, or modenite. Silicoaluminophosphate (SAPO) is the aluminophosphate that has been substituted P atom by Si atom producing more acidity. Therefore its mild acidic property is appropriate for DME synthesis reaction. The four different kinds of aluminophosphate ($AlPO_4$) and silicoaluminophosphate (SAPO) were prepared. Three of them possess one dimensional pore structure but differ in T-atom membered ring; $AlPO_4$-5 has 12 membered-rings with AFI framework structure, $AlPO_4$-11 and SAPO-11 has 10 membered-rings with AEL framework structure. And SAPO-46 has constructed by 12 membered-rings 3 dimensional pore and possess AFS framework structure.

The Cr/ZnO and various types of $AlPO_4$ and SAPO molecular sieve were prepared as mixed catalysts in the weight ratio of 10 to 2 of methanol synthesis catalyst and methanol dehydration acidic catalyst. The various characterization techniques were performed to investigate the catalyst properties.

4.1 Catalyst characterization

The XRD patterns of as-synthesized AlPOs and SAPOs are presented in **Figure 4.1**. The results correspond to the patterns found in the literature [16, 17, 37]. For aluminophosphate, the patterns illustrated the highly crystalline nature of the samples without impurities, while the patterns of silicoaluminophosphates were synthesized and showed some impurities of amorphous phase. The crystallinity of the as-synthesized SAPO-46 was 35% and SAPO-11 was 65% determined by a Bruker 8D Advance X-Ray diffractometer. The XRD patterns of the mixed catalyst were also compared with each type of zeolites and shown in **Figure 4.2**. It can be observed the identical diffraction peak at every parent peak of as-synthesized zeolite with the mixed catalysts. This indicates the existence of zeolite in the mixed catalyst. SEM micrographs of the samples are presented in **Figures 4.3** and **4.4**. The morphology of $AlPO_4$-5 and $AlPO_4$-11 was spherical shapes formed by agglomeration of a great number of small crystals. The SEM images of SAPO-11 and SAPO-46 shows that rectangle-like shape of the crystallines. The chemical composition of the calcined silicoaluminophosphate was given in **Table 4.1**. The mole ratio of Si/Al in SAPO-11 is slightly lower than that of SAPO-46 which is 0.16 and 0.18, respectively. The mole ratio of $AlPO_4$-5 and $AlPO_4$-11 is quite similar. All the yield of the as-synthesized zeolites is presented in Appendix A. The elemental composition of SAPO-46 and SAPO-11 zeolite is quite different from the pure standard zeolites. This is due to the impurity amorphous phase troubled while quenching the mixture solution after the hydrothermal synthesis. The proper way to cool down the hydrothermal reactor is by rinsing the hot hydrothermal reactor with water. The too much different temperature when quenching resulted in crystallization of P and Al particles in mother liquor increasing the amorphous phase contaminated in the as-synthesized zeolite.

The structural properties of samples are illustrated in **Table 4.2**. The properties are closely related with their structure except for SAPO-46. The SAPO-46 with three-dimensional pore shape should have shown high surface area, but the as-synthesized SAPO-46 in this study showed low surface area. This could be from the impurity of SAPO-46 in the form of amorphous phase as we can see from the bump curve of SAPO-46 zeolite in the XRD patterns. The $AlPO_4$-5 possesses nearly

spherical cages linked throughout the structure by twelve membered ring channels (diameter 0.73 nm) shows high surface area. The $AlPO_4$-11 and SAPO-11 with one-dimensional pore shape possess ten membered ring channels with an elliptical opening of 0.4 nm × 0.65 nm also give high surface area. The size and shape of AlPO-11 is comparable with SAPO-11, only Si species incorporate in the framework structure is different.

The acidic properties of different molecular sieves evaluated by NH_3-TPD, and the ammonia profiles are shown in **Figure. 4.5**. There showed one peaks corresponding to adsorption on acid sites. For aluminophosphate, similar shoulder peak at around 100 °C to 150 °C was observed corresponding to the weak acid sites originating from P-OH groups. The present of the P-OH group indicates a flaw of framework structure [6]. For silicoaluminophosphate, one huge desorption peak was observed at around 200 °C corresponding to moderate acid sites [17]. The introducing of silicon atoms into the framework of AlPOs resulted in the appearance of moderate acid sites. The amount of acid sites in $AlPO_4$-5 and $AlPO_4$-11 is quite similar, while the amount of acid sites of silicoaluminophosphate was observed as SAPO-11 > SAPO-46. The NH_3-profiles of mixed catalyst with various zeolites are shown in **Figure 4.6**. There are mainly two peaks observed on these mixed catalysts. The first shoulder peak at 250 °C and the smaller peak at 320 °C were observed. As we known the Cr/ZnO catalyst is the base catalyst. The shift of desorption peak occurred when we mixed the weak acid catalyst with the base Cr/ZnO catalyst. Although the pure SAPO-11 showed the highest amount of acidity it presented the lower acidity when mixed with Cr/ZnO catalyst. The order of acidity of these mixed catalysts are Cr/ZnO/SAPO-46 > Cr/ZnO/SAPO-11> Cr/ZnO/$AlPO_4$-5, Cr/ZnO/$AlPO_4$-11.

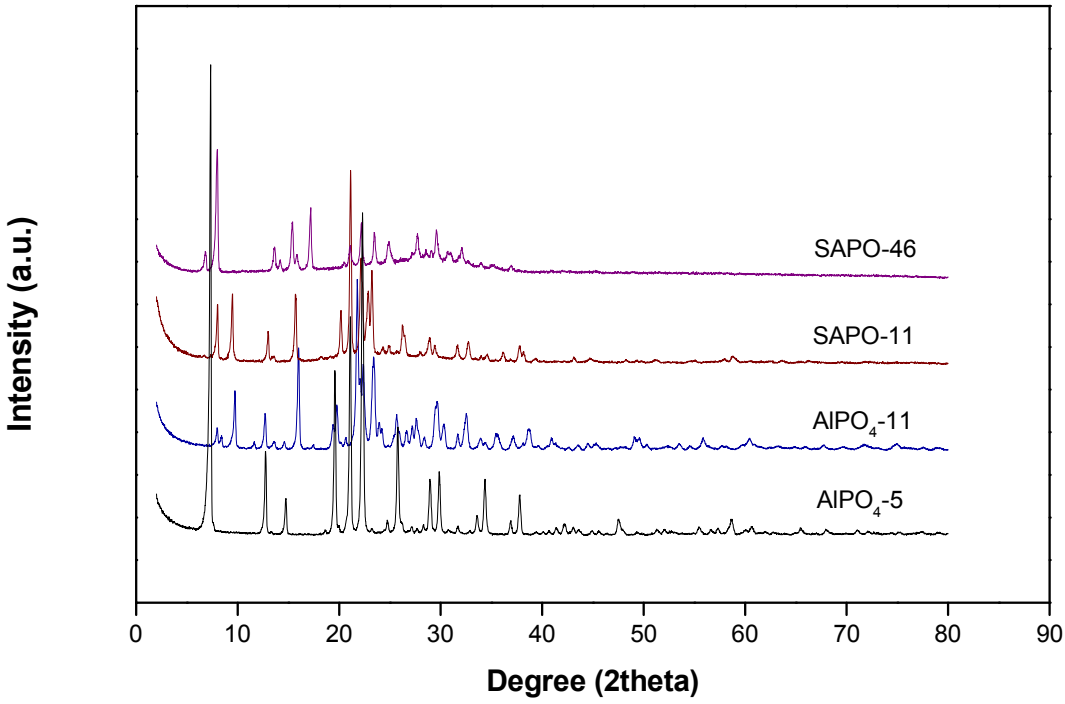

Figure 4.1 XRD patterns of as-synthesized $AlPO_4$-5, $AlPO_4$-11, SAPO-11, and SAPO-46

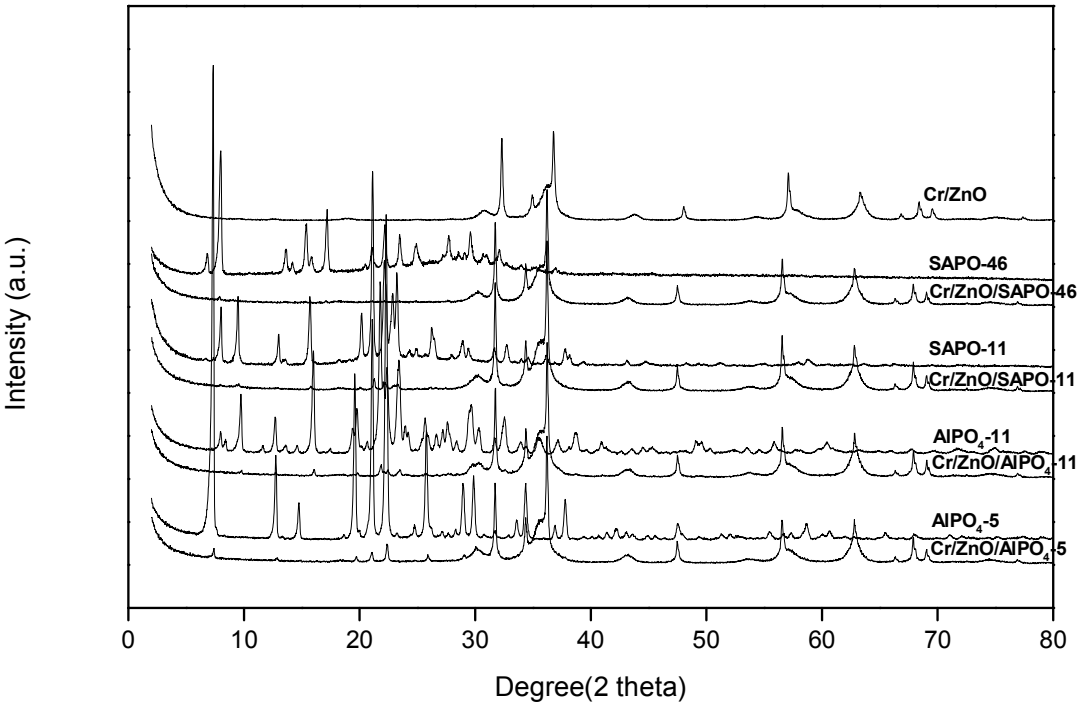

Figure 4.2 XRD patterns of mixed catalysts of Cr/ZnO and $AlPO_4$-5, $AlPO_4$-11, SAPO-11 and SAPO-46

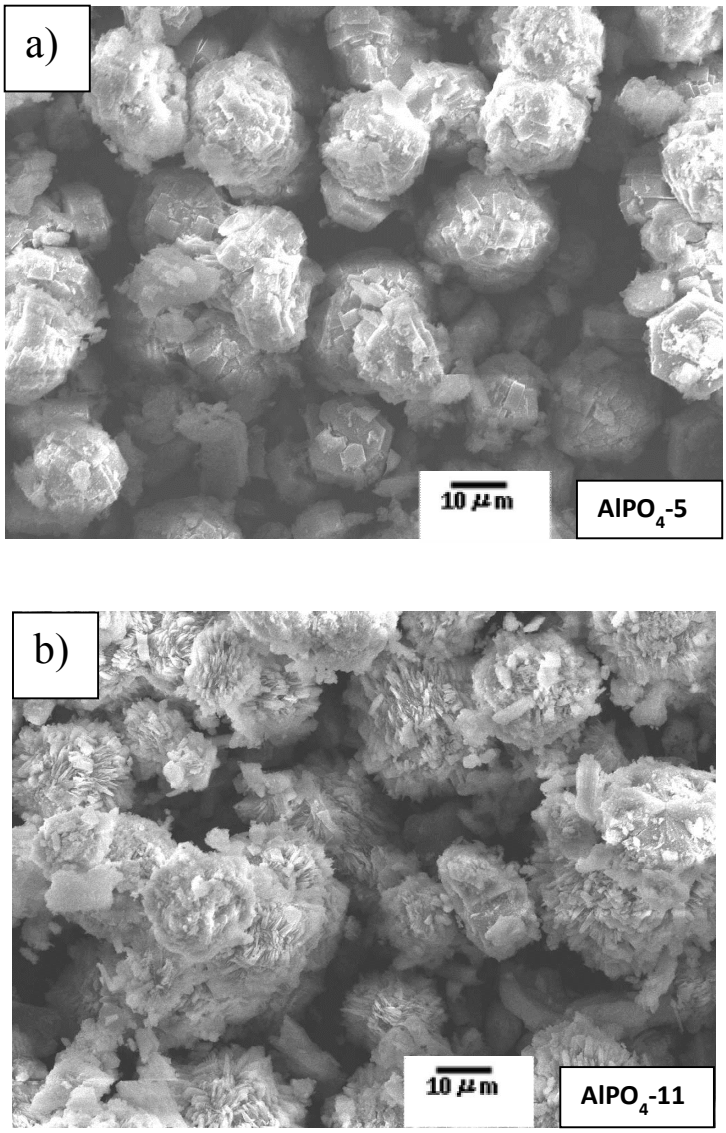

Figure 4.3 SEM images of as-prepared molecular sieve a) $AlPO_4$-5, b) $AlPO_4$-11

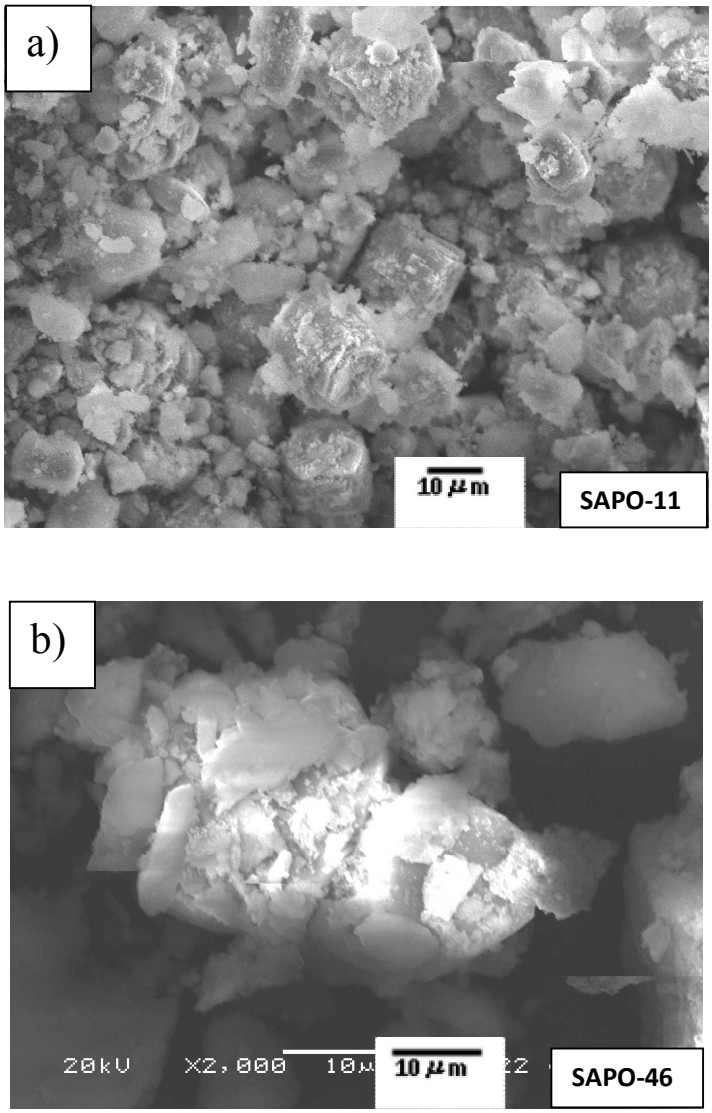

Figure 4.4 SEM images of as-prepared molecular sieve a) SAPO-11 and b) SAPO-46

Table 4.1 EDX analysis of aluminophosphates and silicoaluminophosphate

Sample	Elemental composition (mol %)			
	Al	P	Si	Si/Al
$AlPO_4$-5	58.9	41.1	-	-
$AlPO_4$-11	57.9	42.1	-	-
SAPO-11	59.7	31.0	9.3	0.16
SAPO-46	65.8	22.3	11.9	0.18

Table 4.2 The properties of as-synthesized $AlPO_{4s}$ and SAPOs

Sample	BET surface area (m^2/g)	Total pore volume (cc/g)	Acidity (mmol NH_3/g cat)
$AlPO_4$-5	214.1	0.205	1.042
$AlPO_4$-11	161.1	0.206	1.637
SAPO-11	154.3	0.622	8.922
SAPO-46	71.0	0.124	5.350

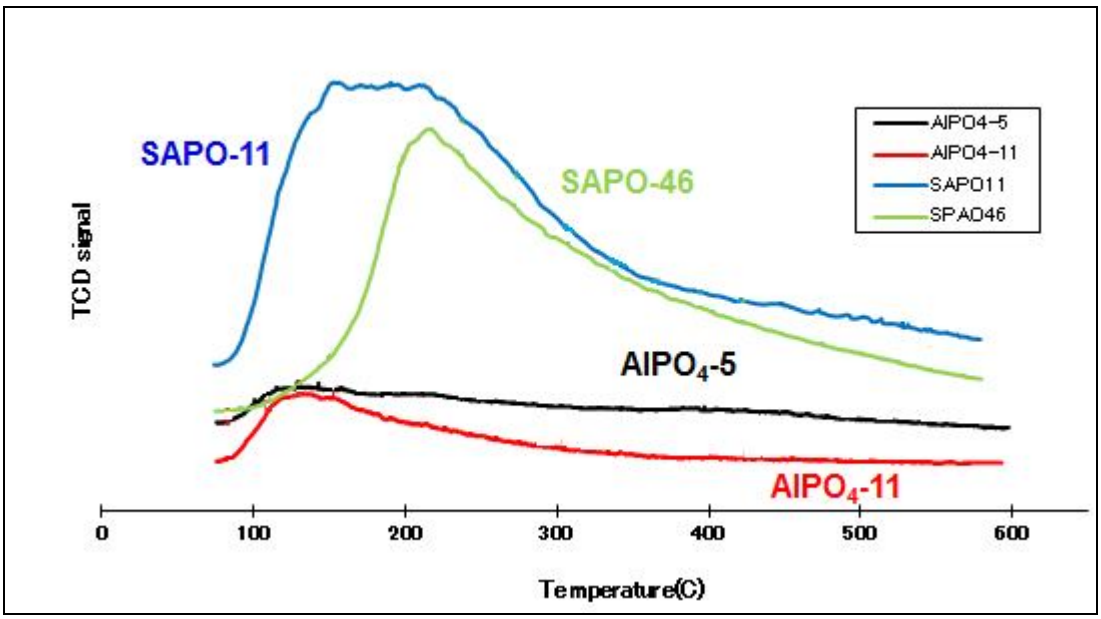

Figure 4.5 NH_3-TPD profiles of as-synthesized $AlPO_4$-5, $AlPO_4$-11, SAPO-11, and SAPO-46

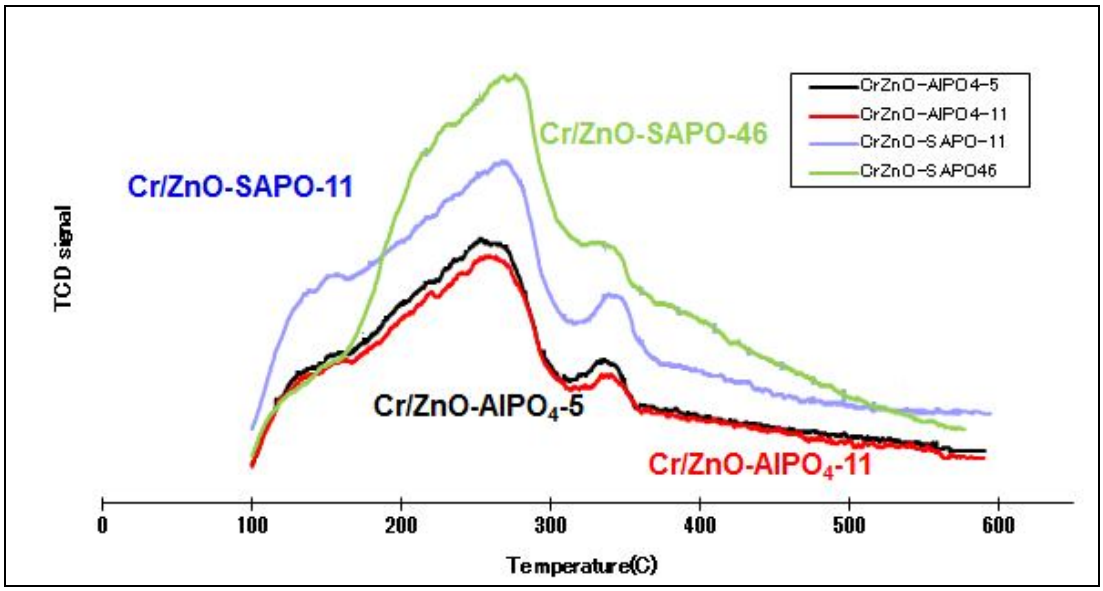

Figure 4.6 NH_3-TPD profiles of mixture catalysts of Cr/ZnO and $AlPO_4$-5, $AlPO_4$-11, SAPO-11, and SAPO-46

4.2 Catalytic activity of mixed catalysts

The STD reaction is mainly consists of methanol synthesis and methanol dehydration in the catalytic process. The first reaction and the second will occur at the different active sites. The methanol synthesis will occur on Cr/ZnO catalyst and then the intermediate methanol will be converted into DME on the acidic site of zeolite. Some side reaction might further convert DME into alkane/alkene or higher hydrocarbon on the acid sites of zeolite. The STD was performed on mixed catalysts to test the catalytic performance of aluminophosphate ($AlPO_4$-5, $AlPO_4$-11) and silicoaluminophosphate (SAPO-11, and SAPO-46). The catalytic performance of these mixed catalysts with time on steam is presented in **Figure 4.7**. The SAPO-46 possesses large pore 3-dimensional with 12 membered ring belongs to AFS framework structure. The large pore channel should have provided large cages for intermediate methanol to contact with the acidic site of SAPO-46 lead to higher DME selectivity. But the results showed that the mixed catalyst Cr/ZnO/SAPO-46 gave the lowest catalytic activities compared with the others. The bad catalytic activities of the Cr/ZnO/SAPO-46 catalyst probably arose from the presence of some amorphous phase of as-synthesized SAPO-46 as we can see from XRD analysis. The results showed that $AlPO_4$-5 and $AlPO_4$-11 with the low acidity properties is promising to be the good catalyst for STD synthesis due to the low acidic requirement of the dehydration reaction. However, the SAPO-11 which is 1-dimensional with 10 membered ring channels showed the best catalytic activity among these catalysts. The highest DME selectivity is obtained when using mixing catalyst of Cr/ZnO and SAPO-11. The pore dimensional structure of each type molecular sieve tends to be one factor controlling catalytic performance of STD reaction. Considering acidity properties of acid catalysts was found that SAPO-11 showed the highest amount of acid sites compared with others. Although the NH_3-TPD profiles of the mixed catalyst of Cr/ZnO and SAPO-46 present higher amount of acidity, it shows the lowest catalytic activity. The pore dimensional structure of silicoaluminophosphate should be considered as one factor as well. The catalyst activity was summarized again in **Table 4.3**. The major product among these catalysts is DME except for the Cr/ZnO/SAPO-46 catalyst. Although the as-synthesized SAPO-46 presented small crystallinity and

contaminated with amorphous phase it showed the confinement effect for encapsulated capsule catalyst. (result is shown in the next Chapter) Then we could say that the three-dimensional pore structure should play an important role in the catalytic performance of STD synthesis on AlPOs and SAPO mixed catalysts. The yield of DME was calculated based on only CO conversion and presented in **Table 4.3**. The DME yield are lined up in the trend of DME selectivity and CO conversion that is Cr/ZnO/SAPO-11 > Cr/ZnO/$AlPO_4$-5 > Cr/ZnO/$AlPO_4$-11 > Cr/ZnO/SAPO-46. For more clearly comparable, the catalytic performance of STD synthesis on these mixed catalysts is presented in **Figure 4.8**.

Moreover, the catalysts with relatively mild acid strength showed low hydrocarbons formation. This result attributed to the fact that mainly simply hydrocarbon process by mild acid sites over acid catalyst does not allow the formation of coking material causing catalyst deactivation. Furthermore, in some literature they claimed that the desirable pore shape of AFI framework structure which belong to $AlPO_4$-5 and AEL framework structure which belong to $AlPO_4$-11 and SAPO-11 and altogether with the mild acid site properties are suitable for methanol dehydration [6]. This reason helps support the catalytic reaction obtained in this study.

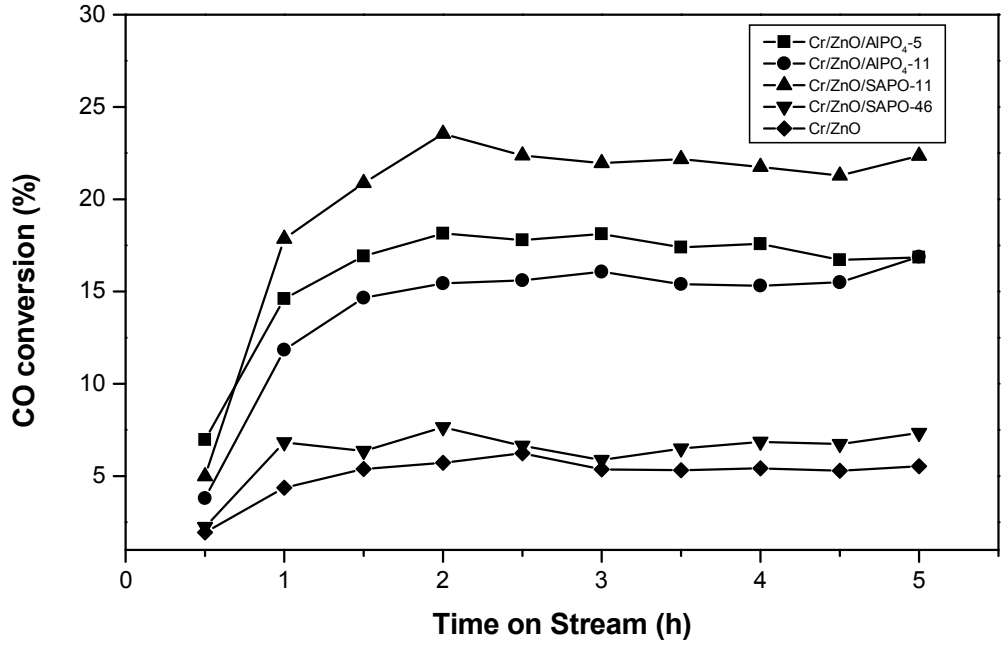

Figure 4.7 STD synthesis on mixed catalyst of Cr/ZnO (◆); Cr/ZnO/$AlPO_4$-5 (■) Cr/ZnO/$AlPO_4$-11 (●); Cr/ZnO/SAPO-11 (▲) and Cr/ZnO/SAPO-46 (▼)

Table 4.3 Catalyst activity of STD reaction on Cr/ZnO, Cr/ZnO-$AlPO_4$-5, Cr/ZnO-$AlPO_4$-11, Cr/ZnO-SAPO-11, Cr/ZnO-SAPO-46 catalysts

Sample	Conversion[a] (%)			Selectivity (%)				Yield of DME (%)
	CO	CO_2	total	CH_4	MeOH	DME	Others	
Cr/ZnO-$AlPO_4$-5	17.6	-25.5	11.9	1.5	18.1	75.5	4.8	13.3
Cr/ZnO-$AlPO_4$-11	15.4	-21.6	10.6	1.9	21.4	70.0	6.7	10.8
Cr/ZnO-SAPO-11	21.7	-36.2	14.1	1.3	12.1	81.1	5.6	17.6
Cr/ZnO-SAPO-46	6.7	-1.6	5.7	2.6	61.2	30.5	5.8	2.0
Cr/ZnO	4.9	2.0	4.5	5.7	87.1	0.5	6.7	0.02

[a] reaction condition: 350°C, pressure at 5 MPa, $W_{Cr/Zno}/F_{syngas}$ = 10 g·mol/h, reaction time 5 h.

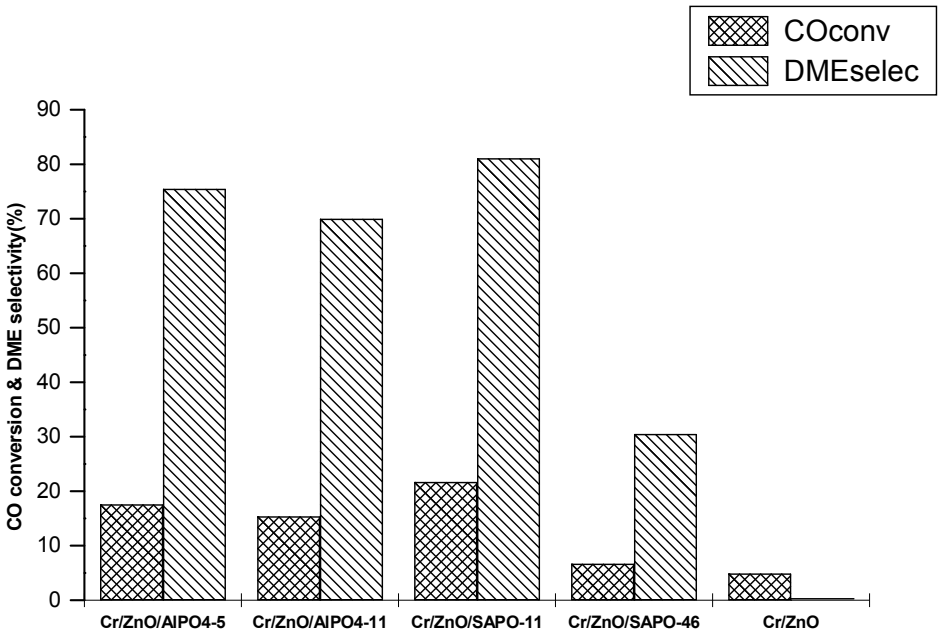

Figure 4.8 Catalytic performance of STD synthesis on mixed catalysts Cr/ZnO-$AlPO_4$-5, Cr/ZnO-$AlPO_4$-11, Cr/ZnO-SAPO-11, and Cr/ZnO-SAPO-46

CHAPTER V

PHYSICAL COATING CAPSULE CATALYSTS

Direct dimethyl ether synthesis from syngas was studied with mixed catalyst and capsule catalyst of Cr/ZnO, CuZnAl and SAPOs and AlPOs. The first topic is already talked on the various types of zeolite framework structure; that is $AlPO_4$-5, $AlPO_4$-11, SAPO-11, and SAPO-46. The second topic is focused on the performance of capsule catalyst by studying on confinement effect of encapsulation capsule catalysts. The Cr/ZnO and CuZnAl catalyst have been used as a core catalyst and SAPO-46 and -11 have been used as an acidic zeolite shell catalyst. In this chapter, various characterization techniques such as XRD, SEM &EDS, BET were used to analyze the properties of the Cr/ZnO/SAPO46-PhyC, CuZnAl/SAPO-11/SAPO11-PhyC capsule catalyst for example, surface SEM & EDS to obtain morphology and elemental composition of capsule catalyst, EDX analysis was used to examine elemental composition of powder sample, XRD analysis for identifying the substance, N_2 physisorption analysis for evaluating surface area, pore volume and pore size diameter of the samples.

The capsule catalyst has well-organized structure which is composed of the core catalyst inside and covered by another active site outside. Moreover, the structure of core-shell-like catalyst is effective to combine two different active sites together. Recently, lots of studies have been performed on the catalyst parameters which affect the effective production of DME, especially the type of acidic catalyst (like γ-Al_2O_3, HZSM-5, AlPO or SAPO) usually used for methanol dehydration. [38-42] Cr/ZnO and CuZnAl encapsulated by SAPOs capsule catalysts were prepared by a new approach named physical coating method. The new physical coating method has advantages over the conventional hydrothermal synthesis method because of the mild condition of synthesizing. The catalytic performance of these catalysts was presented in this chapter.

5.1 A study of core-shell like capsule catalyst SAPO-46 encapsulated Cr/ZnO

We have known that silicoaluminophosphate (SAPO-11 and SAPO-46) has higher acidity than the aluminophosphate ($AlPO_4$-5 and $AlPO_4$-11) from the previous chapter. Therefore in this chapter we selected the SAPO-11 and SAPO-46 zeolite to encapsulate the core catalyst for further study on the capsule catalyst.

5.1.1 Catalyst Characterization

The core shell catalyst synthesized by conventional hydrothermal synthesis was founded that it might have been damaged core catalyst due to the long period of time sitting in the precursor solution. As we can see from **Figure 5.1 (a)**, the capsule catalysts produced by hydrothermal synthesis showed less complete crystallinity of SAPO-46 on the surface of core catalyst than that prepared by physical coating method. By the latter preparation, the SAPO-46 crystal on the surface was prevented from problem of chemical corrosion and the formation of metal coordination compound during synthesizing. Therefore in order to avoid those problems and still maintain the competence of two kinds of active site, the new method named physical coating (PhyC) is introduced to prepare the core-shell-like capsule catalyst. The well-designed catalyst usually lead to the better catalytic performance, the PhyC catalysts have benefited the concept of this idea. The PhyC method is easily prepared at room temperature without any special equipment needed.

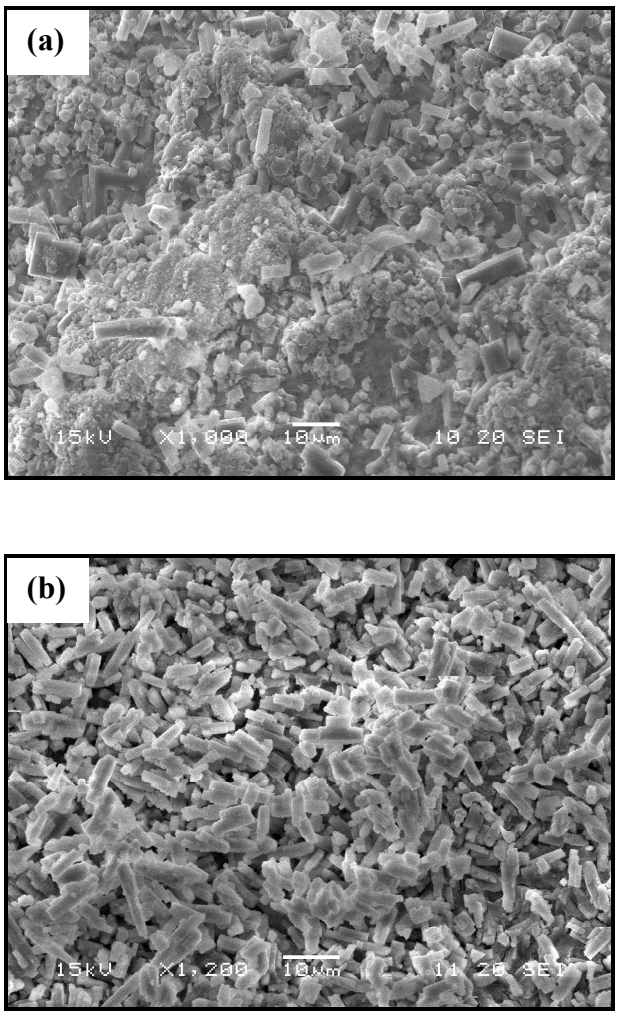

Figure 5.1 The morphology of capsule catalyst synthesized by (a) hydrothermal method and (b) physical coating method

The Cr/ZnO catalyst in the weight ratio of 1:2 was used as the core catalyst for preparing physical coating capsule catalyst. The elemental composition of Cr and Zn was 14.8 and 25.7 % which was approximately close to the original ratio (Cr : Zn = 1 : 2 by mol). The surface SEM and EDS analysis of Cr/ZnO catalyst was showed in **Figure 5.2**. After covering the Cr/ZnO with SAPOs by this physical coating method, the morphology of the core catalyst was clearly observed roughly. The Si/Al ratio of SAPO shell was 0.35. This is higher than those of the original ratio of the as-prepared SAPO-46; the latter one was 0.18. This is more reasonable if considering of using silica colloid as a binder. The as-synthesized SAPO-46 was analyzed by EDX to obtain the elemental composition showed in **Table.5.1**.

In this study, we developed the new PhyC method for encapsulating capsule catalyst by physical approach. This method is easily accessible, repeatable and enlargeable overcoming the coating problems from the hydrothermal synthesis method. Surface SEM image presenting the magnified morphology on the capsule catalyst were showed in **Figure 5.3 (b)** and **(c)**. Comparing to the **Figure 5.3 (a)**, it was clearly noticed the crystal of SAPO-46 on the surface membrane of the core catalyst. **Figure 5.3 (d)** shows the EDS analysis at the surface outer membrane of PhyC catalyst, no signal of Cr and Zn were detected indicating the success of PhyC method. Furthermore, the EDS analysis of SAPO shell membrane have shown that the dilution silica used as a binder was not give any change to the structure of core shell catalyst.

The XRD pattern of as-prepared SAPO-46, physical coating Cr/ZnO-SAPO46-PhyC, mixed Cr/ZnO-SAPO46-M and core Cr/ZnO catalysts are presented in **Figure 5.4**. The diffraction profiles of SAPO-46 were found from as-prepared silicoaluminophosphate according to the literature [6, 8] indicating it was the real zeolite identity. The diffraction profiles of SAPO-46 were found in both of the PhyC and mixed catalysts but in the very small intensity probably due to the small content of SAPO-46 in the catalyst. The crytallinity of as-prepared SAPO-46 is 35%.

These analysis results indicate the formation of a SAPO-46 zeolite layer on the Cr/ZnO core catalyst, suggesting the success of this newly developed PhyC method on the core-shell-like zeolite capsule catalyst preparation. This method is very accessible, repeatable and scalable, and it can be performed under ambient conditions, especially without any complex equipment or technologies.

Table 5.1. The elemental composition of SAPO-46 from EDX analysis

Sample	**Elemental molar composition (mol%)**			**Si/Al**	**Si/(Al+P+Si)**
	Al	P	Si		
SAPO-46	65.8	22.3	11.9	0.18	0.12

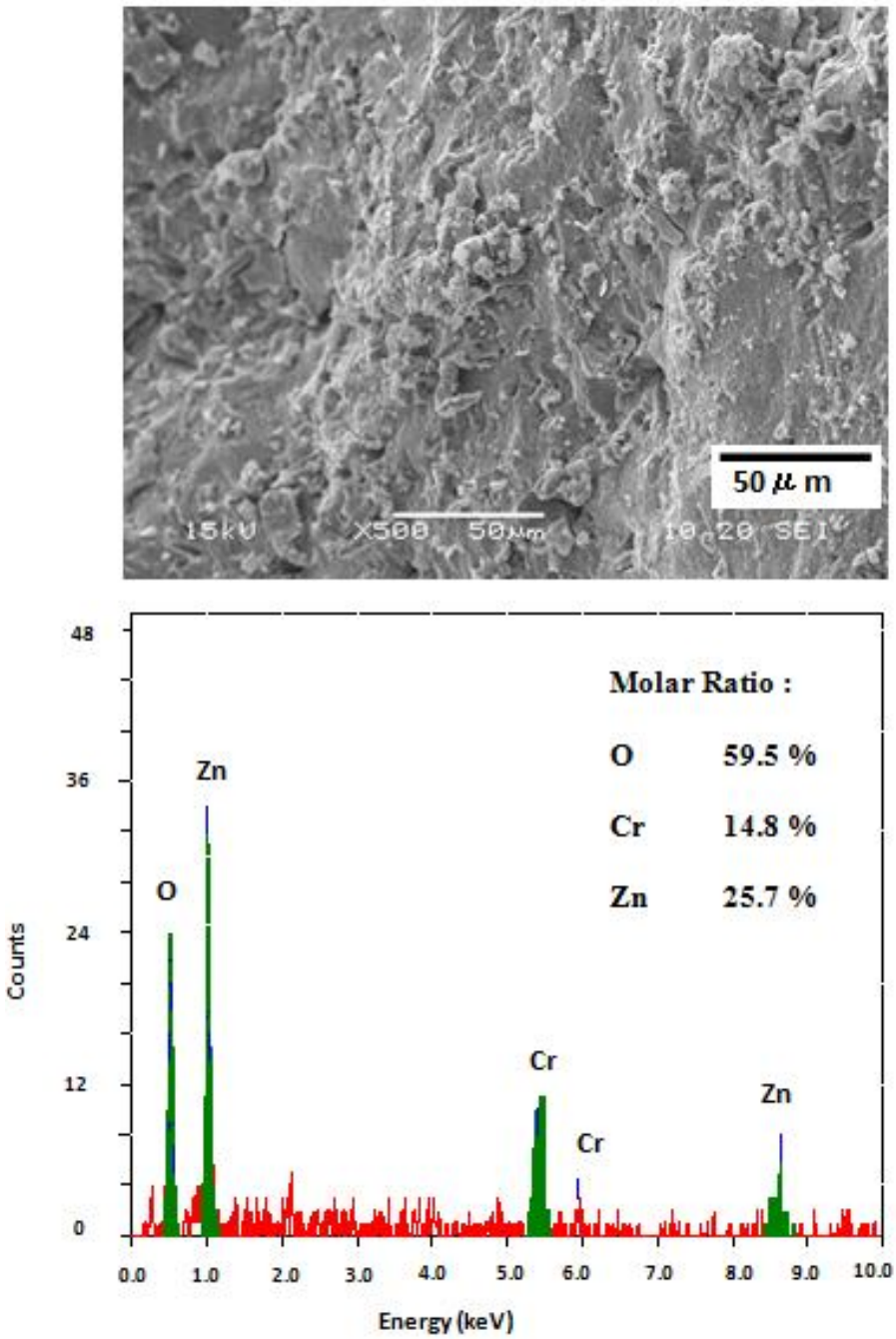

Figure 5.2 Surface SEM and EDS analysis of the Cr/ZnO core catalyst

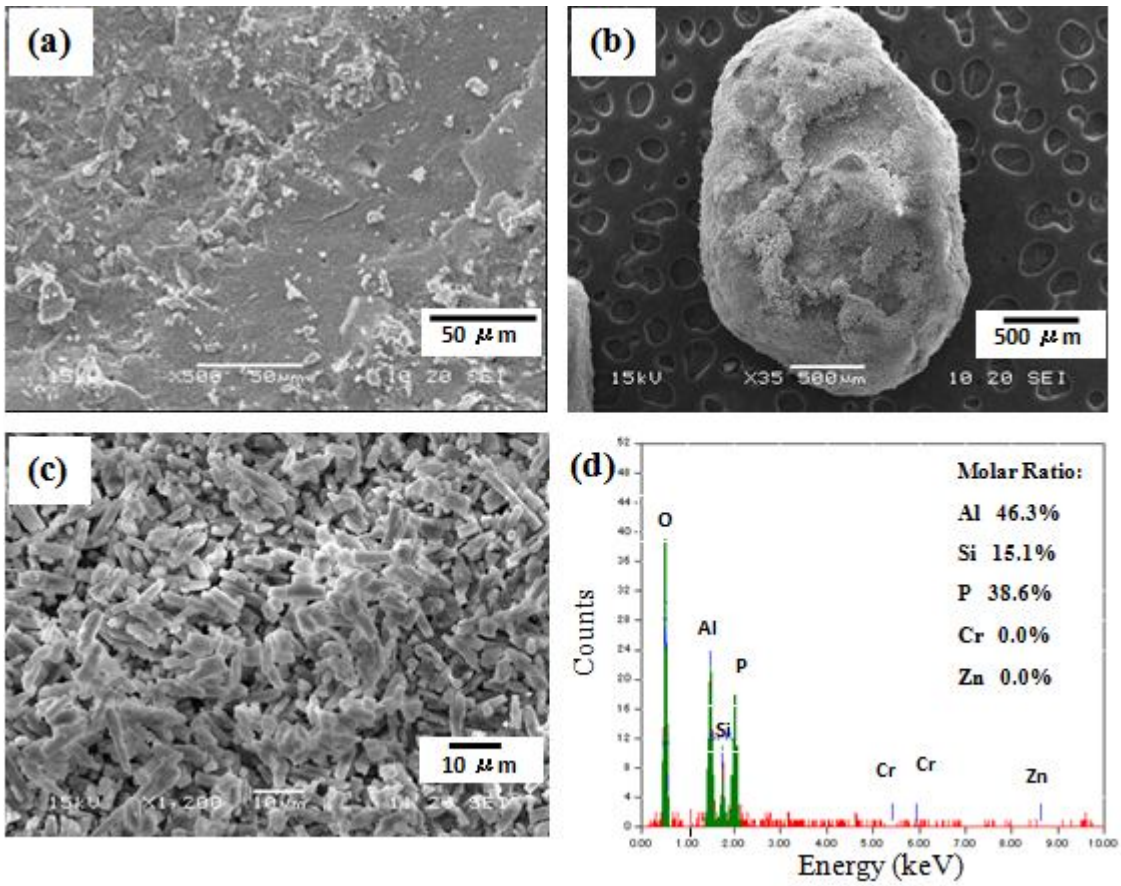

Figure 5.3 The surface morphology of (a) the bare Cr/ZnO catalyst, (b) the capsule catalyst Cr/ZnO-SAPO46-PhyC; (c) the magnified surface morphology of capsule catalyst Cr/ZnO-SAPO46-PhyC and (d) the EDS surface analysis of capsule catalyst Cr/ZnO-SAPO46-PhyC.

For the acidic properties of these catalysts, the NH_3-TPD was used to investigate the acidity property (results were showed in Appendix C). The acidic peak between 200 and 300°C represented the similar acidic strength between two catalysts. The amount of acidity was found that Cr/ZnO/SAPO46-M > Cr/ZnO > Cr/ZnO/SAPO46-PhyC indicating the mechanical preparation might effected to the acid properties of the catalyst. In literature we found that the zeolites particle sizes obtained from crushing by ball-milled preparation resulted in breaking the crystal size of crystalline particles consequently reduce the acidity of the catalyst [21]. But in this case, the mixed catalyst showed the higher amount of acid sites compare with capsule catalyst. The mixed catalyst prepared by mechanical blending had the same amount of

SAPO-46 zeolites and Cr/ZnO with the capsule catalyst but represented different amount of acidity. This could be attributed to the different structure between these two kinds of catalysts. The coating catalyst should have presented the highest acidity among others due to the structure that had been designed to place the SAPO membrane at the outside, while the mixed catalyst should present the acidity less than the coating catalyst because of the random structure. In case of core-shell-like-capsule catalyst, the arranged structure of SAPOs shell was fixed as the membrane over the core catalyst. The SAPO would not been crushed with the Cr/ZnO during the preparation, the crystalline particle of SAPO was still remained as the original shape. But treating the coating catalyst with calcination after all at 500°C for 2 h to make the whole catalyst stronger might damage the pore structure of zeolite causing the lower amount of NH_3 adsorption. Therefore it could be noticed the lower amount of NH_3-desorption on the PhyC catalysts which can inform to the acidity of the catalysts. It might say that the heat treatment cause damages to the zeolite structure resulted in reversion of the acidity trend of catalysts.

5.1.2 Catalytic test of Cr/ZnO encapsulated with SAPO-46 for STD reaction

The catalytic performance of catalysts had been tested by STD reaction. Generally, the consecutive reactions composed of two reactions, methanol synthesis and methanol dehydration. The STD reaction is one of the famous sequential catalysis processes. It mainly includes the MeOH synthesis from syngas on the methanol synthesis catalyst, the methanol dehydration forming DME on the acidic catalysts and the formation of alkane/alkene through further DME dehydration. The STD process, furthermore, is widely known since it is more thermodynamically favorable and more productive than the conventional two-step DME synthesis process. (i.e., methanol synthesis from syngas and methanol dehydration forming DME are performed individually).

DME production from synthesis gas was performed over Cr-based catalyst with two different structures. One is a core-shell-like capsule catalyst, and the other is a mixed catalyst. The results are shown in **Table 5.2**. The Cr/ZnO-SAPO46-PhyC

capsule catalyst showed a slightly higher CO conversion rate than the mixed catalyst. The higher catalytic reaction rate of the capsule catalyst over the mixed catalyst can be explained by increased the syngas to methanol reaction rate. This is the first step of STD synthesis. The methanol that formed in the first step further converted to DME as the second step of the consecutive reaction. This resulted in more thermodynamic favorable. The Cr/ZnO-SAPO46-PhyC capsule catalyst has been designed with the layer of powdered SAPO-46 cover over the core catalyst, forming a thin membrane over the outside. This core-shell-like structure promoted the intermediate product to change into DME when passed through the layer of zeolite. This coating layer formed a restrictive area and also made an inevitable way for methanol to convert to DME. This conversion resulted in a higher catalytic activity of the capsule catalyst over a mixed catalyst. In contrast, the conventional mixed catalyst Cr/ZnO-SAPO46-M was prepared by mixing a methanol synthesis catalyst and an acid catalyst, pressurized, and ground into 0.85-1.7 mm particles resulting in lower contact area between these catalysts due to some part of SAPO-46 being covered by Cr/ZnO catalyst.

The high DME selectivity can be reached at around 37.0% for the capsule catalyst. The lower DME selectivity can be found approximately a half lower at 16.5% for the mixed catalyst. For the bare Cr/ZnO catalyst, MeOH and DME selectivity was accounted for 90.7% and 0.5%, respectively. For better comparison, **Figure 5.5** showed product selectivity of these catalysts. Considering the capsule catalyst of SAPO-46 prepared by the new physical coating method, its DME selectivity reached up to 37.0%. This implies that most of the intermediate product changed to DME and some of those further reacted into the other hydrocarbon which normally occurs on the acid catalyst. The capsule catalyst with the core-shell-like structure was designed aiming to gain the possibility of converting intermediate products to the final products when passing through the zeolite membrane. Moreover, the advantage of this core-shell-like catalyst over the mixed catalyst is the contact area between the SAPO-46 and the core catalyst. For the core-shell-like catalyst, the contact area is greater than the mixed catalyst which resulted from the perfect and well-organized layer of zeolite outside the core. Its more contact area affected in the

more chances of convert intermediate product to DME. This resulted in higher DME selectivity of the core-shell-like catalyst over the mixed catalyst.

In addition, it should be considered that the weight increase of the SAPO-46 layer in the PhyC catalyst was different from the amount of SAPO-46 in the mixed catalyst. Even though the PhyC catalyst still presented the higher specific selectivity, it has a lesser amount of SAPO-46 on the surface (about 5 wt% increase). This is a good evidence to confirm the effective structure of the core-shell-like catalyst. The mixed catalyst was prepared in the weight ratio of 10:1 of Cr/ZnO catalyst and SAPO-46 in order to use as reference of a small ratio of methanol synthesis catalyst and methanol dehydration catalyst.

The extremely controlled DME synthesis by employing this Cr/ZnO-SAPO46-PhyC capsule catalyst should be attributed to its special core-shell-like structure. Each individual reaction of the STD process can be confined to different, but the most suitable, locations on this capsule catalyst. Methanol synthesis from syngas occurred on the Cr/ZnO core catalyst and the following methanol dehydration to DME reacted on the SAPO-46 zeolite coating layer. **Figure 5.6 a** shows the reaction partway the SAPO-46 shell membrane, offering the sequential order of syngas to methanol and then methanol dehydration to DME. The syngas firstly passed through the shell membrane, reached the core Cr/ZnO catalyst, then started the methanol synthesis reaction. Methanol synthesized afterwards will convert into DME while escaping from the core-shell catalyst. The core-shell-like structure offers an inevitable way for methanol to convert to DME. In contrast, the mixed catalyst (as showed in **Figure 5.6 b)** may offers the non-sequential order, providing the random possibility of changing syngas into methanol without further reacting into DME. Syngas changed into methanol and then escaped from the catalyst without touching the SAPO-46. This resulted in maintaining the high amount of methanol left and also would result in lower DME selectivity in the final product. Furthermore, for the mixed catalyst, after methanol dehydrated to DME, the DME might further dehydrate into alkane/alkene products on the acidic site of SAPO-46 because it was not fixed properly in a similar way as in the case of PhyC catalyst. The new physical coating method provided a new way of encapsulation and it obviously showed the higher desired DME selectivity

compared with the mixed catalyst at an even lower amount of SAPO-46 in the catalyst.

In brief, the physical coating method has been designed for preparing the encapsulated capsule catalyst with the SAPO-46. The capsule catalyst Cr/ZnO-SAPO46-PhyC showed higher selectivity of DME synthesis through STD reaction compare with the mixed catalyst Cr/ZnO-SAPO46-M. The PhyC catalyst provided an effective controlled synthesis reaction for syngas to convert to target product. These consecutive reactions resulted in higher catalytic performance in the STD synthesis. The reaction results confirmed the core-shell-like structure is effective and practical for DME selective through STD reaction.

Table 5.2 The catalytic activity of different catalysts [a]

Sample	Conversion (%)				Selectivity (%)			Yield DME (%)
	CO	CO_2	total	CH_4	MeOH	DME	Others	
Cr/ZnO	4.9	2.1	4.5	3.7	90.7	0.5	5.1	0.02
Cr/ZnO-SAPO46-PhyC	6.9	-6.0	5.2	4.7	52.2	37.0	6.1	2.5
Cr/ZnO-SAPO46-M	4.7	-2.9	3.7	5.7	71.7	16.5	6.1	0.78

[a] Reactions conditions: 350°C, 5 MPa, $W_{Cr/ZnO}/F_{Syngas}$ = 10 g·mol/h;
Experimental data were obtained at the fifth hour of reaction.

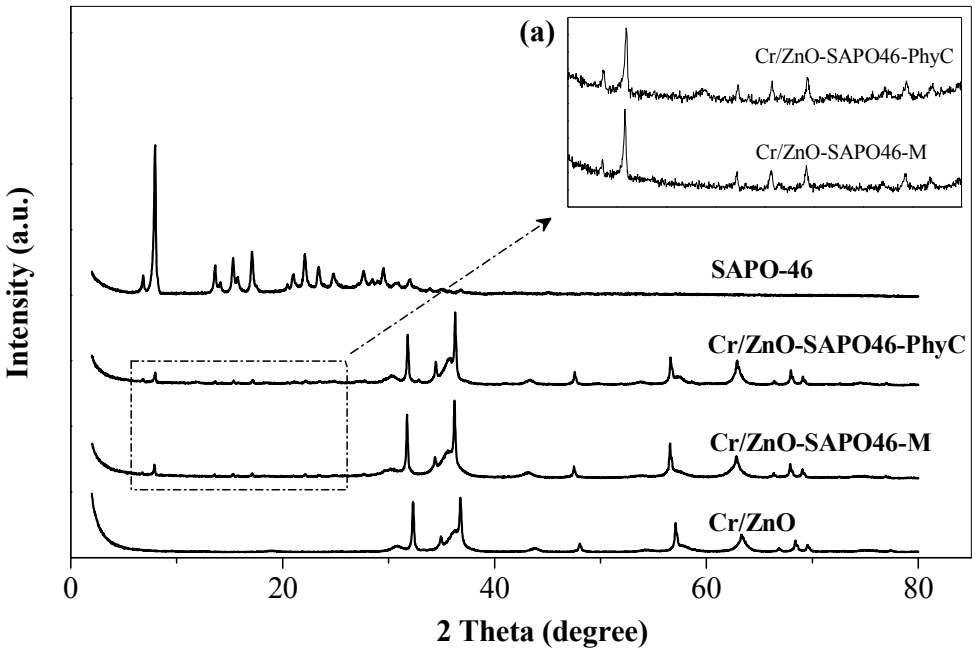

Figure 5.4 XRD patterns of SAPO-46, the CrZnO-SAPO46-PhyC physical coating, the Cr/ZnO/SAPO-46-M mixed and the core Cr/ZnO catalyst and (a) magnified characteractic peaks of SAPO-46 of both Cr/ZnO-SAPO46-PhyC and Cr/ZnO-SAPO46-M catalysts

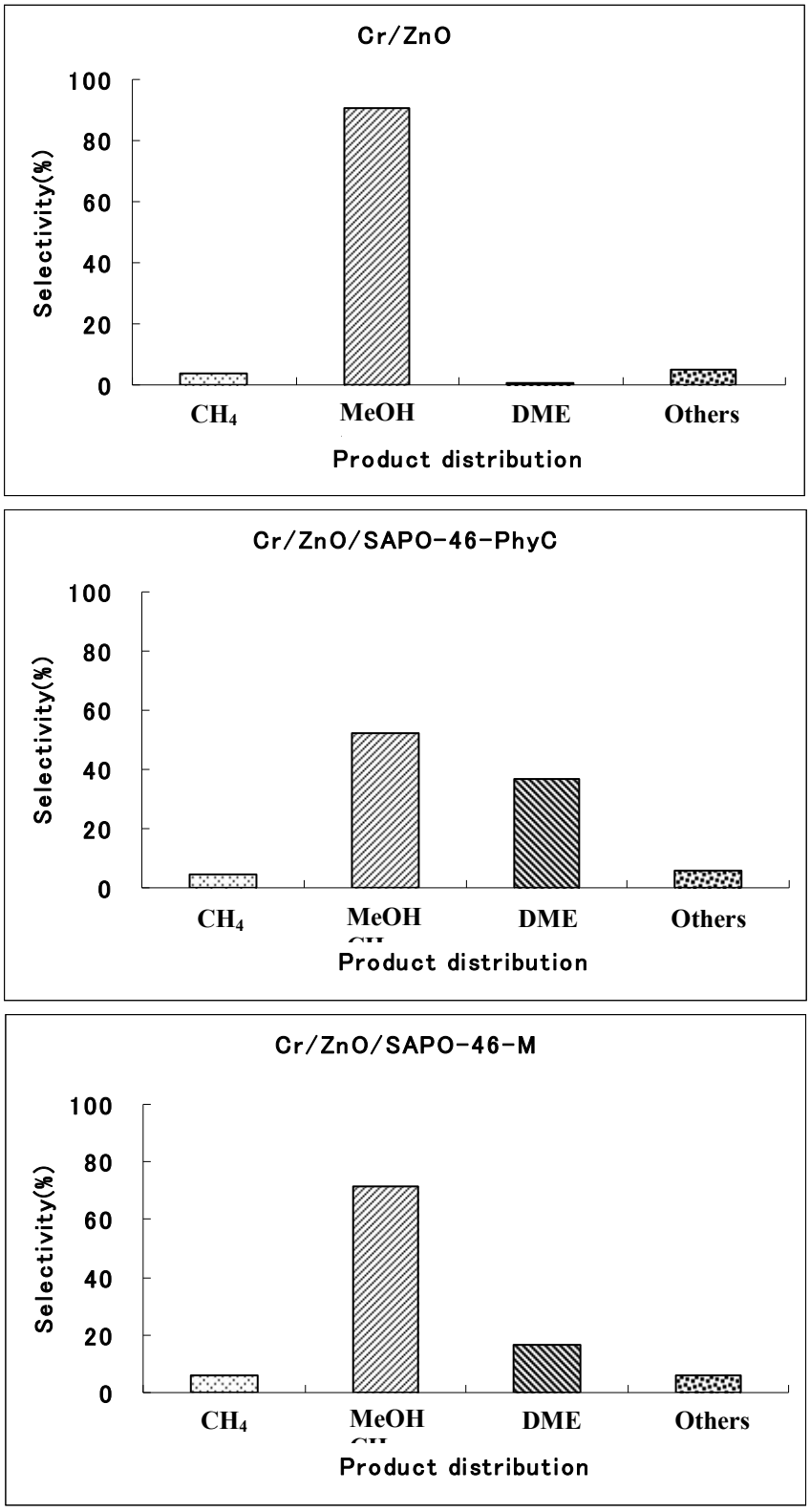

Figure 5.5 Product distribution of STD synthesis on Cr/ZnO, Cr/ZnO-SAPO46-PhyC, Cr/ZnO-SAPO46-M catalysts

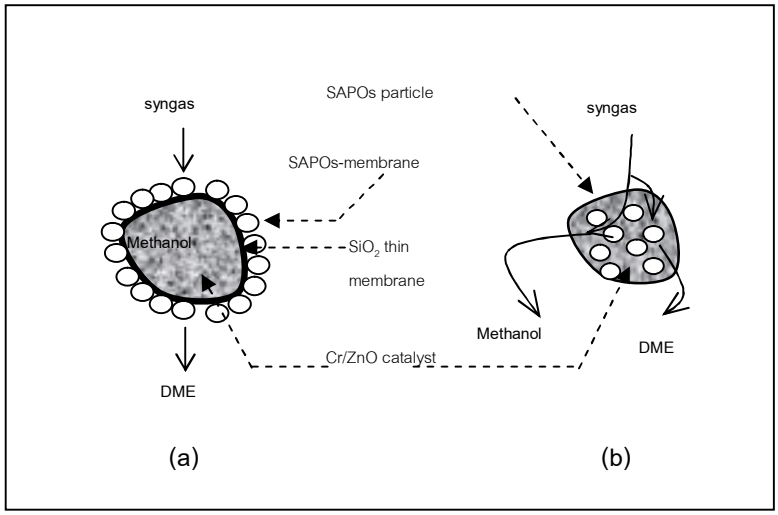

Figure 5.6 The reaction pathway of (a) the physical coating and (b) the mixed catalyst

5.2 A study of core-shell like capsule catalyst SAPO-11 encapsulated with CuZnAl

The previous section was studies about the core Cr/ZnO catalyst, the methanol synthesis catalyst for high temperature DME synthesis, encapsulated with SAPO-46. In this section we will talk about the core CuZnAl catalyst, the low temperature DME synthesis catalyst, encapsulated with SAPO-11. In the previous section, the reaction results showed that the core-shell-like capsule catalysts caused the better DME selective through STD reaction. In the same way, in this section we will expand the idea of the core-shell-like structure prepared by the new physical coating method into the SAPO-11 zeolite encapsulated the core CuZnAl catalyst. The catalyst characterization and reaction results were showed in the section below.

5.2.1 Catalyst characterizations

The CuZnAl catalyst used here is widely known as the good methanol synthesis catalysts for low temperature process. It was selected as the core catalyst for coating the SAPO-11 zeolite on the surface with the physical coating method. The surface SEM and EDS analysis of the bare CuZnAl core catalyst gives the surface

morphology and elemental composition of silicoaluminophosphate membrane. The EDS analysis in **Figure 5.7** had molar composition of Cu, Zn and Al as 66.6%, 29.3% and 4.1% by mole. The molar ratio of Cu to Zn to Al determined by EDS was slightly different from the original ratio in catalyst preparation recipe (60/30/10).

In this study, the new PhyC (physical coating) method was adopted to construct silicoaluminophosphate (SAPO-11) on the core catalyst. The capsule catalyst is the improvement of attempt to develop the restriction area between two active sites, making the closer contact area between them. The conventional capsule catalysts synthesized by the hydrothermal method have been applied to synthesize many capsule catalysts earlier such as Co/Al_2O_3-H-beta zeolite, Cr/ZnO-H-ZSM-5, Pd/SiO_2-H-ZSM-5 and so on [38-40, 43], in which these catalysts have been limited to prepare under the high temperature and heat treatment. Moreover, the capsule catalysts synthesized by this method were unsafe from damages on the core catalyst during the synthesis because of the chemical corrosion from precursor solution itself. For those reasons, in this report we develop the new PhyC method to encapsulate the CuZnAl core catalyst by only the physical approach. This method defeats disadvantages cause by the hydrothermal method as previous mentioned and also tend to be enlargeable for industrial preparation.

The surface SEM of CuZnAl/SAPO11-PhyC gives the surface morphology of silicoaluminophosphate encapsulated the core CuZnAl catalyst was showed in **Figure 5.8b** and **5.8c**. The bare CuZnAl core catalyst, as a reference of silicoaluminhosphate capsule catalyst, had also been captured by SEM and the image was presented in **Figure 5.8a**. The CuZnAl core catalyst was constructed SAPO-11 silico-aluminophosphate on the surface by the PhyC method using diluted silica as a binder. After physically coating the core catalyst with SAPO-11, its surface became rougher as shown in **Figure. 5.8c**, compared with that of the bare CuZnAl core catalyst in **Figure. 5.8a**, it can be clearly observed the prism shape of SAPO-11 layer. The CuZnAl core catalyst was completely covered and looked uniform and homogeneous by SAPO-11 which it is difficult to find the substrate CuZnAl profile. This indicates the achievement of this new PhyC method for core-shell-like silicoaluminophosphate capsule catalyst preparation. The surface elemental composition of CuZnAl/SPAO11-

PhyC had also been analyzed by EDS and the analysis results are showed in **Figure. 5.8d**. The Si/Al ratio came by EDS on the capsule catalyst surface is 0.45. This is higher than that of the original SAPO-11 silicoaluminophosphate ratio as shown in **Table 5.3**. The latter one was 0.16. The increase of Si content in the SAPO-11 silicoaluminophosphate layer can be clearly understandable if considering the use of silica sol as a binder. Besides, the zero signals of Cu and Zn profiles came by on this SAPO-11 silicoaluminophosphate membrane can prove that the SAPO-11 membrane prepared by this new PhyC method has no crack and hole.

The XRD patterns of the CuZnAl, CuZnAl/SAPO11-PhyC, CuZnAl/SAPO11-M catalysts and pure SAPO-11 were showed in **Figure 5.9**. The diffraction line is identical to the AEL (SAPO-11) framework structure as in the literature, identifying the same structure. The diffraction profiles of SAPO-11 are observed in both of these catalysts. It also found the identical peaks of CuZnAl at 2 theta equal 31, 35, 38 and 47 degree were hardly changed among these catalysts. Therefore it can be concluded that preparation capsule catalyst by this PhyC method does not cause any damages to the core catalyst. Moreover, we can say that the identical peaks to SAPO-11 of CuZnAl/SAPO11-PhyC and CuZnAl/SAPO11-M are weak which can be ascribed by small amount of SAPO-11 content in the catalyst. The nitrogen adsorption is used to determine the specific surface area, total pore volume, and average pore diameter. The properties of catalysts are showed in **Table 5.4**. The PhyC capsule catalyst shows the higher specific surface area over the mixed catalyst. The structure of mixed catalyst consist of CuZnAl and SAPO-11 that blended together may cause the overlap between them resulted in lower specific surface area. The pore volume and average pore diameter of capsule catalyst also higher than those of mixed catalyst. The structure of the catalyst plays the important role on different specific surface area.

The acidic properties of catalysts are evaluates by NH_3-TPD (results showed in Appendix C). For both of PhyC and mixed catalysts, the desorption peaks were found at the same temperature indicating the same kind of acid strength. The amount of acid sites of mixed catalyst was found different from those of PhyC catalyst according to the area under the peak. The amount of acid sites were observed as

CuZnAl/SAPO11-PhyC > CuZnAl/SAPO11-M. The quantitative information on the acidic property was showed in Appendix C.

From these characteristic results, it can be said that the new physical coating method is successful to prepare the SAPO-11 layer on the core CuZnAl catalyst unlike the conventional hydrothermal method which might cause damage to the core catalyst during the long period of time in the hydrothermal unit. This new physical coating method overcomes the disadvantage of the conventional method.

Table 5.3 Elemental analysis of SAPO-11 obtained from EDX analysis

Sample	**Elemental molar composition (mol%)**			**Si/Al**	**Si/(Al+P+Si)**
	Al	P	Si		
SAPO-11	59.7	31.0	9.3	0.16	0.09

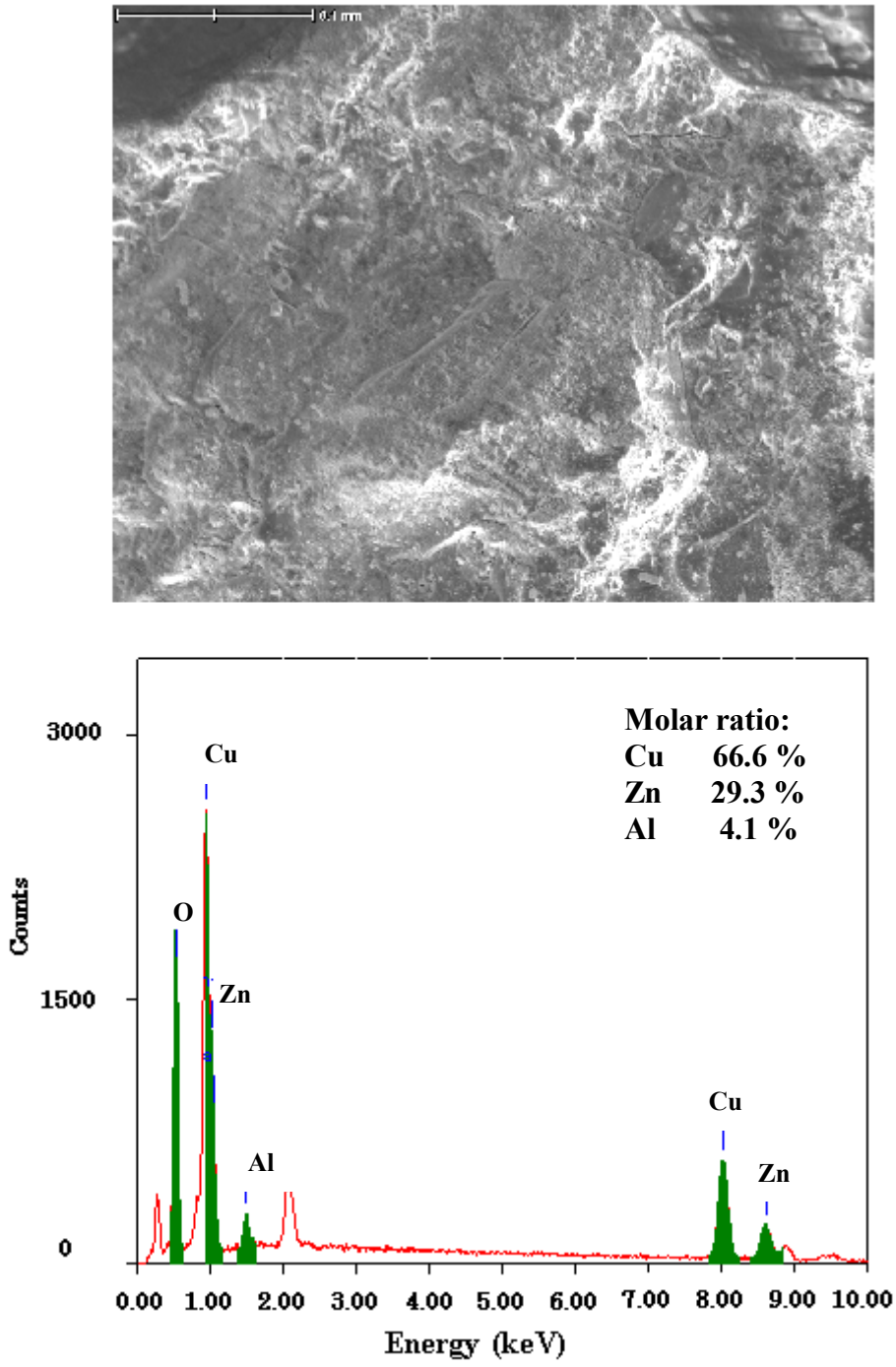

Figure 5.7 Surface EDS analysis of the bare CuZnAl catalyst

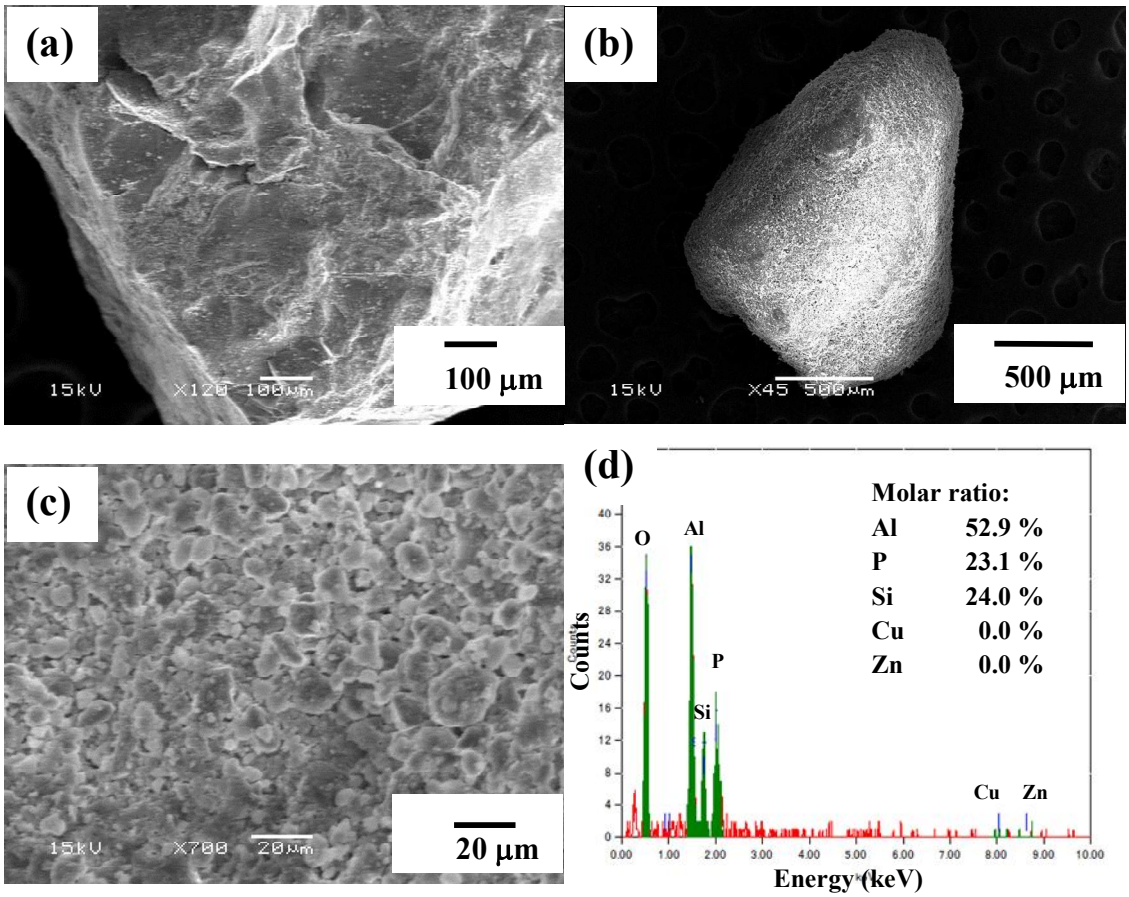

Figure 5.8 SEM images of (a) the CuZnAl catalyst, (b) the physical coating CuZnAl/SAPO-11 catalyst, (c) the surface of the physical coating CuZnAl/SAPO-11 catalyst, and (d) the surface EDS analysis of the physical coating CuZnAl/SAPO-11 catalyst

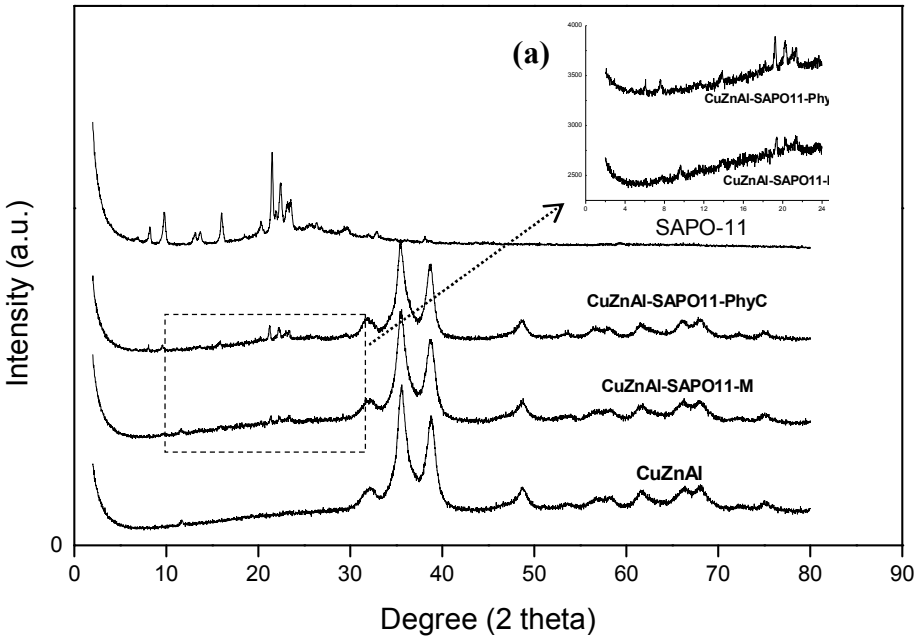

Figure 5.9 XRD diffraction lines of pure SAPO-11, CuZnAl/SAPO11-PhyC, CuZnAl/SAPO11-M, and CuZnAl, catalysts and (a) the magnified characteristic peaks of SPAO-11 of both CuZnAl/SAPO11-PhyC and CuZnAl/SAPO11-M catalysts

Table 5.4 The properties of capsule and mixed catalysts

Sample	**BET surface area (m^2/g)**	**Total pore volume (cc/g)**	**Ave pore diameter (Å)**
CuZnAl	85	0.207	52
CuZnAl/SAPO11-PhyC	90	0.311	138
CuZnAl/SAPO11-M	77	0.243	127

5.2.2 Catalytic test of CuZnAl encapsulated with SAPO-11 for STD reaction

Direct DME production from syngas was performed over the PhyC and mixed catalyst. Also the as-synthesized CuZnAl and Cu-based commercial catalyst had been performed under the same condition to use as references. The catalytic performance of the catalysts is showed in Table 5.5. The high catalytic conversion of capsule catalyst was accounted for 92% was obviously noticed. The capsule catalyst composes of two parts, the core CuZnAl and the membrane SAPO-11. The methanol synthesis reaction occurred at the core center. The formed methanol is systematically converted into DME on the acidic site of SAPO-11 shell via methanol dehydration, which will accelerate the overall reaction rate. It is well known that the one-step DME production from syngas is more thermodynamically favorable than solely methanol dehydration. It should be noted that even though the high CO conversion was obtained from capsule catalyst, the high CO_2 conversion was promoted at the same time, indicating the high rate of water-gas-shift reaction (WGS) was generated.

When consider the higher catalytic activity of the capsule compared with the bare CuZnAl and mixed catalyst, we found that this new coating method protect the core catalyst from crystallization of SAPO-11 in the pores and also from occurring the metal coordination compound which generally occurs in case of using hydrothermal synthesis. The crystallized SAPOs will block pores of the core CuZnAl catalyst leading to the lower Cu species contact are. This problem has been claimed that it was an important factor for DME production in many studies.

The product distribution of the catalysts was showed in **Figure 5.10**. It clearly sees that the extremely high DME selectivity at around 90% can be obtained from the PhyC catalyst. The PhyC catalyst gave almost two times higher DME selectivity than that on the mixed catalyst. This implied that most intermediate product was changed into DME on the acidic sites of SAPO-11 membrane. The confinement effect of core-shell structure of capsule catalyst was the main reason to obtain the high DME yield. This proves that the restricted area all outside core catalyst can help increasing desire product selectivity. The shell membrane created the certain way for formed methanol to pass through the SAPO-11 producing spatial restriction between the core catalyst

particle and the SAPO-11 shell at the same time. On the other hand, for mixed catalyst prepared by mechanical blending, the random converting of methanol into DME on the acid sites of SAPO-11 occurred on this random structure. There was still high amount of remaining methanol in final products. However, the DME selectivity was the major product on this mixed catalyst. Considering the structure of mixed catalyst, that has not been fixed properly, the syngas converted on the CuZnAl to form methanol, and then some part of methanol might be randomly converted into DME on the nearby SAPO-11 acidic sites of the CuZnAl catalyst in the mixed catalyst. The DME might further be converted into higher hydrocarbons on the nearby acidic sites since it diffused away without spatial restriction. However, it was a little amount of higher hydrocarbons formed on this the mixed catalyst of Cr/ZnO and SAPO-11. The remaining methanol might not be converted into DME without contact acidic sites of SAPO-11. By the structure of mixed catalyst, the random reactions took place in unordered sequential reactions. Unlike the spatial core-shell structure of capsule catalyst, the sequential reaction took place at the core and shell membrane. This is effective not only for ordering the consecutive reaction to occur at the specific active sites, but also for preventing DME diffuse back to further react into alkane/alkene by products. Consequently, the high DME selectivity and low amount of alkanes/alkenes was obtained. The moderate acid sites of SAPO-11 should be considered to give an influence on products selectivity too. Its moderate acid strength of SAPO-11 was suitable for methanol dehydration into DME in STD synthesis. Considering the results between bare CuZnAl catalyst and mixed catalyst, the major product DME selectivity was accounted for 47% for mixed catalyst whereas that from CuZnAl catalyst was zero. The obviously high DME selectivity should be ascribed to the core-shell-like structure of capsule catalyst and the suitable acid catalyst SAPO-11 membrane.

The catalytic conversion of CO on PhyC catalysts was surprisingly high at 92% whereas those on mixed and bare core catalysts were 65 and 51%, respectively. The methanol synthesis rate occurred on core catalyst has been affected by methanol dehydration rate occurred on SAPO-11 shell membrane. It should be note that the methane selectivity was zero for capsule catalyst and very small for mixed catalyst, this result can be suggested that the methanol dehydration rate on SAPO-11 is much

higher than methanol synthesis rate. Hence, the properties of acid catalyst such as framework structure and acid strength of the SAPO-11 for direct DME synthesis might play an important role for higher catalytic performance. The AEL framework structure possesses one-dimensional 10 member ring channel size which tends to provide easily accessible route for small molecule such as methanol to diffuse through and convert into DME. This is also true when we consider on the random structure of mixed catalyst.

These results showed that the CuZnAl/SAPO11-PhyC capsule catalyst is not only a successful catalyst for enhancing DME selectivity but also is a promising catalyst for STD synthesis. The new physical coating catalysts were prepared without any special equipment or technologies but presented the remarkable reaction results in direct STD synthesis. Therefore this new method should be applied to other zeolites to coat on the core catalyst to benefit the spatial structure of the capsule catalyst.

In brief, the core CuZnAl catalyst coated by SAPO-11 was successfully prepared by mechanical physical coating method. The characterization SEM & EDS and XRD showed the coated membrane was finely covered and uniformly attached. The high catalytic activities over capsule catalyst were obtained. The moderate acid sites of SAPO-11 accelerated reaction rate of the overall sequential reaction leading to the high catalytic conversion. The same partway of capsule and mixd catalyst in **Figure 5.6** could be referred to explain the good results of catalytic activity of capsule catalyst over mixed catalyst as well.

Table 5. 5 Catalytic performance of CuZnAl/SAPO-11 catalyst

Sample	Conversion[a] (%)			Selectivity (%)				Yield DME (%)
	CO	CO_2	total	CH_4	MeOH	DME	Others	
CuZnAl	51.0	-16.7	42.1	0.3	96.8	0.0	2.9	0.0
CuZnAl/SAPO11-PhyC	92.0	-163.7	58.5	0.0	9.2	90.3	0.5	83.1
CuZnAl/SAPO11-M	64.9	-77.3	46.2	0.1	51.4	46.6	1.9	30.2
Cu based commercial	50.7	-10.9	42.7	0.3	98.9	0.5	0.3	0.25

[a] Reactions conditions: 250°C, 5.3 MPa, $W_{Cr/ZnO}/F_{Syngas}$ = 10 g·mol/h;

Experimental data were obtained at the fifth hour of reaction.

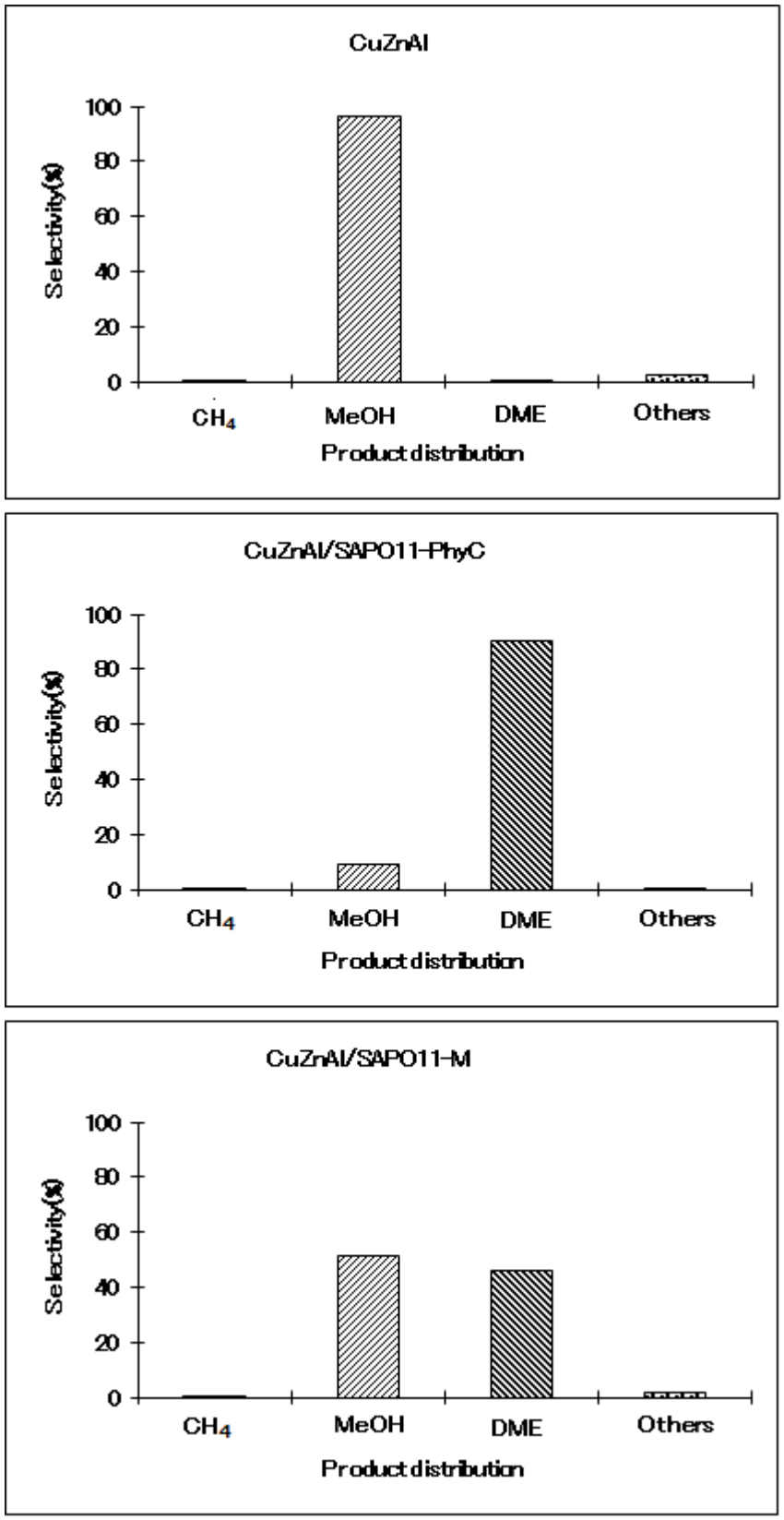

Figure 5.10. Product distribution and selectivity of the CuZnAl, CuZnAl/SAPO11-PhyC, CuZnAl/SAPO-M, and commercial based catalyst

CHAPTER VI

FACTORIAL DESIGN OF Cr/ZnO AND SAPO-11 MIXED CATALYST

The study about the experimental design by using 2^k factorial was focus on 3 parameters that is $W_{core\ catalyat}/F_{syngas}$ ratio, reaction temperature, and weight ratio of Cr/ZnO and SAPO-11. The optimum desire parameter was evaluated among these 3 factors by normal 2^3 experiments and also added another 3 face center point including the face center cubic 8 run. The interpretation from the data shows the optimum contour graph and mathematical model.

Factorial design has been applied to many studied for studying the main effect or interaction effect between each parameters. Furthermore, it can optimize the factor effects to improve the response. The analysis procedure for factorial design is as follow—the first step is to estimate the factor effects and their magnitude. The second step is forming the initial model which usually is the full model providing at least one of the design points has been replicated. Then in step 3, use the analysis of variance to test the significant main effects or interaction effects. Step 4, adjust the model by removing the non-significant variables. Step 5, analyze the residuals to check adequacy and assumptions. Finally, report the graphical analysis in the form of either main effect or interaction graph or contour and response plots.

In this study we focus on the of effect of three important parameters that are W/F ratio, reaction temperature, and weight ratio of SAPO11 : Cr/ZnO. The maximum and minimum values of three parameters were showed in **Table 6.1**. Variable A is W/F ratio, Variable B is Temperature and Variable C is SAPO11: Cr/ZnO weight ratio. Coded variables and catalytic performance of each condition were showed in **Table 6.2**. The Table shows the catalytic conversion and product selectivity of all experiments in low and high level and also including 3 center points

and another 6 face center cubic points. The contrast constant for 2^3 factorial design was showed in **Table 6.3**.

Table 6.1 The maximum and minimum levels of parameters

Variable	Name	(-1) Low	(0) center	(+1) High	[unit]
A	$W_{Cr/ZnO}/F_{sysgas}$ ratio	10	15	20	-
B	Temperature	300	350	400	°C
C	SAPO11:Cr/ZnO ratio	0.1	0.5	0.9	-

The simplified method to manage the high level and low level of each effect is to do process called coded variables which it will change the large value of the parameter's conditions to be the smallest number and easier to calculate. We named the coded variable as the following below.

Coded variable A: $$x_1 = \frac{\frac{W}{F} - \frac{(20+10)}{2}}{\frac{(20-10)}{2}}$$

Coded variable B: $$x_2 = \frac{Temp - \frac{(400+300)}{2}}{\frac{(400-300)}{2}}$$

Coded variable C: $$x_3 = \frac{SAPO11:Cr/ZnO - \frac{(0.9+0.1)}{2}}{\frac{(0.9-0.1)}{2}}$$

The reaction procedure was similar to that described in Chapter 3. The reaction conditions were as follow temperature 350 °C, pressure 5 MPa, W/F ratio 10 g.mol/h. The catalytic results of all factorial experiments were showed in **Table 6.2**.

In order to study the significance of the process operating parameters and compare the response of each variable on the system target, selected as DME selectivity and CO conversion, and to optimize the latter parameter values, a contrast constant table was prepared according to 2^k factorial design method. In the analysis, 3 factors with 2 levels and center points were selected. Parameter W/F ratio and reaction temperature both affect mainly on reaction kinetic. Whereas SAPO11: Cr/ZnO weight ratio have impact on thermodynamic on fixed bed system. The operating parameters for the reaction systems were determined from Experimental design and the results are summarized in **Table 6.2**.

Table 6.2 Contrast constant for 2^3 Design and responses

Treatment Combination	Factorial Effect							Outcome1	Outcome2
	A	B	AB	C	AC	BC	ABC	CO conversion (%)	DME selectivity (%)
(-1)	-1	-1	1	-1	1	1	-1	7.9	58.8
a	1	-1	-1	-1	-1	1	1	13.1	75.3
b	-1	1	-1	-1	1	-1	1	9.2	38
ab	1	1	1	-1	-1	-1	-1	10.3	29.4
c	-1	-1	1	1	-1	-1	1	6.2	80.9
ac	1	-1	-1	1	1	-1	-1	12.8	81.3
bc	-1	1	-1	1	-1	1	-1	26	3.6
abc	1	1	1	1	1	1	1	65.2	0.2

The main effect of A, B and C and interaction effect

Three main effects of A, B and C are plotted in **Figure 6.1**. All of these variables are positive if we consider only CO conversion, but there are negative for DME selectivity. The BC, AC, and AB interactions effects are plotted in **Figure 6.2**. The graph that has intersection point is pointing out that how each parameter affects the responses. In this experiment, we found that BC interaction might affect both response, CO conversion and DME selectivity.

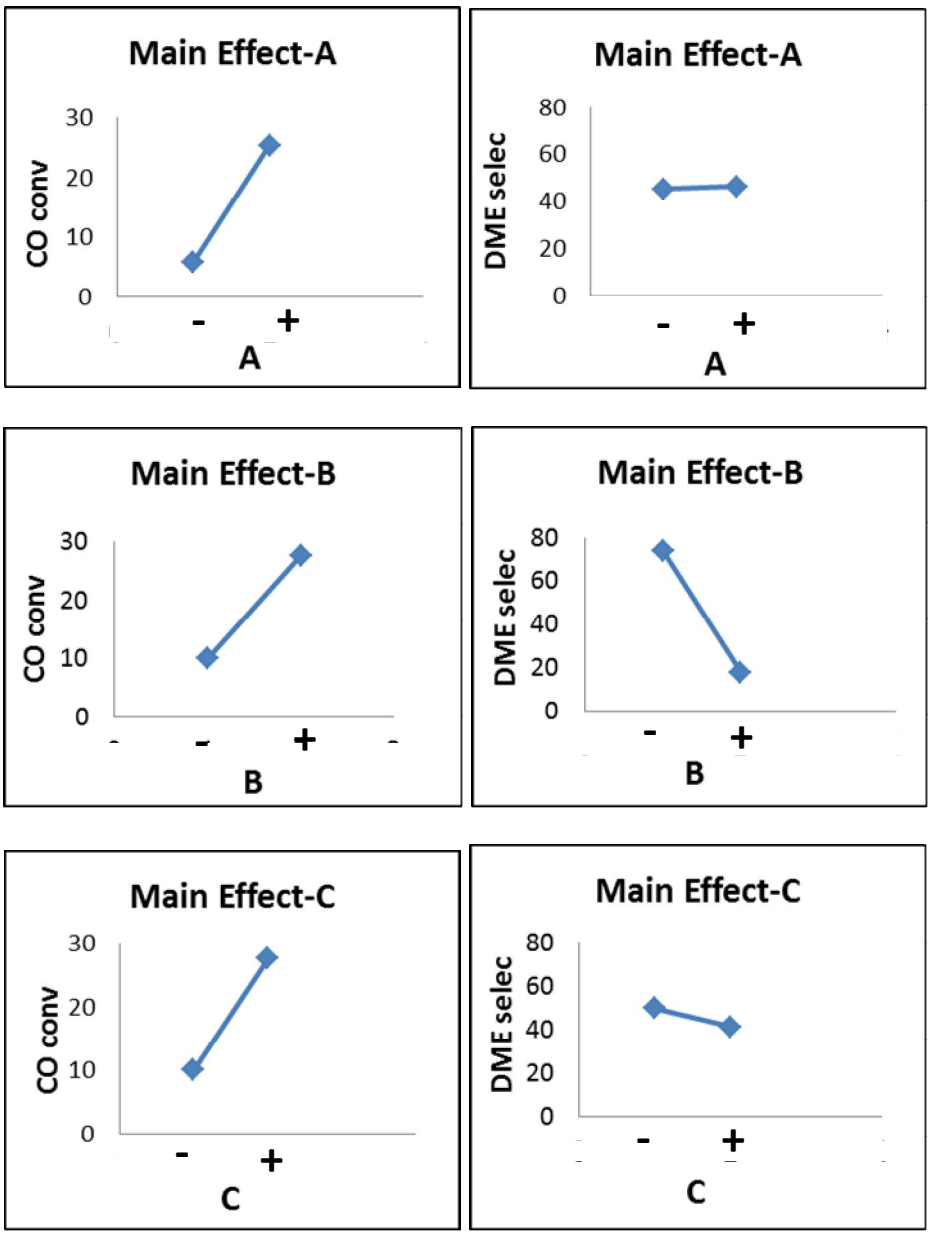

Figure 6.1 The main effect plots

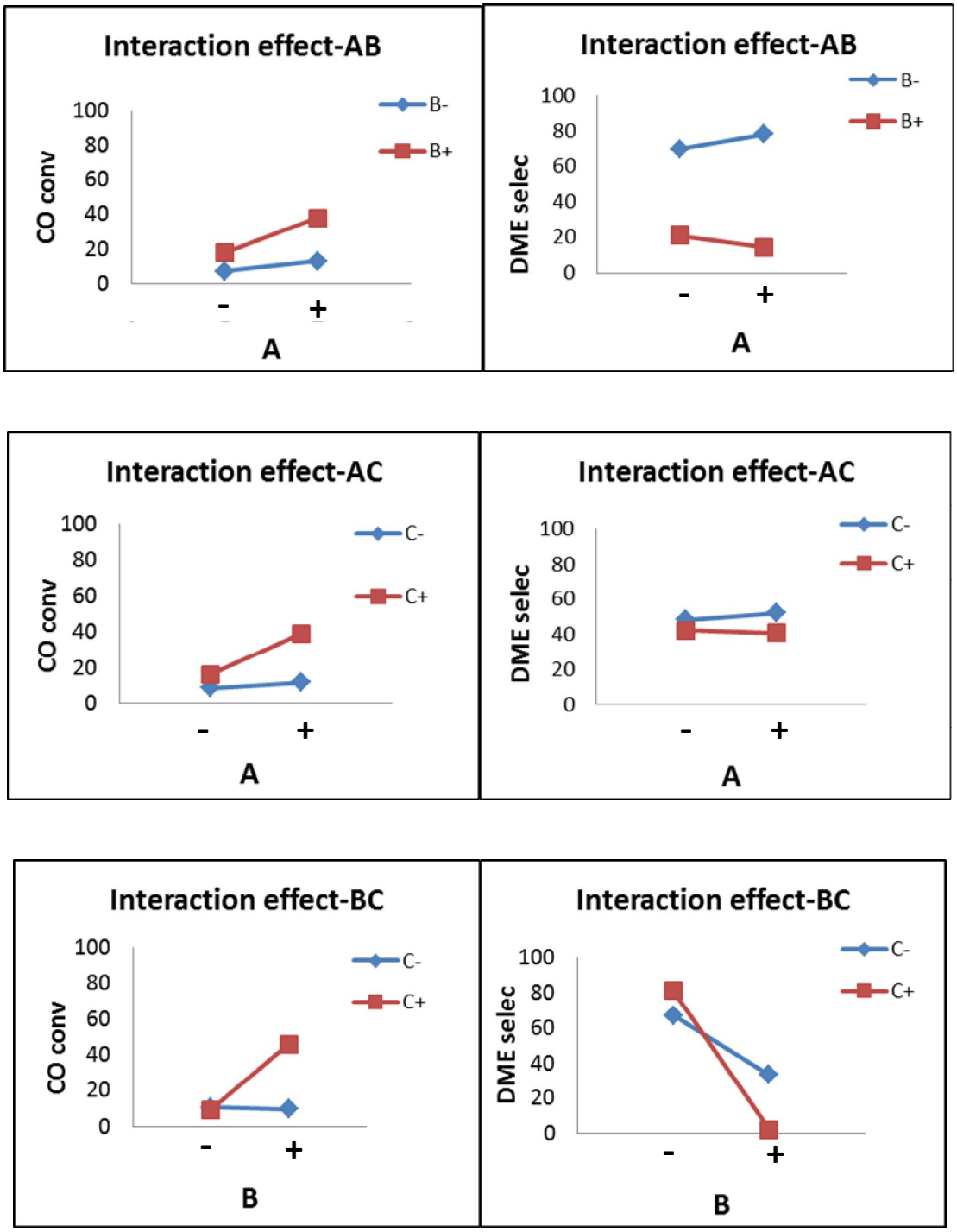

Figure 6.2 The interaction effect plots

6.1 The CO conversion modeling

Furthermore, we further calculated the effect estimated and sum of square for all of the factorial effect as shown in **Table 6.3**. We found that effect B, C and BC tend to be the important factor for this experiment, and then we choose these three effects to do the analysis of variance (ANOVA) as shown in **Table 6.4**. ANOVA is now used to reconfirm that each effect gave impacts in this experiment considering from the P-value. If P-value is very low (normally less than 0.05) that mean the effect we chose is the right one. For the ANOVA of outcome 1 the P-value is low but not lowers than 0.05 which implied that our results might not enough to fit this experiment. If we further calculate the mathematical model for predicting CO conversion we will find the large residual and when we plotted the residual with the predicted value, we get the divergent structure-like graph as shown in **Figure 6.3**. This graph can implied this model is not complete and not the right model for predicting CO conversion. Then the author have introduced more the experiments, pure quadratic center, into these experiments to check whether it has the effect of the second order term or not. It found the second term order might give effects considering from the P-value of curvature as shown in **Table 6.5**. The ANOVA table for reduced model of outcome 1 was showed in **Table 6.6**. The interpretation from the reduced model showed the difference. It interpretation obtained from the ANOVA for reduced model found that the curvature term did not give significant effect to the model consider from the P-value higher than 0.05. However, if we further do more experiment or replicate of all the experiment we might get the complete model.

The model from the preliminary analysis is

$$\hat{y}_1 = 18.84 + 6.51x_1 + 8.84x_2 + 8.71x_3 + 9.21x_2x_3$$

Table 6.3 The summary of effect estimate table for outcome1

Factors	Regression Coefficient	Estimated Effect	Sum of Squares	Percent distribution
Overall ave	18.8375			
A	6.5125	13.025	339.3013	12.49609
B	8.8375	17.675	624.8113	23.01111
AB	3.5625	7.125	101.5313	3.739285
C	8.7125	17.425	607.2613	22.36477
AC	4.9375	9.875	195.0313	7.182787
BC	9.2125	18.425	678.9613	25.0054
ABC	4.5875	9.175	168.3613	6.20056

Table 6.4. Analysis of Variance (ANOVA) of outcome1

Source of variation	**Sum of square**	**DF**	**Mean square**	**F_0**	**P-values**
B	624.8113	1	624.8113	4.1462	0.0435
C	607.2613	1	607.2613	4.0297	0.0465
BC	678.9613	1	678.9613	4.5056	0.0354
Error	1054.8517	7	150.6931		
Total	2965.885	10			

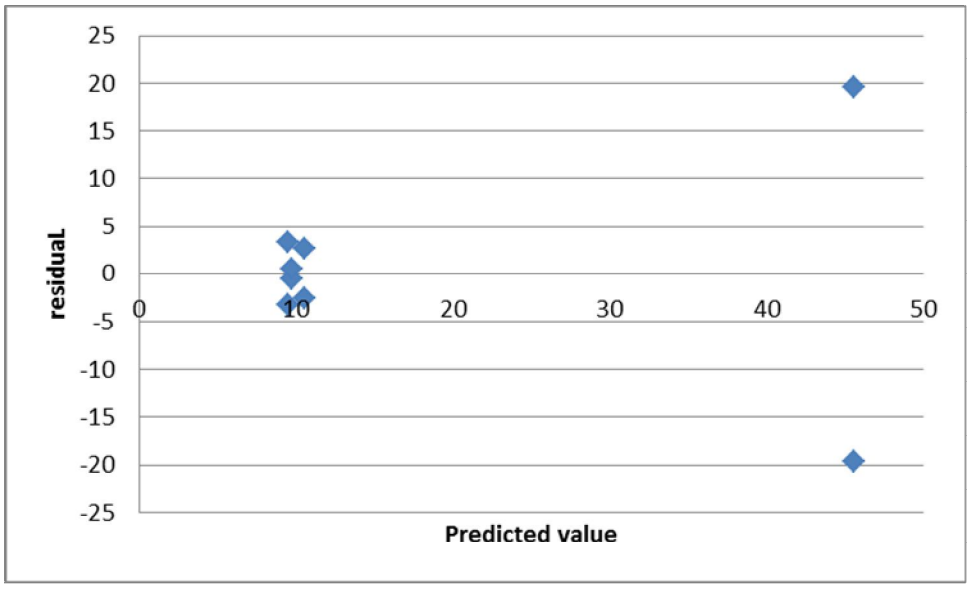

Figure 6.3 The divergent structure-like graph for out come1

Table 6.5 ANOVA for the full model (of outcome1)

Source of variation	Sum of square	DF	Mean square	F_0	P-values
Model	2715.26	7	387.89	39.99	0.0246
A	339.30	1	339.30	34.98	0.0274
B	624.81	1	624.81	64.41	0.0152
AB	101.53	1	101.53	10.47	0.0837
C	607.26	1	607.26	62.60	0.0156
AC	195.03	1	195.03	20.11	0.0463
BC	678.96	1	678.96	69.99	0.0140
ABC	168.36	1	168.36	17.36	0.0531
Pure quadratic					
Curvature	195.08	1	195.08	20.11	0.0463
Pure error	19.40	2	9.70		
Core total	2929.74	10			

Table 6.6 ANOVA for reduced model (of outcome1)

Source of variation	Sum of square	DF	Mean square	F_0	P-values
Model	2250.33	4	562.58	5.81	0.0403
A	339.30	1	339.30	3.5	0.1202
B	624.81	1	624.81	6.4	0.0519
C	607.26	1	607.26	6.27	0.0542
BC	678.96	1	678.96	7.00	0.0455
Pure quadratic					
Curvature	195.08	1	195.08	2.01	0.2151
Residuals	484.32	5	96.86		
Pure error	19.4	2	9.7		
Lack of fits	464.92	3	154.97	15.97	0.0595
Core total	2929.74	10			

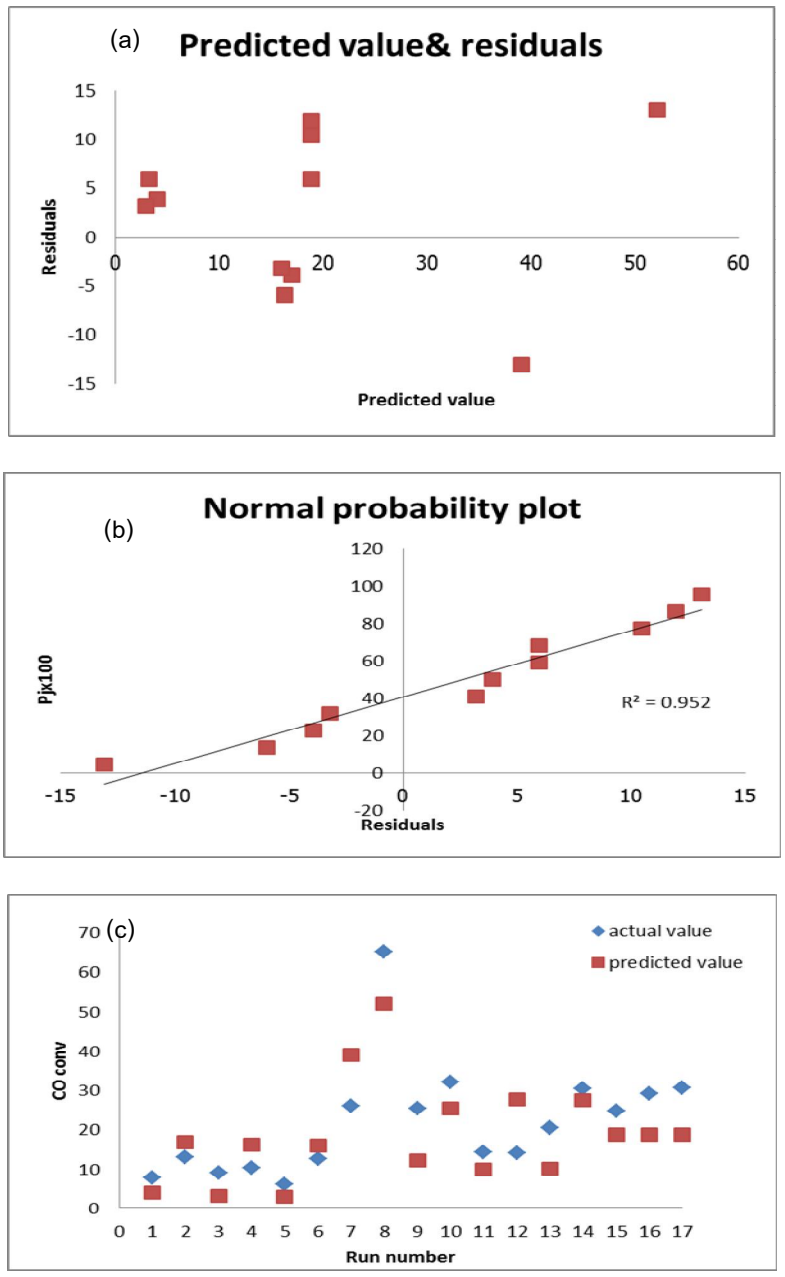

Figure 6.4 (a) the predicted value and residual plot, (b) the normal probability plot, and (c) the CO conversion of predicted and actual value

In order to check the structure less of the predicted and residual plot, the Modified Levene test was introduced to the analysis (the Modified Levene can be done by minus each outcome with the median and then do ANOVA again to check P-value). And after that the ANOVA analysis was done again to check the significant P-

value. The results showed that the P-value of curvature term was 0.1566 which higher than 0.05, therefore, it can be implied that curvature term does not affect the model we obtained so we still resist the same equation that is

$$\hat{y}_1 = 18.84 + 6.51x_1 + 8.84x_2 + 8.71x_3 + 9.21x_2x_3 \quad \text{.....eq. 6.1}$$

Or replaced the coded variable with the actual parameter, we obtained

$$COconv = 18.84 + 6.51\left(\frac{\frac{W}{F} - \frac{(20+10)}{2}}{\frac{(20-10)}{2}}\right) + 8.84\left(\frac{Temp - \frac{(400+300)}{2}}{\frac{(400-300)}{2}}\right) +$$
$$8.71\left(\frac{SAPO11:Cr/ZnO - \frac{(0.9+0.1)}{2}}{\frac{(0.9-0.1)}{2}}\right) +$$
$$9.21\left(\frac{Temp - \frac{(400+300)}{2}}{\frac{(400-300)}{2}}\right)\left(\frac{SAPO11:Cr/ZnO - \frac{(0.9+0.1)}{2}}{\frac{(0.9-0.1)}{2}}\right)$$

The contour graph of this mathematical model was created by the program named DX6 were showed in **Figure 6.5**. From the graph we can should the condition for the experiment in order to determine the result beforehand.

Table 6.7 ANOVA of the model after operating the Modified Levene

Source of variation	Sum of square	DF	Mean square	F_0	P-values
Model	2094.51	7	299.21	30.85	0.0317
A	86.46	1	86.46	8.91	0.0962
B	439.56	1	439.56	45.31	0.0214
AB	311.25	1	311.25	32.09	0.0298
C	454.51	1	454.51	46.85	0.0207
AC	189.15	1	189.15	19.50	0.0476
BC	369.21	1	369.21	40.84	0.0236
ABC	217.36	1	217.36	22.41	0.0418
Pure quadratic					
Curvature	47.80	1	47.80	4.93	0.1566
Pure error	19.40	2	9.70		
Core total	2161.71	10			

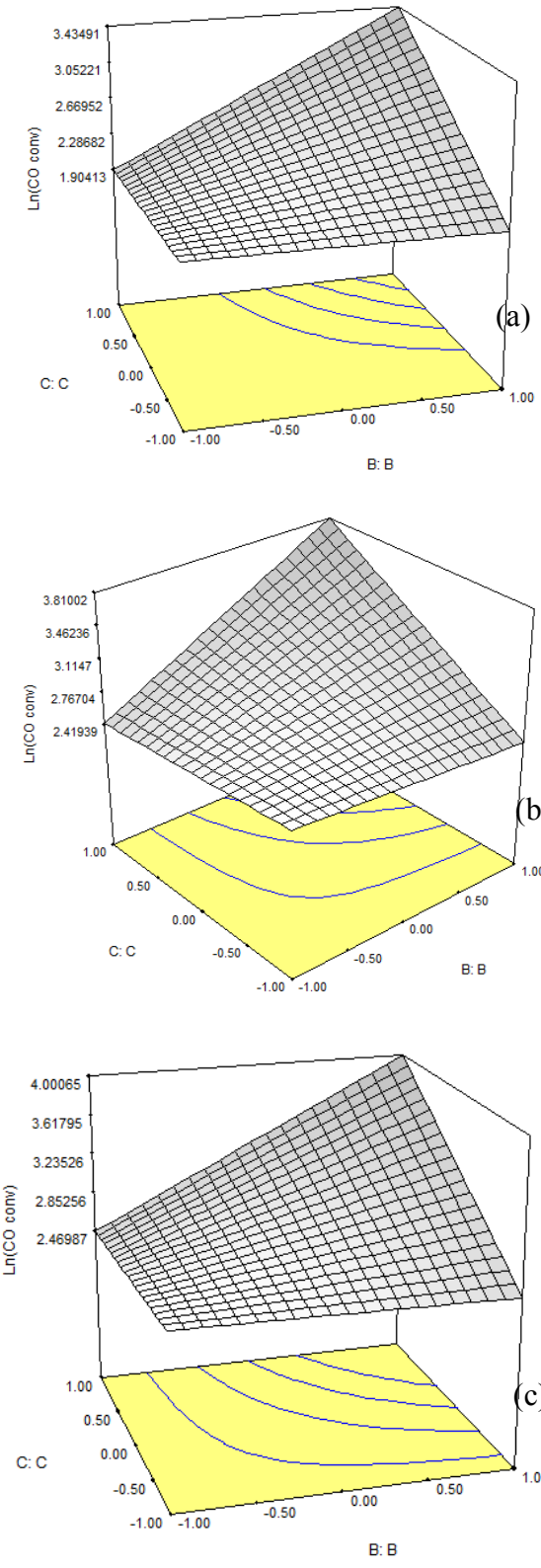

(a) at low(-) level of A

(b) at middle level of A

(c) at high(+) level of A

Figure 6.5 The contour graph of parameter B and C at (a) low, (b) middle, and (c) high level of parameter A on CO conversion

6.2 The DME selectivity modeling

For analysis of outcome 2 (DME selectivity), the similar analysis procedure was doing for this analysis as well. The effect estimate of each parameter was showed in **Table 6.8**. The effect B, C, and BC covered large proportion for of all effect estimates. Therefore, the ANOVA analysis of reduced model of B, C and BC was calculated and showed in Table 6.9. The model obtained from this preliminary analysis is

$$\hat{y}_2 = 45.94 - 28.14x_2 - 4.44x_3 - 11.46x_2x_3 \qquad \text{.....eq. 6.2}$$

After that, the residual was calculated from the different between the predicted value from the model and the actual value and was plotted in **Figure 6.6**. It can be clearly seen the divergent-like structure of the graph which means to the inadequate of the data analysis to evaluate the model therefore, more experiments needed to be added. The extra center point experiments were performed. Both the full and reduced ANOVA analysis said the curvature term gave impact to the model as the P-value went much lower than 0.05. As a result, to further evaluated the good model, more experiment at the face center cubic point were added and with the help of regression equation we obtained the regression coefficient showed in **Table 6.13**. The ANOVA analysis was made to confirm the results and showed in **Table 6.12**. Finally, we obtained the mathematical model evaluated from these data.

$$\hat{y}_2 = 76.45 - 28.83x_2 - 11.39x_2x_3 - 22.48x_2^2 \qquad \text{.....eq. 6.3}$$

This equation is the simplified form of coded parameter. In order to apply to use in STD reaction, each coded variable in the equation should be replace by the actual parameter. That is

$$DMEselectivity = 76.45 - 28.83\left(\frac{Temp - \frac{(400+300)}{2}}{\frac{(400-300)}{2}}\right) -$$

$$11.39\left(\frac{Temp - \frac{(400+300)}{2}}{\frac{(400-300)}{2}}\right)\left(\frac{SAPO11:Cr/ZnO - \frac{(0.9+0.1)}{2}}{\frac{(0.9-0.1)}{2}}\right)$$

$$-22.48\left(\frac{Temp - \frac{(400+300)}{2}}{\frac{(400-300)}{2}}\right)^2$$

The predicted value and residuals graph, normal probability plot value are showed as following. And also the actual and predicted values were showed in **Figure 6.7**. The contour graph of this model was showed at the low and high level of parameter A in **Figure 6.8**.

As we can see from both model of CO conversion and DME selectivity, we found that parameter of reaction temperature (B) and catalyst weight ratio (C) showed the significant impact to the catalytic activity of STD reaction. And also the interaction effect of reaction temperature and catalyst weight ratio (BC) and the square term of reaction temperature, B^2 show the significant meaning in the model as well. The reaction temperature is the kinetic parameter which it tends to give lots impacts to the catalytic activity and is confirmed by the factorial design.

Table 6.8 The summary of effect estimate for outcome 2

Effect	Regression Coefficient	Estimated Effect	Sum of Squares	Percent Distribution
Overall ave	45.9375			
A	0.6125	1.225	3.00125	0.038869
B	-28.1375	-56.275	6333.7513	82.02897
AB	-3.6125	-7.225	104.40125	1.35211
C	-4.4375	-8.875	157.53125	2.040201
AC	-1.3625	-2.725	14.85125	0.19234
BC	-11.4625	-22.925	1051.1113	13.61303
ABC	2.6625	5.325	56.71125	0.734472

Table 6.9 ANOVA of STD synthesis of outcome2

Source of variation	Sum of square	DF	Mean square	F_0	P-values
B	6333.7513	1	6333.75125	25.1592	9.994E-07
C	157.5313	1	157.53125	0.62575	0.42966
BC	1051.1113	1	1051.11125	4.17526	0.04206
Error	1762.2317	7	251.7474		
Total	9304.6254	10			

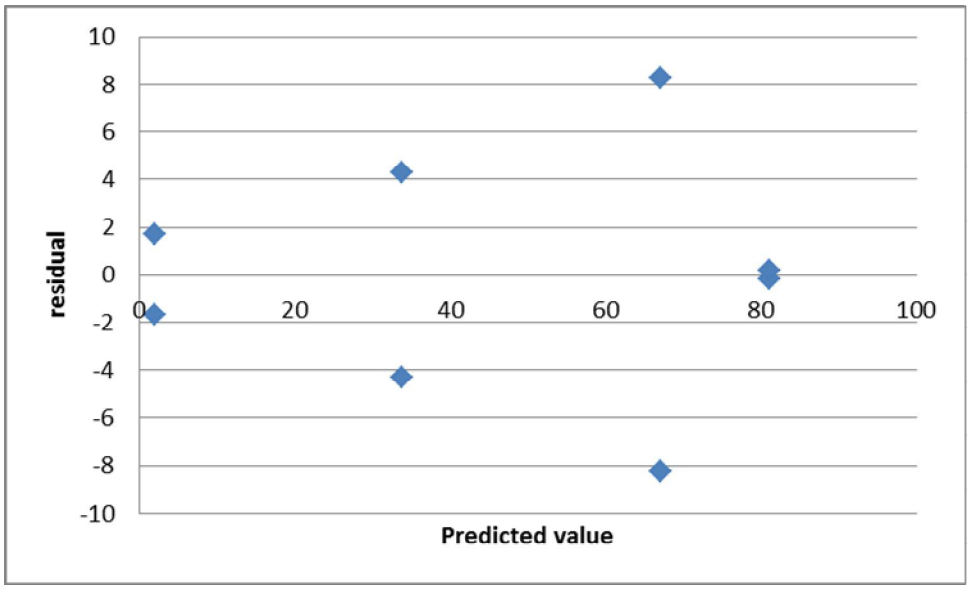

Figure 6.6 The divergent structure-like graph of predicted value and residual of outcome 2

Table 6.10 ANOVA for the full model of outcome 2 after add the center point experiments

Source of variation	Sum of square	DF	Mean square	F_0	P-values
Model	7721.3588	7	1103.05125	248.4349662	0.048814
A	3.0013	1	3.00125	0.675957207	0.561935
B	6333.7513	1	6333.75125	1426.520552	0.016852
AB	104.4013	1	104.40125	23.51379505	0.129471
C	157.5313	1	157.53125	35.48001126	0.105891
AC	14.8513	1	14.85125	3.344876126	0.318542
BC	1051.1113	1	1051.11125	236.736768	0.041318
ABC	56.7113	1	56.71125	12.77280405	0.173688
Pure quadratic					
Curvature	1574.386705	1	1574.386705	354.5916001	0.033776
Pure error	8.8800	2	4.44		
Cor total	9304.6255	10			

Table 6.11 ANOVA for the reduced model of outcome 2 after the center point experiments

Source of variation	Sum of square	DF	Mean square	F_0	P-values
Model	7542.3937	3	2514.1312	80.30444	3.1101E-05
B	6333.7513	1	6333.75125	202.30779	7.5498E-06
C	157.5313	1	157.53125	5.03174	0.06606
BC	1051.1113	1	1051.11125	33.57378	0.001157
Pure quadratic					
Curvature	1574.386705	1	1574.386705	50.28784	0.000394
Residuals	187.845	6	31.3075		
Pure error	8.8800	2	4.44		
Lack of fits	178.965	4	44.74125	10.07685	0.092311
Cor total	9304.6255	10			

Table 6.12 ANOVA for the full model after operating regression model

Source of variation	Sum of square	DF	Mean square	F_0	P-values
Model	12259.23	10	1225.923	14.5771	0.001918
A	1.1552	1	1.1552	0.013736	0.910525
B	6649.351	1	6649.351	79.06557	0.000113
AB	108.7813	1	108.7813	1.293487	0.298777
C	106.58	1	106.58	1.267313	0.303276
AC	13.26125	1	13.26125	0.157686	0.705036
BC	1037.401	1	1037.401	12.33545	0.012638
ABC	59.95125	1	59.95125	0.712864	0.430866
A2	55.49534	1	55.49534	0.65988	0.447625
B2	4044.171	1	4044.171	48.08811	0.000446
C2	183.0782	1	183.0782	2.176931	0.190544
Error	504.5952	6	84.0992		
Total	12763.82	16			

Table 6.13 Regression coefficient obtained from regression equation

Variation	Regression Coefficient	Contrast	Estimated Effect	Sum of Square
Overall	76.4478			
A	0.38	3.04	0.76	1.1552
B	-28.83	-230.64	-57.66	6649.351
AB	-3.6875	-29.5	-7.375	108.7813
C	-3.65	-29.2	-7.3	106.58
AC	-1.2875	-10.3	-2.575	13.261
BC	-11.3875	-91.1	-22.775	1037.401
ABC	2.7375	21.9	5.475	59.951
A_2	-2.6338	-21.07	-5.2676	55.495
B^2	-22.4838	-179.87	-44.9676	4044.17
C^2	-4.7838	-38.27	-9.5676	183.078

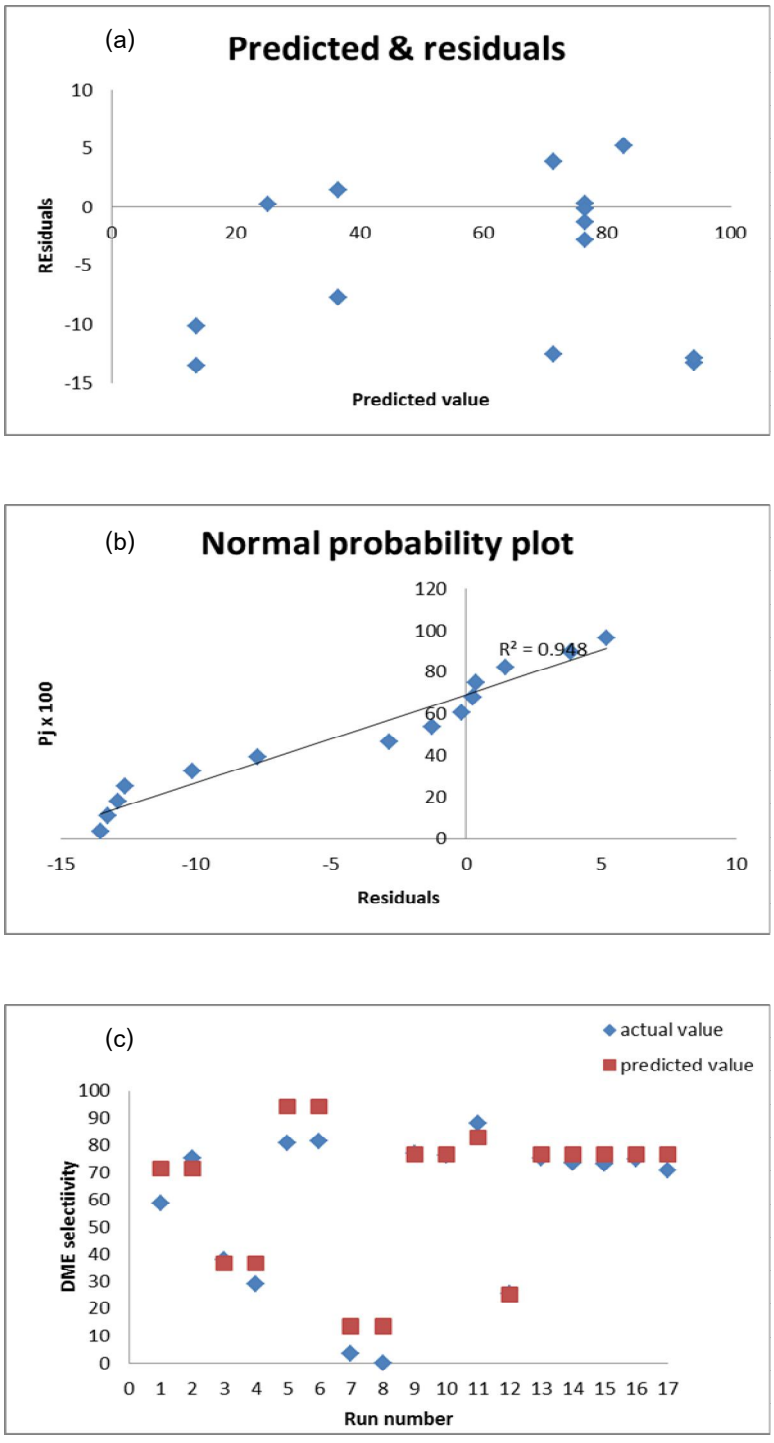

Figure 6.7 (a) the predicted value and residual plot, (b) the normal probability plot, and (c) the DME selectivity of predicted and actual value

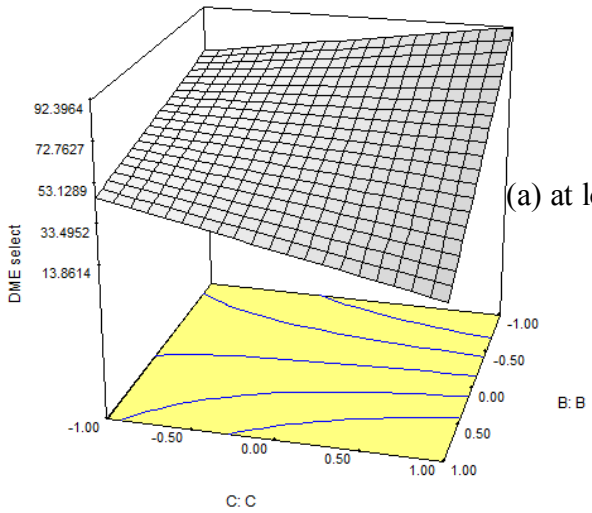

(a) at low (-) level of A

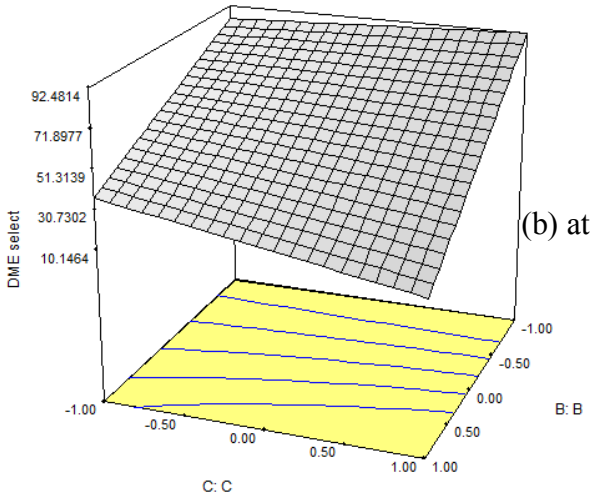

(b) at high (+) level of A

Figure 6.8 The contour graph of parameter B and C at (a) low and (b) high level of parameter A on DME selectivity

CHAPTER VII

CONCLUSIONS

The main study was the capsule catalyst system of Cr/ZnO/SAPO46 and CuZnAl/SAPO11 on direct DME synthesis through STD reaction. The capsule catalysts were characterized by X-ray diffraction (XRD), scanning electron microscopy (SEM) and energy-diffusive X-ray spectroscopy (EDS). Furthermore, the study of mixed catalysts of various zeolites ($AlPO_4$-5, $AlPO_4$-11, SAPO-11 and SAPO-46) and Cr/ZnO were studied and characterized by those analysis methods and also the N_2-physisorption and temperature programmed desorption of ammonia (NH_3-TPD) as well. The experimental design with 2^3 factorial was performed on three parameters; $W_{Cr/ZnO}/F_{syngas}$ ratio, reaction temperature and weight of methanol dehydration to methanol synthesis catalyst (SAPO11: Cr/ZnO). The aim of this work is studying the characterization and catalytic activity of all capsule catalyst synthesized by PhyC (physical coating) method and the supplement section of preliminary study about the activity of acid catalysts and 2^k factorial design.

7.1 The various types of zeolite study

The study of the various types of zeolite in STD synthesis, we can conclude that the SAPO-11 is promising to be a good acid catalyst for DME synthesis through the direct STD reaction which showed DME yield at 17.6% with a good selectivity (81.1%). The SAPO-46 showed the smallest catalytic performance among these catalysts although it showed high amount of acid site. Besides the acidic properties, the framework structure should be considered as an important factor to effluent the catalytic activity of the reaction as well.

7.2 The capsule catalyst study

This study emphasizes on the development of capsule catalyst system Cr/ZnO-SAPO46 and CuZnAl-SAPO11 prepared by the new method. The direct DME synthesis through synthesis gas was selected to test to catalytic performance of them. The summary of these experiments were showed below.

The core catalysts coated by zeolite membrane were successfully prepared by mechanical approach named physical coating method. The physical coating method has been designed for preparing the encapsulated capsule catalyst with the SAPO-46 and SAPO-11. The characterization SEM & EDS and XRD showed the coated membrane was finely covered and uniformly attached. The characterization of the prepared capsule catalyst showed that this new method was easy to prepare the SAPO-46 shell on the Cr/ZnO core catalyst and the SAPO-11 shell on the CuZnAl core catalyst without damaging the core catalyst. The capsule catalyst Cr/ZnO-SAPO46-PhyC and CuZnAl/SAPO11-PhyC showed very good selectivity of DME synthesis through STD reaction compare with the mixed catalyst Cr/ZnO-SAPO46-M and CuZnAl/SAPO11-M. The PhyC catalyst provided an effective controlled synthesis reaction for syngas to convert to target product. These consecutive reactions resulted in higher catalytic performance in the STD synthesis. The benefit of core-shell-like structure will confine the methanol and restrict them to convert to DME on the acid site ofzeolites. This helped the reaction occurs in well-ordered and as a consequence, the high selectivity of DME was obtained. The alkanes/alkenes byproducts was suppressed due to no further deep dehydration of DME into higher hydrocarbons when pass through the membrane structure. The CuZnAl/SAPO11-PhyC capsule catalyst showed high DME yield (83.1%) with a high selectivity (90.3%) whereas the Cr/ZnO-SAPO46-PhyC capsule catalyst showed DME yield at 2.5 % with 37% selectivity. The reaction results confirmed the core-shell-like structure is effective and practical for DME selective through STD reaction. This new method could be performed under normal ambient conditions without any special equipment needed and also is simple, repeatable and accessible for apply to various zeolite catalysts.

7.3 The study of 2^3 factorial design

The 2^3 factorial design was evaluated to obtain the optimum conditions among these three parameters. The mathematical modal obtained from the experiment showed that in the sense of CO conversion, the reaction temperature and catalyst weight ratio between methanol synthesis and acid catalyst gives the important impact on the first order model. While the second order term of reaction temperature plays more impact on the DME selectivity and also the first order term of reaction temperature and weight ratio between methanol synthesis and acid catalyst. The response of CO conversion and DME selectivity showed that there has one effect in common, the reaction temperature.

7.4 Suggestions

Further kinetics study on capsule catalyst should be studied on going together with the mathematical model. And this coating method should be applied to prepare with the various zeolite in order to coat the capsule catalyst for other applications. This idea also should be further brought to the study in other fields that needed the spatial structure of two active sites in two consecutive different reactions. The other effects should be studied more in 2^k factorial design as well in order to obtain more accurate model from the experiments, for example, the effect of calcination temperature after preparing catalyst coating preparation. The long period of time of heating treatment might be one factor damages the pore structure of zeolite and might result in the ability to adsorb NH_3 gas in temperature programmed analysis of capsule catalyst.

REFERENCES

[1] Yaripour, F., Baghaei, F., Schmidt, I. and Perregaard, J. Catalytic dehydration of methanol to dimethyl ether (DME) over solid-acid catalysts. Catalysis Communications 6 (2005) : 147-152.

[2] Herrera, G., Lardizabal, D., Martinez, V.H.C. and Elguezabal, A.A. Dehydroisomerization of n-pentane to isopentene on molecular sieves impregnated with platinum. Catalysis Letters 76 (2001) : 161-166.

[3] Kong, W.B., Dai, W.L., Li, N., Guan, N.J. and Xiang, S.H. A one-step route to SAPO-46 using H_3PO_3-containing gel and its application as the catalyst for methanol dehydration. Journal of Molecular Catalysis a-Chemical 308 (2009) : 127-133.

[4] Wei, Y., Zhang, D., Liu, Z. and Su, B.L. Methyl halide to olefins and gasoline over zeolites and SAPO catalysts: A new route of MTO and MTG. Cuihua Xuebao/Chinese Journal of Catalysis 33 (2012) : 11-21.

[5] Fatourehchi, N., Sohrabi, M., Royaee, S.J. and Mirarefin, S.M. Preparation of SAPO-34 catalyst and presentation of a kinetic model for methanol to olefin process (MTO). Chemical Engineering Research & Design 89 (2011) : 811-816.

[6] Yoo, K.S., Kim, J.H., Park, M.J., Kimb, S.J., Joo, O.S. and Jung, K.D. Influence of solid acid catalyst on DME production directly from synthesis gas over the admixed catalyst of $Cu/ZnO/Al_2O_3$ and various SAPO catalysts. Applied Catalysis a-General 330 (2007) : 57-62.

[7] International DME association. International Conference on Energy and Automotive Technologies. Multi-Source; Multi-Purpose; Low Carbon: DME's Roles in the Energy Mix [online]. 2012. Available from: http://www.icatconf.com/Sunumlar/SESSION1/4_Jean%20Alain%20Taupy.pdf [1 April 2013]

[8] Semelsberger, T.A., Borup, R.L. and Greene, H.L. Dimethyl ether (DME) as an alternative fuel. Journal of Power Sources 156 (2006): 497-511.

[9] Japan DME Forum. About DME. The comparison of physical properties between DME and similar fuels [online]. 2004. Available from: http://www.dmeforum.jp/about/property e.html [2 April 2013]

[10] Lim, H.W., Jun, H.J., Park, M.J., Kim, H.S., Bae, J.W., Ha, K.S., Chae, H.J. and Jun, K.W. Optimization of methanol synthesis reaction on $Cu/ZnO/Al_2O_3/ZrO_2$ catalyst using genetic algorithm: Maximization of the synergetic effect by the optimal CO_2 fraction. Korean Journal of Chemical Engineering 27 (2010) : 1760-1767.

[11] Bekkum H.V., F.E.M., Jacobs P.A. and Jansen J.C. Introduction to Zeolite science and Practice. 2nd ed. The Netherlands: Elsevier Science, 2001.

[12] Wendelbo, R., Akporiaye, D., Andersen, A., Dahl, I.M. and Mostad, H.B. Synthesis, characterization and catalytic testing of SAPO-18, MgAPO-18, and ZncZPO-18 in the MTO reaction. Applied Catalysis a-General 142 (1996) : L197-L207.

[13] The international zeolite association. Database of Zeolite Structures. Zeolite Framework Types [online]. 1973. Available from: http://www.iza-structure.org/databases/ [20 April 2013]

[14] Weitkamp, J.and Puppe, L. Catalysis and zeolites : fundamentals and applications. Germany: Spinger-Verlag Berlin Heidelberg, 1999.

[15] Montgomery, D.C. Disign and Analysis of Experiments. 5th ed. Asia: John Wiley & Sons, 2001.

[16] Dai, W.L., Wang, X., Wu, G.J., Guan, N.J., Hunger, M. and Li, L.D. Methanol-to-Olefin Conversion on Silicoaluminophosphate Catalysts: Effect of Bronsted Acid Sites and Framework Structures. Acs Catalysis 1 (2011) : 292-299.

[17] Dai, W.L., Kong, W.B., Wu, G.J., Li, N., Li, L.D. and Guan, N.J. Catalytic dehydration of methanol to dimethyl ether over aluminophosphate and silico-aluminophosphate molecular sieves. Catalysis Communications 12 (2011) : 535-538.

[18] Buchholz, A., Wang, W., Xu, M., Arnold, A. and Hunger, M. Thermal stability and dehydroxylation of Bronsted acid sites in silicoaluminophosphates H-SAPO-11, H-SAPO-81 H-SAPO-31, and H-SAPO-34 investigated by

multi-nuclear solid-state NMR spectroscopy. Microporous and Mesoporous Materials 56 (2002) : 267-278.

[19] Lim, H.W., Park, M.J., Kang, S.H., Chae, H.J., Bae, J.W. and Jun, K.W. Modeling of the kinetics for methanol synthesis using $Cu/ZnO/Al_2O_3/ZrO_2$ catalyst: Influence of carbon dioxide during hydrogenation. Industrial and Engineering Chemistry Research 48 (2009) : 10448-10455.

[20] García-Trenco, A. and Martínez, A. Direct synthesis of DME from syngas on hybrid CuZnAl/ZSM-5 catalysts: New insights into the role of zeolite acidity. Applied Catalysis A: General 411–412 (2012) : 170-179.

[21] Cui, Y.B., Xu, Y.B., Lu, J.Y., Suzuki, Y. and Zhang, Z.G. The effect of zeolite particle size on the activity of Mo/HZSM-5 in non-oxidative methane dehydroaromatization. Applied Catalysis a-General 393 (2011) : 348-358.

[22] Danilina, N. and Bokhoven, J. A. Control of morphology and mesoporosity of SAPO using engineered surfactants. in A. Gédéon, P. Massiani and F. Babonneau (eds.), The 4th International FEZA Conference: Zeolites and Related Materials: Trends, Targets and Challenges, 213-216. Elsevier B.V., 2008.

[23] Liu, P., Ren, J. and Sun, Y.H. Influence of template on Si distribution of SAPO-11 and their performance for n-paraffin isomerization. Microporous and Mesoporous Materials 114 (2008) : 365-372.

[24] Qi, J.A., Zhao, T.B., Xu, X., Li, F.Y. and Sun, G.D. High activity in catalytic cracking of large molecules over micro-mesoporous silicoaluminophosphate with controlled morphology. Science China-Chemistry 53 (2010) : 2279-2284.

[25] Liu, Z.M. and Liang, J. Methanol to olefin conversion catalysts. Current Opinion in Solid State & Materials Science 4 (1999) : 80-84.

[26] Garcia-Trenco, A., Vidal-Moya, A. and Martinez, A. Study of the interaction between components in hybrid CuZnAl/HZSM-5 catalysts and its impact in the syngas-to-DME reaction. Catalysis Today 179 (2012) : 43-51.

[27] Fu, Y.C., Hong, T., Chen, J.P., Auroux, A. and Shen, J.Y. Surface acidity and the dehydration of methanol to dimethyl ether. Thermochimica Acta 434 (2005) : 22-26.

[28] Jin, D., Zhu, B., Hou, Z., Fei, J., Lou, H. and Zheng, X. Dimethyl ether synthesis via methanol and syngas over rare earth metals modified zeolite Y and dual Cu-Mn-Zn catalysts. Fuel 86 (2007) : 2707-2713.

[29] Siva Kumar, V., Padmasri, A.H., Satyanarayana, C.V.V., Ajit Kumar Reddy, I., David Raju, B. and Rama Rao, K.S. Nature and mode of addition of phosphate precursor in the synthesis of aluminum phosphate and its influence on methanol dehydration to dimethyl ether. Catalysis Communications 7 (2006) : 745-751.

[30] Takeguchi, T., Yanagisawa, K.I., Inui, T. and Inoue, M. Effect of the property of solid acid upon syngas-to-dimethyl ether conversion on the hybrid catalysts composed of Cu-Zn-Ga and solid acids. Applied Catalysis A: General 192 (2000) : 201-209.

[31] Thongkam, M., Yang, G., Vitidsant, T. and Tsubaki, N. Novel three-component zeolite capsule catalyst for direct synthesis of isoparaffin. Journal of the Japan Petroleum Institute 52 (2009) : 216-217.

[32] Kasaie, M. and Sohrabi, M. Kinetic study on methanol dehydration to dimethyl ether applying clinoptilolite zeolite as the reaction catalyst. Journal of the Mexican Chemical Society 53 (2009) : 233-238.

[33] Omata, K., Sutarto, Hashimoto, M., Ishiguro, G., Watanabe, Y., Umegaki, T. and Yamada, M. Design and development of Cu-Zn oxide catalyst for direct dimethyl ether synthesis using an artificial neural network and physicochemical properties of elements. Industrial and Engineering Chemistry Research 45 (2006) : 4905-4910.

[34] Chuab, D.W., Zeng, Y.P. and Jiang, D.L. Synthesis and growth mechanism of Cr-doped ZnO single-crystalline nanowires. Solid State Communications 143 (2007) : 308-312.

[35] Hong, Z.S., Cao, Y., Deng, J.F. and Fan, K.N. CO_2 hydrogenation to methanol over $Cu/ZnO/Al_2O_3$ catalysts prepared by a novel gel-network-coprecipitation method. Catalysis Letters 82 (2002) : 37-44.

[36] Zhang, Y.L., Sun, Q., Deng, J.F., Wu, D. and Chen, S.Y. A high activity $Cu/ZnO/Al_2O_3$ catalyst for methanol synthesis: Preparation and catalytic properties. Applied Catalysis a-General 158 (1997) : 105-120.

[37] Prakash, A.M., Ashtekar, S., Chakrabarty, D.K. and Chilukuri, S.V.V. Synthesis and Characterization of the Large-Pore Molecular-Sieve Sapo-46. Journal of the Chemical Society-Faraday Transactions 91 (1995) : 1045-1050.

[38] Yang, G.H., Tsubaki, N., Shamoto, J., Yoneyama, Y. and Zhang, Y. Confinement Effect and Synergistic Function of H-ZSM-5/Cu-ZnO-Al_2O_3 Capsule Catalyst for One-Step Controlled Synthesis. Journal of the American Chemical Society 132 (2010) : 8129-8136.

[39] Yang, G.H., Thongkam, M., Vitidsant, T., Yoneyama, Y., Tan, Y.S. and Tsubaki, N. A double-shell capsule catalyst with core-shell-like structure for one-step exactly controlled synthesis of dimethyl ether from CO_2 containing syngas. Catalysis Today 171 (2011) : 229-235.

[40] Yang, G.H., Wang, D., Yoneyama, Y., Tan, Y.S. and Tsubaki, N. Facile synthesis of H-type zeolite shell on a silica substrate for tandem catalysis. Chemical Communications 48 (2012) : 1263-1265.

[41] Mao, D.S., Xia, J.C., Zhang, B. and Lu, G.Z. Highly efficient synthesis of dimethyl ether from syngas over the admixed catalyst of CuO-ZnO-Al_2O_3 and antimony oxide modified HZSM-5 zeolite. Energy Conversion and Management 51 (2010) : 1134-1139.

[42] Yaripour, F., Baghaei, F., Schmidt, I. and Perregaard, J. Synthesis of dimethyl ether from methanol over aluminium phosphate and silica-titania catalysts. Catalysis Communications 6 (2005) : 542-549.

[43] Bao, J., He, J., Zhang, Y., Yoneyama, Y. and Tsubaki, N. A core/shell catalyst produces a spatially confined effect and shape selectivity in a consecutive reaction. Angewandte Chemie-International Edition 47 (2008) : 353-356.

APPENDICES

Appendix A

Gel composition calculation of molecular sieve

Calculation details of as-synthesized zeolite

Table A.1 Silicoaluminophosphates gel composition

Chemical formula	Name	Company	Molecular weight
Al_2O_3	Aluminium isoproxide	Aldrich	204.25
H_3PO_4	Phosphoric acid (85%)	Chameleon Reagent	98
SiO_2	Silica Ludox 40 wt% suspension in water	Aldrich	60.08
DPA	di-n-propylamine (99%) Triethylamine (TEA)	Sigma-Aldrich	101.22

Calculation example for design the molar ratio of sol preparation

SAPO11: $1.2Al_2O_3$: $3H_3PO_4$: $0.6SiO_2$: 2DPA: $100H_2O$

Table A.2 The chemical sources and its molecular weight

Chemical	Precursor	Molecular weight
Al_2O_3	Aluminium iso-propoxide	204.25
H_3PO_4	Phosphoric acid (85 wt%)	98
SiO_2	Silica sol (40 % suspension in water)	60.08
DPA	Di-n-propylamine (99%)	101.22
TEA	Triethylamine	101.19
H_2O	Ion exchange water	18

The amount of water of 20 ml is fixed at 100 mol in the recipe and then we have to convert into

20g × 1 mol/ 18 g = 1.1111 mol;
and then we divided by the same molar number and multiplied by the molar number in the recipe to make them have molar ratio as same as the recipe, we obtained;
20g × 1 mol/ 18 g = 1.1111 mol × 100/1.1111 mol = 100

For Al_2O_3, the weight we have to take was
1.2 mol of Al_2O_3 × 2 mol of Al/ mol of Al_2O_3 × 204.25 g/mol of precursor × 1.1111/100 = 5.4466 g

For H_3PO_4, the weight we have to take was
3 mol of H_3PO_4 × 1 mol of P × 98 g/mol of H_3PO_4 × 1.1111/100 = 3.2666 g
But the precursor was only 85% of phosphoric acid in water, then we have to divided by 0.85 to obtain the full real required amount of precursor we have to add in to the SAPO mixture solution. Therefore the actual weight we have to take was;
3 mol of H_3PO_4× 1 mol of P × 98 g/mol of H_3PO_4 × 1.1111/100 = 3.2666 g × 1/0.85 = 3.8431 g

For DPA, the weight we have to take was
2 mol of DPA × 101.22 g/mol of DPA × 1.1111/100 = 2.2493g

For SiO_2, the weight we have to take was
0.6 mol of SiO_2 × 60.08 g/mol of SiO_2 ×1.1111/100 = 0.4005 g
But the precursor was only 40wt% suspension in water, then we have to divided by 0.4 to obtain the full real required amount of precursor we have to add in to the SAPO mixture solution. Therefore the actual weight we have to take was;
0.6 mol of SiO_2 × 60.08 g/mol of SiO_2 ×1.1111/100 = 0.4005 g × 1/0.4 = 1.0013 g

Then we must consider that the molar ratio of water in the recipe is the total amount of water included small fraction of water as the suspension in the H_3PO_4 (85%) or SiO_2 Ludox (40 wt% suspension)

Therefor we recalculate the fraction amount of water from three sources that is
Come from H_3PO_4 for 3.843 × 0.15 = 0.5764 g
Come from SiO_2 Ludox for 1.0013 × 0.6 = 0.60078 g

Therefore the amount of water we have to add into the mixture solution was 20 – 0.5764 – 0.60078 = 18.8228 g

For the SAPO-46 or ALPOs, the same calculation method was used. The summary of used chemical substance was showed in Table A3.

Table A.3 Summary of weight of chemical reactants used

	Weight used (g)					
Type	Al_2O_3	H_3PO_4	SiO_2	DPA	TEA	H_2O
$AlPO_4$-5	5.446	3.266	-	-	1.124	19.4
$AlPO_4$-11	5.446	3.266	-	1.124	-	19.4
SAPO-11	5.454	3.275	1.004	2.252	-	20
SAPO-46	5.446	3.266	1.001	4.499	-	20

Table A.4 Yield of as-synthesized zeolite

Type	in Gel (from the formula)		in calcined zeolite (from EDX analysis)		% Yield (based on Si/Al)
	Si/Al	P/Al	Si/Al	P/Al	
$AlPO_4$-5	-	1.25	-	0.70	56
$AlPO_4$-11	-	1.25	-	0.73	58.4
SAPO-11	0.25	1.25	0.16	0.52	64
SAPO-46	0.25	1.25	0.18	0.34	72

Appendix B

The weight increment of physical coating catalyst

Example of the calculation of the weight increment of the physical coating catalyst CuZnAl/SAPO11-PhyC

The weight of core catalyst was 1.2018 g

The weight of catalyst after soaking by SiO_2 Ludox (after dried) was 1.2835 g

The weight of SAPO-11 powder was 0.4784 g

The weight after calcination is 1.553 g

Therefore the % increment was $\frac{(1.553 - 1.2835)}{1.2018} \times 100 = 22.42\%$

The calculated weight increment is based on the original weight of the core catalyst.

Appendix C

NH_3-TPD Analysis

The NH_3-TPD profiles of all physical coating Cr/ZnO/SAPO46-PhyC, CuZnAl/SAPO11-PhyC, the mixed Cr/ZnO/SAPO46-M, CuZnAl/SAPO11-M and the Cr/ZnO catalysts, and the bare Cr/ZnO and CuZnAl catalyst were investigated by NH_3-TPD. Furthermore, the author also prepared the very low ratio of SAPO-11 to the core Cr/ZnO catalyst. The results were showed in the **Table C.1**

Table C.1 The acid properties obtained from NH_3-TPD of all physical coating and mixed catalysts

Sample	Acid strength	Acidity (mmol NH_3/g cat)
Cr/ZnO/SAPO46-PhyC (<5 wt%)	moderate	3.474
Cr/ZnO/SAPO46-M (10:1)	moderate	5.496
Cr/ZnO	moderate	4.874
Cr/ZnO/SAPO11-PhyC (0.579wt%)	moderate	2.789
Cr/ZnO/SAPO11-M (10:0.0579)	moderate	3.502
CuZnAl/SAPO11-PhyC (20 wt%)	moderate	6.121
CuZnAl/SAPO11-M (10:2)	moderate	8.597
CuZnAl	moderate	7.759

Appendix D

Calculation of W/F ratio of syngas

Calculation of W/F ratio for STD synthesis

1. $W_{core\ cat}/F_{syngas}$ calculation for adjusting flow rate of syngas

For example $\frac{W_{Cr/ZnO}}{F_{syngas}} = 10$ g.h/mol $= \frac{0.5}{x}$

$\therefore$ x = 0.05 mol/h

From ideal gas's law: $n = \frac{PV}{RT}$

$$0.05\ \frac{mol}{h} = \frac{P\ (Pa) \times V(\frac{cc}{\min}) \times 60(\frac{min}{h}) \times \frac{1\ L}{1000cc}}{8.314 \times 10^3 \frac{Pa.L}{molK} \times (273+T)K}$$

$$\therefore\ V = \frac{0.05 \times 8.314 \times 10^5 \times (273+T) \times 1000}{P \times 60}$$

If pressure and temperature are 1026 hPa and 26°C, replace P and T in the equation we will get flow rate of syngas

$$V = \frac{0.05 \times 8.314 \times 10^5 \times (273+26) \times 1000}{102600 \times 60}$$

$$= 20.19\ \frac{cc}{min}$$

Appendix E

Catalytic conversion and product distribution

Calculation formula

1. Calculation of CO conversion of syngas

$$COconversion(\%) = \frac{\left(\frac{CO}{Ar}\right)_{in} - \left(\frac{CO}{Ar}\right)_{out}}{\left(\frac{CO}{Ar}\right)_{in}} \times 100$$

$$CO_2conversion(\%) = \frac{\left(\frac{CO_2}{Ar}\right)_{in} - \left(\frac{CO_2}{Ar}\right)_{out}}{\left(\frac{CO_2}{Ar}\right)_{in}}$$

Total conversion

$$= CO_{conv@5hour} \times \left(\frac{mol\%CO}{mol\%CO + mol\%CO_2}\right) + CO_{2,conv@5hour} \times \left(\frac{mol\%CO_2}{mol\%CO + mol\%CO_2}\right)$$

2. Calculation of outlet flow rate; for example, the pressure at 1018 hPa, Temperature 25 °C, effluent flow rate 30 s/10cc

$$\text{Outlet flow rate (mol/h)} = \frac{1018hPa \times \frac{1kPa}{10hPa} \times \left(\frac{10cc}{30s} \times \frac{60cc}{1\min} \times \frac{60\min}{1h}\right) \times \frac{1L}{1000cc}}{8.31447\left(\frac{LkPa}{K \cdot mol}\right) \times (°C + 273.15)K}$$

$$= 0.04928\frac{mol}{h}$$

3. Calculation of amount of product gas (C mol/h)

3.1 For C.mol/h of each substance for GC 14B FID equipped with PQ column

$$= C_1 mol\%_{s\tan dardgas} \times \frac{AreaC_{n1\ productgas}}{AreaC_{1s\tan dardgas}} \times outletflowrate\left(\frac{mol}{h}\right)$$

Calculation area of C_n for GC 14B (porapaq Q column)

From $\left(\frac{AreaC_n}{AreaC1}\right)_{PQ} = \left(\frac{AreaC_n}{AreaC_1}\right)_{Al2O3} = correctionfactor$; n= 3, 4, 5,…

$$\left(AreaC_n\right)_{PQ} \quad correctionfactor \times AreaC_{1,PQ}$$

Therefore they will have a factor for calculating

Correction factor of $\frac{f_{PQ}}{f_{Al_2O_3}} = \frac{\left(\frac{AreaC_n}{AreaC_1}\right)_{Al_2O}}{\left(\frac{AreaC_n}{AreaC_1}\right)_{PQ}}$; let $f_{Al_2O_3} = 1$

3.2 For C.mol/h of each substance for GC 14B FID equipped with Alumina-30

$$= C_1 mol\%_{s\tan dardgas} \times \frac{Area_{MeOH}}{AreaC_{1,FID-AL30}} \times factor_{MeOH} \times outletflowrate\left(\frac{mol}{h}\right)$$

Calculation area of MeOH

$$\left(\frac{Area_{MeOH}}{AreaC_1}\right)_{AL-30} = \left(\frac{Area_{MeOH}}{AreaC_1}\right)_{PQ}$$

$$\left(Area_{MeOH}\right)_{AL-30} = \left(\frac{Area_{MeOH}}{AreaC_1}\right)_{PQ} \times AreaC_{1,AL-30}$$

The SHIMAZU GC14B was used to analyze the amount of MeOH, DME and higher hydrocarbons with two different column, PQ column and Aluminar-30 column, in two different apparatus. The PQ column was used to analyzed MeOH and DME, and Aluminar-30 column was used to analyze higher hydrocarbons.

Table E.1 Show the detectable substance of each column

Substance	PQ column	Alumina
C_1	Yes	Yes
C_2	Yes	Yes
C_3^+	No	Yes
MeOH	Yes	No
DME	Yes	No

4. Calculation for selectivity (%) = $\frac{\text{amount of product}}{\text{Total amount of product}} \times 100$

Example for CO conversion and DME selectivity

From run number 36. (CuZnAl/SAPO11-M)

GC raw data of synthesis and standard gas analyzed from GC 8A equipped with TCD column

Table E.2 Standard data

Syn gas	**Area TCD GC**	**Comp (mol%)**
Ar	13050	3.09%
CO	134680	33.80%
CO_2	22229.333	5.10%
CO/Ar	10.320306	
CO_2/Ar	1.7033971	
Standard gas	**Area TCD GC**	**Comp (mol%)**
Ar Area	12807.833	3.19%
CO Area	38778.167	5.05%
CH_4 Area	15869.5	5.25%
CO_2 Area	22205	5.02%

Collection factor for each product

Hydrocarbons	**MeOH**	**DME**	**CH_4**
FID Factors	1.4681	2.0958	1.0000

Correction factor between GC 14B FID detector of PQ column and Alumina-30 column

	FID-PQ	**FID-Al-30**
CH_4 Area	78799	1848806

Table E.3 Reaction data of catalyst CuZnAl/SAPO11-M (10:2)

Time	Area				flow rate	outlet gas flow rate	W/F	Conversion		
(hr)	Ar	CO	CH_4	CO_2	sec/10 cc	(mol/h)	g. h/mol	CO	CO_2	Total
0.5	12353	124468	-	30988				2.37	-47.27	-4.14
1	16509	112843	-	46238	55.95	0.0259	19.26	33.77	-64.42	20.89
1.5	20025	102550	-	60674				50.38	-77.87	33.56
2	23658	96947	-	67451	60.23	0.0241	20.74	60.30	-67.37	43.55
2.5	22872	95860	-	71315				59.39	-83.05	40.71
3	24228	95553	-	72401	71.78	0.0202	24.71	61.78	-75.43	43.79
3.5	23652	97347	-	72927				60.12	-81.01	41.61
4	24383	98411	119	73604	75.57	0.0192	26.02	60.89	-77.21	42.78
4.5	23776	99205	84	71840				59.57	-77.38	41.61
5	25120	100556	111	71258	57.26	0.0254	19.71	61.21	-66.53	44.46
5.5	23780	101944	108	72680				58.46	-79.43	40.38

Table E.4 Reaction data of catalyst CuZnAl/SAPO11-M (10:2)

FID (PQ column)			
Substance	Area	Amount of pdt. (C-mol/h)	Selectivity proportion
C_1	323	6.99337E-06	0.001364001
$C_2^=$	330	7.14493E-06	0.001393562
C_2	-	0	0
$C_3^=$	-	0	0
C_3	-	0	0
C_4	3070	6.64695E-05	0.012964345
C_5	93.8194	2.03131E-06	0.000396191
C_6	95.1981	2.06116E-06	0.000402013
C_7	76.1675	1.64913E-06	0.000321649
C_8	-	0	0
C_9	614.1317	1.32968E-05	0.002593425
MeOH	130359	0.002822442	0.550494823
DME	101842	0.002205012	0.43006999
CO_2		0.003197647	
total		0.008324748	1

FID (Alumina column			
Substance	Area	Amount of pdt. (C-mol/h)	Selectivity proportion
C_1	14291	7.79842E-06	0.000931497
C_2	13924	7.59815E-06	0.000907576
$C_2^=$	78	4.25636E-08	5.08409E-06
C_3	1632	8.90562E-07	0.000106375
C_4	3280	1.78986E-06	0.000213793
C_5	4151	2.26515E-06	0.000270565
C_6	4212	2.29844E-06	0.000274541
C_7	3370	1.83897E-06	0.000219659
C_8	-	0	0
C_9	27172	1.48274E-05	0.001771089
MeOH	5767679	0.004620608	0.551917032
DME	3245681	0.003711968	0.44338279
CO_2		0.003197647	
total		0.011569573	1

At the 2nd hour :

$$\text{CO conversion} = \frac{\frac{134680}{13050} - \frac{96947}{23658}}{\frac{134680}{13050}} \times 100 = 60.295\%$$

$$\text{CO}_2 \text{ conversion} = \frac{\frac{22229}{13050} - \frac{67451}{23658}}{\frac{22229}{13050}} \times 100 = -67.379\%$$

Total conversion

$$= 60.295\% \times \left(\frac{33.80\%}{33.80\% + 5.10\%} \right) + (-67.379\%) \times \left(\frac{5.10\%}{33.80\% + 5.10\%} \right) = 43.556\%$$

For GC 14B equipped with FID detector, the one with PQ column had been used for MeOH and DME analysis and the other one with Alumina column had been used for higher hydrocarbons analysis. The analysis results had been interpreted from both GC to obtain the reaction results.

Amount of product (C-mol/h) calculated based on GC 14B, PQ column

$$\text{for } C_1 = C_1 mol\%_{s\tan dardgas} \times \frac{AreaC_{1\,productgas}}{AreaC_{1s\tan dardgas}} \times outletflowrate\left(\frac{mol}{h}\right)$$

$$= 5.25\% \times \frac{323}{78799} \times 0.019216 \times correctionfactor_{C_1, AL30/PQ}$$

$$= 5.25\% \times \frac{323}{78799} \times 0.019216 \times 1.6911$$

$$= 6.99315E-06 \text{ C.mol/h}$$

Amount of product (C-mol/h) calculated based on GC 14B, Alumina column

$$\text{For } C_{1=}\ 5.25\% \times \frac{14291}{1848806} \times 0.0192165 = 7.798E-06$$

$$\text{Area of MeOH} = 14291 \times \frac{130359}{323} = 5767679$$

C.mol/h for MeOH = $5.25\% \times \frac{5767679}{1848806} \times 1.4681 \times 0.019216 = 0.0046205$

Selectivity consider from PQ column

$$selectivityC_1 = \frac{6.99337E-06}{5.127101E-03} \times 100 = 0.1364$$

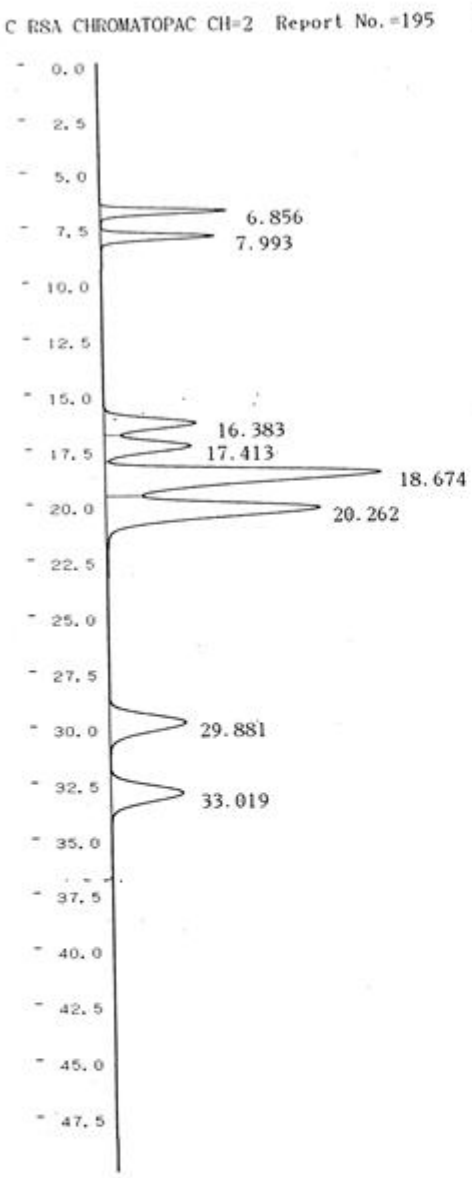

** CALCULATION REPORT **

CH	PKNO	TIME	AREA	HEIGHT	MK	IDNO	CONC	NAME
2	4	6.856	22003	1287	V		5.2206	
	5	7.993	22645	1160			5.373	
	6	16.383	32550	940			7.723	
	7	17.413	32137	884	V		7.6251	
	8	18.674	127083	2803	V		30.1528	
	9	20.262	104359	2172	V		24.7611	
	10	29.881	42005	783			9.9664	
	11	33.019	38681	740	V		9.1779	
		TOTAL	421464	10768			100	

Figure E.1 Chromatogram of GC-14B SHIMADZU

Appendix F

Details and raw data of design of experiments

Table F.1 DME experiment results

Std	Coded factor				Conversion (%)			Selectivity (%)			
	A	B	C	Label	CO	CO_2	total	CH_4	MeOH	DME	Others
1	-	-	-	(-1)	7.9	-3.2	5	1.1	39.3	58.8	0.8
2	+	-	-	a	13.1	-20.8	8.7	1	22.8	75.3	0.9
3	-	+	-	b	9.2	-15.6	6	13.2	9.7	38	39.1
4	+	+	-	ab	10.3	-14.1	7.1	29	26.3	29.4	15.3
5	-	-	+	c	6.2	-6	4.6	2.5	12	80.9	4.6
6	+	-	+	ac	12.8	-18.1	8.8	3.2	9.8	81.3	5.7
7	-	+	+	bc	26	-75.1	12.8	13.1	2.7	3.6	80.6
8	+	+	+	abc	65.2	-178	33.3	32.1	0.3	0.2	67.4
9	0	0	0	center	28.4	-57.7	17.2	1.7	9	73	16.3
10	0	0	0	center	29.3	-56.7	18	1.7	9.1	74.8	14.4
11	0	0	0	center	30.8	-64.1	18.3	3	8.8	70.6	17.6
12	-	0	0	Fcc	25.4	-49.3	15.6	1.5	9.3	76.8	12.4
13	+	0	0	Fcc	32.1	-64.3	19.5	1.7	7.9	76.3	14.1
14	0	-	0	Fcc	14.4	-25	9.2	0.6	10.1	88	1.3
15	0	+	0	Fcc	14.2	-24.4	9.1	15.6	7.1	25.4	51.9
16	0	0	-	Fcc	20.5	-31.1	13.7	1.7	16.3	75.2	6.8
17	0	0	+	Fcc	30.5	-64.9	18	1.7	8	73.6	16.7

BIOGRAPHY

Miss Kitima Pinkaew
Birthday: 28 June 1985, Bangkok, Thailand

Education :

Master's Degree - Master of Engineering, 2009, Chulalongkorn University, Bangkok, Thailand
Bachelor's Degree - Bachelor of Science, 2007, Chulalongkorn University, Bangkok, Thailand

Academic publication :

1. "A new core-shell-like capsule catalyst with SAPO-46 zeolite shell encapsulated Cr/ZnO for the controlled tandem synthesis of dimethyl ether from syngas" Fuel, inpress, 2013
2. "Effect of nanocrystallite size of TiO_2 on Co/TiO_2 catalysts over methanation" Proceeding of *the 2nd Asian Conference on Innovative Energy & Environmental Chemical Engineering*, Phuket, Thailand, 2010
3. "Carbonmonoxide hydrogenation over Co/TiO_2-Ru catalysts" Proceeding of *the 18th Thailand Chemical Engineering and Appiled Chemical Conference*, Pattaya, Thailand, 2008
4. " Dimethyl ether synthesis at low temperature" Proceeding of *the 15th Academic Conference, the 2007 Annual Meeting, Faculty of Science*, Chulalongkorn University, Bangkok, Thailand, 2007

Award and Scholarship :

1. The financial support from Chulalongkorn University, Dutsadi Phiphat Scholarship (2009-2013)
2. The financial support from Chulalongkorn University, Department of Chemical Engineering (2007-2009)
3. The Second Class Honors in the bachelor's degree from Department of Chemical Technology, Chulalongkorn University (2007)